

INFLUENCE OF INTERFERENCE, TURBULENCE
INTENSITY AND SURFACE ROUGHNESS ON THE
FLOW-INDUCED VIBRATION OF A CIRCULAR
CYLINDER

BY

MOHAMMAD SALEH HIJAWI

MEMORANDUM

SUPERVISORS

Dr. BASSAM A. JUBRAN

Dr. MOHAMMAD N. HAMDAN

0
2194

Submitted in partial fulfillment of the requirements for the degree of master of science
in mechanical engineering.

Faculty of Graduate Studies,

University of Jordan.

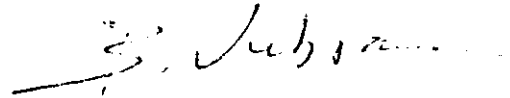
Amman , Jordan

April , 1991

The Examining Committee considers this thesis satisfactory and acceptable for the award of the Degree of Master of Science in Mechanical Engineering in April 2, 1991.

Dr. Bassam A. Jubran
Mechanical Engineering Department
University of Jordan

Chairman of Committee



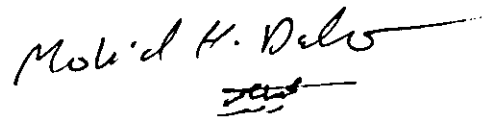
Dr. Mohammad N. Hamdan
Mechanical Engineering Department
University of Jordan

Member of Committee



Dr. Mohammad Al-Dado
Mechanical Engineering Department
University of Jordan

Member of Committee



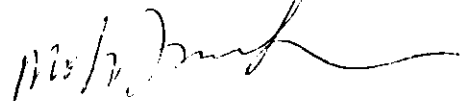
Dr. Ala Al-Deen Shehab
Industrial Engineering Department
University of Jordan

Member of Committee



Dr. Mohammad Al-Jarrah
Mechanical Engineering Department
Jordan University of Science and Technology

Member of Committee



ACKNOWLEDGEMENTS

It is of my pleasure to express my gratitude to all people who helped me in completing the present work. Special thanks are indebted to my supervisors Dr. B. Jubran and Dr.M. Hamdan; whom without their support, encouragement, sound guidance, and advice, my work could have been infinitely more difficult. Also I highly appreciate the great assistance conducted through the mechanical engineering labs staff, especially Mr.Aref Shahin and the computer center staff at the Faculty of Engineering and Technology.

Finally, not to forget, the support and great help given to me by all my friends throughout my research.

ABSTRACT

The present investigation is an experimental work involving the study of the effects of interference, free stream turbulence intensity and surface roughness on the flow induced vibration of a single cylinder clamped as a cantilever. The dynamic response of the single cylinder clamped at one end is characterized by one resonance peak at $U/FD = 15.5$.

The effect of interference was examined in tandem, side-by-side and staggered arrangements for different gap spacings and relative dimensions of the diameter of the interfering circular body to the diameter of the test cylinder (d/D). It is found that the effect of interference is more clear in tandem arrangement than that of the other arrangements. The vibration amplitude increases significantly for small gap spacing (g/D) especially when (d/D) is large. For (g/D) > 6.0 the response of the cylinder is similar to that of a single cylinder.

Free stream turbulence intensity and surface roughness were studied for a single cylinder, as well as, tandem and side-by-side arrangements. The effects of the free stream turbulence intensity on the dynamic response of the test cylinder are very much depending on the turbulence intensity, Reynolds number, relative dimensions (d/D) and the gap spacings (g/D) or (T/D). The surface roughness is found to reduce the vibration amplitude significantly even for small gap spacing in tandem arrangement, while for the side-by-side arrangement the effect of the surface roughness is smaller. Finally, conclusions and recommendations are presented, thoroughly expressed and discussed.

Contents

ACKNOWLEDGEMENTS	i
ABSTRACT	ii
CONTENTS	iii
NOMENCLATURE	vii
1 INTRODUCTION AND OBJECTIVES	1
1.1 Introduction	1
1.2 Forms of Flow-Induced Vibration	3
1.2.1 Vortex Shedding From Cylindrical Bodies	3
1.2.2 Fluid-Elastic Excitation (Galloping)	4
1.2.3 Flutter	5
1.3 Factors Affecting Flow-Induced Vibration	6
1.3.1 Interference Effects	6
1.3.2 Turbulence Intensity Effects	7
1.3.3 Surface Roughness Effects	8
1.3.4 End-Plates Effects	9
1.4 Present Work Contribution	9
1.5 Outline of The Experimental Program	10
1.6 Layout of The Thesis	10
2 LITERATURE SURVEY	13

2.1	Introduction	13
2.2	Single Cylinder Response	13
2.3	Effects of Interference	18
2.4	Effects of Turbulence Intensity	22
2.5	Effects of Surface Roughness	24
2.6	Effects of End Plates	25
3	INSTRUMENTS AND APPARATUS	27
3.1	Introduction	27
3.2	Apparatus	27
3.2.1	Wind Tunnel	27
3.2.2	Clamping and Position of the Test Cylinder	28
3.2.3	Interfering Bodies	28
3.2.4	Turbulence Generating Grids	29
3.2.5	Standard Sand Papers	29
3.2.6	End Plates	30
3.3	Velocity and Turbulence Measurements	30
3.4	Vibration Measurements	33
3.5	Experimental Conditions	34
3.6	Preliminary Tests	34
3.7	Experimental Procedures	36
3.7.1	Single Cylinder Measuring Procedure	36
3.7.2	Interference Arrangements Measuring Procedure	37
3.7.3	End Plates Measuring Procedure	37
3.8	Repeatability of Measurements	38
4	DISCUSSION OF RESULTS	30

4.1	Introduction	39
4.2	Single Cylinder Results	39
4.3	Effects of Interference	40
4.3.1	Interference Effects for Tandem Arrangement	41
4.3.2	Interference Effects for Side-By-Side Arrangement	44
4.3.3	Interference Effects for Staggered Arrangement	45
4.4	Effects of Turbulence Intensity	47
4.4.1	Turbulence Intensity Effects for Single Cylinder	47
4.4.2	Turbulence Intensity Effects for Tandem and Side-By-Side Arrangement	49
4.5	Effects of Surface Roughness	52
4.5.1	Surface Roughness Effects for Single Cylinder	52
4.5.2	Surface Roughness Effects for Tandem and Side-By-Side Arrangements	53
4.6	Effects of Turbulence Intensity, Surface Roughness on Tandem and Side-By-Side Arrangements	54
4.7	Effects of End Plates	55
4.8	Effects of Experimental Conditions on the Response Signal Wave	55
5	CONCLUSIONS AND RECOMMENDATIONS	57
5.1	Conclusions	57
5.1.1	Single Cylinder	57
5.1.2	Effects of Interference	58
5.1.3	Effects of Turbulence Intensity	58
5.1.4	Effects of Surface Roughness	59
5.2	Recommendations	60

NOMENCLATURE¹

- A*: Vibration amplitude.
- A_v*: Transverse vibration amplitude.
- A_h*: Streamwise vibration amplitude.
- A/D*: Dimensionless vibration amplitude.
- D*: Diameter of the test cylinder.
- d*: Diameter of the interfering cylinder.
- d/D*: Relative dimension.
- EP*: Distance between end plate and tunnel wall.
- F*: Natural frequency of the test cylinder.
- f*: Oscillating cylinder frequency.
- f_s*: Vortex shedding frequency.
- g*: Gap spacing in the streamwise direction.
- g/D*: Relative gap spacing in the streamwise direction.
- I*: Electric current.
- k*: Roughness height.
- k/D*: Relative roughness height.
- K_s*: Damping factor = $2m\delta/\rho D^2$.
- l*: Length of the test cylinder.
- l/D*: Aspect ratio.

¹This list is confined mainly to frequently-used symbols.

m : Mass per unit length.

Nu : Nusslet number.

P : Power.

Q : Heat loss.

R : Resistance of the hot wire.

Re : Reynolds number= UD/ν .

RMS: Root mean square.

S : Strouhal number= $f_s D/U$.

Sc : Scruton number= $2m\delta/\rho D^2 H$.

t : Thickness of the test cylinder.

T : Gap spacing in the transverse direction.

T/D : Relative gap spacing in the transverse direction.

TU : Free stream turbulence intensity.

U : Free stream velocity.

U/FD : Reduced velocity.

ρ : Density of air.

ν : Kinematic viscosity of air.

δ : Logarithmic decrement.

Chapter 1

INTRODUCTION AND OBJECTIVES

1.1 Introduction

The flow of fluids around structural members can cause destructive vibrations. These flow-induced vibrations have become increasingly important in recent years because designers are using materials to their limits, causing structures to become progressively lighter and more flexible.

Any structure with sufficiently bluff trailing edge sheds vortices in a subsonic flow. The vortex streets tend to be very similar regardless of tripping structure. Periodic forces on the structure are generated as the vortices are alternately shed from each side of the structure. This phenomena have been observed for many years ago, although the mechanics of vortex formation are not yet fully understood.

The oscillations in a normal direction of the flow are called crossflow oscillations and the oscillation in the direction of flow are called in-line oscillations, which are due to the cylinder installation.

The susceptibility of an elastic or rigidly clamped cylinder to flow-induced oscillation depends on the flowing dimensionless parameter:

$$\frac{\lambda(x, y)}{D} = f''(W, S_c, DF, Re, AR, SR, TU)$$

where;

A/D is the relative amplitude with components, usually, in both streamwise and transverse directions.

$W = U/FD$ is the reduced velocity based on the natural frequency F of the cylinder in Hz.

$Sc = 2M\delta/\rho D^2 H$ is the Scruton number, which is a product of the mass ratio and damping expressed through the logarithmic decrement .

DF is the number of degree of freedom of the rigidly clamped cylinder.

Re is the Reynolds number based on the diameter of the cylinder.

AR is the aspect ratio expressed as the height to diameter ratio of the cylinder.

SR is the surface roughness.

TU is the free stream turbulence intensity.

The fluid flow and the structure are iterative system, and their interaction is dynamic. These systems are coupled by the force exerted on the structure by the fluid. The fluid force causes the structure to deform. As the structure deforms it changes its orientation to the flow, and the fluid force may change.

Given a structural system incorporating supported cylindrical elements exposed to fluid flow, one would like to be able to analytically predict the structural response directly as a function of the structural and flow parameters. This could be done by constructing an approximate model for the fluid-structure interaction problem. This model should retain as much of the fluid dynamics as possible while remaining tractable analytically. Unfortunately, the theory of vortex shedding, especially in the near wake region, is very complex and no exact solution to the fluid- elastic problem has yet been found.

1.2 Forms of Flow-Induced Vibration

There are three forms of flow induced vibration; vortex shedding, fluid-elastic or galloping and flutter. These forms are described in the following sections.

1.2.1 Vortex Shedding From Cylindrical Bodies

Vortex-Shedding has been the most common form of fluid dynamic excitation for a single cylinder. Observations show that above $Re \simeq 50$ vortices are formed and shed periodically downstream of the cylinder. The mechanism of separation and vortex shedding was described by Blevins (1977). In general, as a fluid flows toward the leading edge of a bluff cylinder the pressure in the fluid rises from the free stream pressure to the stagnation pressure. This will develop boundary layers about both sides of the cylinder. These boundary layers separate from each side of the cylinder surface near the widest section and form two free shear layers which bound the wake. Since the innermost portion of the free shear layers moves much slowly than the outermost portion of the layers which are in contact with the free stream, the free shear layers tends to roll up into descent, swirling vortices. A formation mechanism of alternating vortices behind a circular cylinder is shown in Fig(1-1).

The shedding of the formed vortices alter the pressure distribution, and the cylinder experiences a time-varying force at the frequency of vortex shedding. If the cylinder is flexible or flexibly mounted, interactions can arise between the vortex shedding mechanism and the cylinder deflections. If the vortex shedding frequency coincides with the natural frequency of the oscillating structure, the resonance could exist with large amplitude of vibrations.

Experiments show that the frequency of shedding is given in terms of Strouhal number S , and this in turn is a function of the Reynolds number. The Strouhal number is

defined as:

$$S = \frac{f_s D}{U}$$

where f_s is the frequency of vortex shedding from one side of cylinder, in Hz, D is the diameter of cylinder, and U is the free-stream velocity, Blevins (1977).

Lock-in or Synchronization of Vortex Shedding

Lock-in phenomena is an important feature of vortex-shedding excitation. If the frequency of the vortex shedding is in resonance with the natural frequency of the member that produces it, large amplitude oscillations with consequent large stresses can develop.

These oscillations begin when the flow velocity increased or decreased so that the shedding frequency approaches the natural frequency of the structure. Lock-in occurs over a certain range of velocities depending on the structure properties (i.e. mass, surface roughness, stiffness and damping) and the flow properties (i.e. velocity, density and turbulence intensity). This is the difference between the lock-in and the usual case of resonance which exhibits a single resonance point.

As the lock-in phenomena begins and the motion of the vortex shedding locks into the structural frequency, a feed path is completed so that the motion of the structure controls the vortex shedding. Lock-in phenomena disappears beyond a critical conditions due to the limited capacity of the oscillating structure to alter the frequency of vortex shedding.

1.2.2 Fluid-Elastic Excitation (Galloping)

The flow-induced vibration of bluff structure is commonly referred to as stall flutter or galloping. Galloping can arise in any lightweight, flexible, structure exposed to a flow. A wide variety of cross sections, including square, rectangular, right angle, and stalled aerofoil is potentially unstable owing to aerodynamic galloping.

The fluid elastic forces result from the strong nonlinear interaction of the cylinders and the flow around them. These forces occur when the cylinders are arranged within the regions where the discontinuous change of flow regime take place, (i.e. the cylinders are within the wake-interference region). The fluid-elastic oscillations are not defined within a finite range of reduced velocities. Once initiated, they continue up to the highest velocity.

The main assumption of galloping analysis is that the fluid force on the structure is determined solely by the instantaneous relative velocity and the angle of attack of the flow to the structure. This implies that the information about the fluid force can be measured by wind tunnel test on stationary models held at various angles.

The most fascinating feature of the interference galloping is that both the mean position of the motion and the body's oscillation frequency may vary appreciably with increasing flow velocity. Another notable feature is that the vibration amplitude always approaches asymptotically a constant value. The instability is either in the form of a vortex-resonance or a galloping. The cylinder never exhibits a combined vortex-resonance and a galloping or a vortex-resonance followed by a galloping, Bokain (1987).

Galloping vibration can be prevented by increasing the internal damping of the structure, reducing the flow velocity, stiffening the structure and increasing the mass of the structure without lowering its natural frequency or damping.

1.2.3 Flutter

Flutter has been defined as the dynamic instability of an elastic body in an airstream and is produced by aerodynamic forces which result from the deflection of the elastic body from its undeformed state, Arnold (1972).

Flutter can be occurred in any engineering application of more than two degrees of freedom, such as long-span suspension bridges and turbine blades. The main reason of

sitioned at right angles to the approaching flow direction. The two cylinders can be positioned in tandem arrangement; with one cylinder behind the other at any stream-wise spacing, or in side-by-side arrangement; the cylinders face the flow side by side at any transverse spacing. Any other combinations represent staggered arrangements. These positions are extensively used in engineering situations due to the need for more compact structures like heat exchangers.

The flow interference of two parallel pipes are classified into four kinds by Zdravchovich (1985,1987) as shown in Fig(1-2) and (1-3). However, the four kinds can be distinguished as follows:

1. **Proximity interference;** the two cylinder are close to each other , but none of them in the wake of the other.
2. **Wake interference;** one cylinder is near to or submerged in the wake of the other. This kind is related to the downstream cylinder in tandem and staggered arrangements inside the interference boundary.
3. **Proximity and wake interference;** in which an extreme vibration of forces in magnitude and direction was found to occur.
4. Finally, there is a substantial region marked by 'no interference' in which the interference is negligible.

1.3.2 Turbulence Intensity Effects

Flow-induced vibrations caused by turbulent flow are a common one. These could be seen in the vibration of an automobile antenna, an anchored ship bobs in a complex turbulent flow, fuel rods in a nuclear reactor, etc. In each case induced vibrations occur due to the fluctuating pressures caused by the turbulent fluctuations.

Turbulence in the flow can have a profound effect upon flow-induced vibration. Turbulence effects on the behavior of structures can be in the form of a complex interaction between the turbulence and the body which results in changing the flow around the body. These effects depends on the shape of the body and its response to vortex shedding, galloping and torsion flutter. However, knowledge on the turbulence effects is not complete, and it is still not known how precise the simulation needs to be. One of the main reasons for this is that the effect of turbulence on vortex shedding is not sufficiently understood.

The vibration excited forces can either be reduced or increased in a turbulent flow. These excited vibrations may generally be reduced either by reducing the intensity of the turbulence, modifying the structure, increasing the stiffness of the structure and increasing the damping.

1.3.3 Surface Roughness Effects

The influence of surface roughness is important because of the fundamental flow phenomena involved and the significance of its effects in several practical applications. For example, important reduction in the magnitude of mean peak suction on cooling tower shells can be obtained if the surface is roughened by external ribs.

It has been well recognized that surface roughness can not only promote the boundary layer transition from laminar to turbulent, but also affect significantly the subsequent flow development at Reynolds numbers well beyond the critical.

It is found that for large roughness, the critical transition can be characterized as a range over which sporadic, asymmetric turbulent reattachment of the shear layers occurs resulting in unstable flow configurations and disappearance of organized shedding.

Despite many efforts, information that has been obtained on this subject still remains complex. It is thus necessary to make further investigations, either experimentally or

analytically, to understand the precise rule played by roughness on the flow past circular cylinders.

1.3.4 End-Plates Effects

The cylinder end boundaries, whether they be end plates or simple free ends, alter the vortex-shedding mechanism near these boundaries. Most investigators have studied the effect of the ratio (l/d), but insufficient information is available on the effect of end plate shape and size on the flow. In some studies they have determined the distance from the leading edge of the end plates to the cylinder axis which is sufficient to eliminate the effect of the horseshoe vortices at the junction of cylinder and wall. For very low length-to-diameter ratios ($l/d \approx 15$), however, the shedding from a cylinder can be solely determined by the boundary conditions.

1.4 Present Work Contribution

The present work is an experimental study of some factors that affect the flow-induced vibration of a circular cylinder. These factors are; (a) the presence of interfering bodies around the cylinder, (b) the turbulence intensity of the freestream, (c) the surface roughness of the cylinder, and finally the end plates. The coupling effect of these factors are presented.

The test cylinder is fixed at one end and free at the other (i.e. as a cantilever). The interfering bodies are circular with different diameters proportional to the diameter of the cylinder. The turbulence intensity is changed using different turbulence generating grids. They are positioned at different gap spacings in different arrangements. Standard sand papers are used to obtain different surface roughness. Finally, circular metal sheets are used as end plates.

392970

are discussed in chapter 5 which also include the recommendation for future work.

Some selected remarks for operating and calibrating of some instruments are presented in the appendix.

Chapter 2

LITERATURE SURVEY

2.1 Introduction

The behavior of flexible bodies in fluid flow has been the subject of several researches. One of the most interesting aspects of the problem is the effect of body oscillation on the mean and unsteady bluff-body flows, where the complex interaction between the body oscillation and the formation and shedding of vortices plays a central part, since it could be the cause of costly structural failures.

The problems associated with flow-induced oscillations and their important consequences have proved to be exceedingly difficult both theoretically and experimentally. The difficulty arises from the fundamental problem of interaction between the structure and the flow.

In this chapter, some of the investigations that have been reported were summarized to show a comprehensive account of recent contributions to the literature on the flow-induced vibrations and related aspects.

2.2 Single Cylinder Response

There have been numerous investigation of the response characteristics of freely vibrating cylinders. These investigations studied the effects of large number of structure and flow parameters on the flow induced vibrations on a single cylinder. Most of these works

deal in detail with resonant response and fluctuating pressure.

Griffin et al (1973) studied the vortex-excited resonant vibration of circulator cylinders by measuring the response characteristics and flow fields about circular cylinders that were mounted on springs in a wind tunnel. The measured vibration frequencies and amplitudes of vibrations were compared with a developed wake oscillator model for the vortex-excited vibrations. Measurements were done for an oscillating circular cylinder in cross flow with various flow conditions at Reynolds number between 350 and 1000. A series of flow visualization was used to show the cylinder motion and the accompanying vortex formation.

Skop and Griffin (1975) introduced a mathematical model that enables one to predict the vortex-excited resonant response of bluff elastic cylinders in cross-flow with differing end conditions. They coupled a modified Van Der Pol equation to the equation of motion of the cylinder. The practical case of uniform flow over a uniform elastic cylinder has been treated in detail and response have been made for taut strings and circular beams with differing end conditions. Good agreement has been obtained between the predicted and experimental results.

Chen and Jenderzejczyk (1979) investigated single tube subjected to liquid cross flow. The experiments have two distinct features: (1) the damping in the lift and drag direction is measured as a function of reduced flow velocity; (2) the detailed response characteristics of the tube (frequency spectra, RMS tube displacement, and orbital path of tube motion) are obtained at various reduced flow velocities. An analytical model is also provided to correlate with the experimental data. They have drawn the following conclusion:

1. Tube response in the drag direction becomes significant for a reduced velocity between 1.5 and 4.5.

1. Low U/FD :

(a) $1 < U/FD < 3$ and $Sc < 1.2$: The initial displacement of the cylinder in the streamwise direction disrupts the natural vortex shedding. A subsequent symmetric formation of two vortices terminates with a forced symmetric shedding when the cylinder reaches the maximum downstream amplitude. There is a significant difference in drag force when the cylinder moves upstream and the vortices are small compared with the downstream stroke when the vortices are more developed. The variation of the drag force maintains the self-excitation and produces amplitudes up to 0.2 diameters at very low values of Sc .

(b) $2.5 < U/FD < 4$ and $Sc < 1.0$: Excited oscillations occurs in the streamwise direction so that the cylinder synchronizes vortex shedding at its natural frequency

2. Medium U/FD ; $4 < U/FD < 8$ to 11 and $Sc < 15$ to 20 for a finite cylinder with a free end or $Sc < 60-80$ for a nominally two-dimensional cylinder between end plates.

The excitation is mostly into the transverse direction for amplitude up to 0.6 diameters. The interaction between the cylinder and the vortex shedding passes through the following phases :

(a) when the frequency of vortex shedding approaches the natural frequency of the cylinder, the fluctuating transverse lift force excites the cylinder to oscillate near the resonance condition.

(b) As U/FD increases, the amplitude of oscillations rises beyond the resonance condition causing a significant change in the near-wake.

(c) A rapid variation of the phase angle between the excitation force and the displacement takes place in the middle of the synchronization range.

3. High U/FD ; $U/FD > 20$ to 40: Far beyond the synchronization range, the cylinder starts to oscillate again gradually and builds up considerable amplitude, mostly in the transverse direction.

Berger (1988) studied the mechanism of vortex shedding oscillation of elastically mounted rigid cylinder. He found that the stability analysis of the so-called "lift-oscillator model" with feedback coupling by the oscillation velocity to a spring mass-system (cylinder) reveals that stability is not given in the near vicinity of phase angle of 90° and also at phase angles larger than or equals $115^\circ/120^\circ$. The reason for this is the amplitude dependance of the coupling and damping ratio caused by viscosity. He concluded that the amplitude dependance of the damping and coupling-ratio of the system is the most significant effect on the stability of the system.

Humphries et al (1988) used a slender cylinder to study the nature of vortex shedding from flexible cylinders undergoing large amplitude vortex excited motions in sheared flow. The cylinder used in the experiments was either allowed to vibrate as a vertical cantilever or held rigidly. The main conclusions of their study are:

1. For rigid cylinder in shear flow, the vortex shedding was found to follow the Strouhal relationship.
2. The measurements of the vortex shedding from a rigid cylinder in uniform flow agreed with the Strouhal relationship and expected Strouhal number.
3. For a flexible cantilever undergoing vortex induced vibrations in uniform flow, the wake frequency was found to match the structural response frequency throughout lock-on. However, only at the peak amplitude response did the measured fre-

quencies equal the structural natural frequency. During the rest of lock-on the measured frequencies were some 10% higher. The wake frequency was constant along the length of the cylinder.

4. A cantilever subject to a linear shear approach flow exhibited vortex induced vibrations and lock-in. At the peak amplitude response the wake frequency, the Strouhal response frequency and the cylinder's natural frequency were equal. During the rest of lock-on the response frequency was 5-10% higher than the natural frequency and the wake frequency was 4% higher.

Bedoor (1989) studied the flow-induced vibrations of an elastically mounted cylinder in wind tunnel. He found that the lock-in region starts at reduced velocity of about 5 and ceases at reduced velocity of about 12.5. The lock-in region is found to have two distinct resonance hills with nearly sinusoidal waveform.

2.3 Effects of Interference

Most investigated feature is the pressure field around two rigid circular cylinder of equal diameters in tandem and side-by-side arrangements for various spacings. In some studies one cylinder was elastically mounted while in most studied both cylinders were elastically mounted. Also most of the studies used equal diameter cylinders. There is a lack of studied when the relative dimensions are varied and when the front cylinder is elastically mounted while the rear one is rigid.

Zdravkovich (1977) identified two distinct groups of arrangements: (1) tandem arrangement; with one cylinder behind the other at any streamwise spacing, (2) side by side arrangement; the cylinders face the flow side by side at any transverse spacing. Other combinations of the two group represent staggered arrangements.

For tandem arrangement Zdravkovich investigated the pressure distributions, veloc-

ity profiles and force measurements. He found two flow patterns; the first one produce vortex shedding behind the upstream cylinder and distinctly influences the vortex shedding behind the downstream one. The second flow pattern produces periodic vortex shedding behind both cylinders . He also found that the most neglected feature of the flow around two staggered cylinders was the measurements of vortex shedding.

Zdravkovich (1980) studied the flow patterns caused by the interference of flow between two circular cylinders in some critical arrangements. By measuring the simultaneous pressure distribution, he found that the bistable flow in the side-by-side arrangement is prominent feature for the cylinder of finite height.

Yeung and Weaver (1983) studied the cross flow induced vibrations of different triangular array orientation in water tunnel. They found that only parallel triangular array has significant amplitude vorticity response . The fluid elastic that hold for the normal triangular array was found to be about twice that of the parallel triangular array. Their study was done to be taken into account for heat exchangers design.

Zdravkovich (1985) categorized the wide variety of fluid-elastic responses into three characteristic types for two cylinders with identical properties : (1) instability rapidly builds up to extremely large amplitude predominantly in the streamwise direction, (2) instability slowly builds up amplitude to a certain level, the oscillations begin mostly in the streamwise direction, (3) instability gradually builds up to large amplitude predominantly in the transverse direction. He found that all types of the fluid-elastic oscillations were related to the regions of interference.

Lakshmana (1986) presented the interference effects of a single in-line rigid body on the transverse vibrations of a spring-mounted circular cylinder in a uniform flow of low turbulence intensity. He has been used circular and rectangular interfering bodies located downstream of the test cylinder which was positioned vertically at the centre of a rectangular frame supported by four springs.

The results have shown that lock-in region begins at a reduced velocity of 5.0. The peak dimensionless amplitude was 0.25 over a range of reduced velocity between 6.6 and 7.6. The tests were conducted at three typical reduced velocities:

1. $U/FD = 4.5$ with diameter ratios (d/D) of 0.5, 1.0, 1.5 and 2.0. The amplitude of vibration was zero whatever was the gap to diameter ratio (g/D).
2. $U/FD = 7.0$ at which steady vibrations with a dimensionless amplitude of 0.25 occurred. With varying the ratio (g/D) gradually for different (d/D) ratios, there was a dual-peaked response except in the case of (d/D) = 0.5.
3. $U/FD = 11.45$. For $d/D = 0.5$, the effects of the presence of the downstream cylinder were not evident until (g/D) as low as 0.75 and for further reduction in (g/D) the dimensionless amplitude reached a value of 0.9.

Lakshmana concluded that the effects of circular interfering bodies are very much influenced by the reduced velocity. The oscillatory amplitudes depends on the relative dimensions (d/D) and the relative gap widths (g/D). Also he concluded, by using the flow visualization studies, that the interference effects observed are due to the changes in the vortex shedding phenomenon and the changes in the flow field that occur due to the interfering body.

Bokaian (1987) described a quasi-steady theory for predicting the galloping motion of an elastic circular cylinder, with oscillations constrained to a plane normal to the incident flow, as induced by the vicinity of a rigid parallel circular cylinder placed inside the wake. He concluded that the reduced amplitude in tandem arrangement varied with the twice-reduced velocity independently of the cylinder mass and damping. Also, the relative mean position of the moving cylinder in staggered arrangement was observed to be dependent only on the dimensionless free-stream dynamic pressure and the lift forces.

Zdravkovich (1987) studied various cluster arrangement in term of the number of cylinders, the spacing and orientation to the oncoming flow. He classified the basic interference flow regimes in all possible arrangements. The results have revealed that the most complete physical picture of the flow patterns was developed for only two cylinders in various arrangements.

Lakshmana (1988) investigated the interference effects of a rigid circular cylinder on the transverse vibrations of a spring-mounted circular cylinder exposed to a uniform flow at a reduced velocity of 7.0. The results showed that there is a critical combination of relative dimensions and spacing which gives the maximum amplitude of vibration. For staggered and side-by-side arrangements, he found that the oscillatory response of the test cylinder is strongly dependent upon whether the ratio $(d/D) < 1.0$ or otherwise.

Albrecht et al (1988) measured the frequencies of vortex shedding from two cylinders in tandem. In the first set of experiments they have used two circular cylinders. The downstream cylinder was the same during the experiment, while the upstream one was changed for different diameters. They found that the changing of the upstream cylinder diameter changed the frequency of vortex shedding for a constant free-stream velocity. The frequency of vortex shedding from the downstream cylinder locked-in to that from the upstream cylinder such that the two frequencies were equal. In the second set of experiments they replaced the upstream cylinder with a flat plate. They found that for low frequencies of shedding from the flat plate, were equal as the first part. However, the lock-in broke down for higher frequencies.

Shasrakashi et al (1989) investigated the interference effect on the oscillation behaviour of an elastically supported cylinder in cross flow caused by a downstream cylinder in a criss-crossed (cruciform) arrangement in a wind tunnel. They found that the Karman vortex resonance of the upstream cylinder is effectively depressed by the approaching of the downstream cylinder, and vanishes when the gap is smaller than half

turbulence intensity to the free stream on the characteristics of the bistable flow which takes place around two square prisms in tandem arrangement. They found that the bistable flow regime is shifted toward lower value of s/w (s : spacing between two prisms, w : width of prisms) as the turbulence intensity increased. It was found that the presence of the freestream turbulence intensity caused the formation of the wake behind the upstream prism to narrow. As the intensity of the freestream turbulence increases the flow around the two prisms becomes more unstable. Also they have found that the freestream turbulence intensity have a significant effect on the vortex shedding frequency.

Howell and Novak (1988) studied experimentally the vortex shedding from vibrating circular cylinders in turbulent flow at subcritical Reynolds numbers. The types of turbulent flow used were grid generated homogeneous turbulence and turbulent boundary layers. Pressures and their correlation, lift coefficient and response were studied.

The experiments were divided into two parts; in the first the cylinder was positioned horizontally while in the second it was vertically. The main conclusions were: (1) Turbulence weakens the spanwise pressure correlation and broad the pressure spectra while amplitude of motion increases the correlations and narrows the spectra, (2) The pressure correlations in boundary layers are similar to those obtained in grid generated-turbulence, (3) The response of cylinders is insensitive to exposure for small damping but increases with turbulence for larger damping.

Sviadosch et al (1990) investigated the vibrations of finned tubes in a cross flow of water for turbulence level of the incident flow from 1.0 to 12.0% and Reynolds number from 10^3 to 2.0×10^3 . The study was performed with flexibly-mounted tubes. The turbulence grids were two rows of stainless steel cylindrical rods. The main conclusions of their study can be summarized as below :

1. In the low turbulence flow ($TU = 1.0\%$) two maxima were obtained; one when the frequency of vortex shedding was coincident with the natural frequency of the

tubes, and the other in the case when the reduced velocity was 50.0%.

2. In the turbulized flow the vortex-induced vibrations of finned tubes do not vanish as in the case of the smooth tube.
3. As the reduced velocity reduced, the maximum amplitudes of vortex-induced vibration of smooth and finned tubes become greater in the streamwise direction. However, the amplitudes will be greater in the transverse direction as the reduced velocity is increased.

Jubran et al (1991) investigated the effects of the turbulence intensity oscillations of an elastically supported single cylinder in a cross flow. They found that increasing the turbulence intensity seems to suppress the lock-in region or as the turbulence intensity is increased the fluid elastic tends to dominate the oscillations even for the low reduced velocity range and tends to increase the vibration amplitude. For rough cylinder they found that increasing the turbulence intensity to 2.8% leads to a decrease in the vibration amplitude, while, a further increase in the turbulence intensity to 4.2% results in an increase in the vibration amplitude.

2.5 Effects of Surface Roughness

Güven et al (1980) presented the results of an experimental and analytical investigation undertaken to clarify the influence of surface roughness on the mean pressure distribution and boundary-layer development in uniform stream. The measurements are conducted on five sizes of distributed sand paper roughness over Reynolds-number range 7×10^4 to 5.5×10^5 . The cylinders were mounted vertically. They found that the drag coefficient, as well as the pressure-distribution parameters, become independent of Reynolds number as it is increased, but a definite dependence on the relative roughness is shown. This

is bounded by two end plates less than 20 to 30 diameters apart.

Farrell and Fedeniuk (1988) measured the mean and fluctuating pressures on a rough circular cylinder in a uniform flow with and without end plates. The experiments were carried out at critical and transcritical Reynolds number. The leading edge of the plates was given the form of horseshoe vortex that forms at the junction of the cylinder and the tunnel wall, approximated by a circular arc. They revealed that in or near the critical range, the end plates appear to produce a flow behavior corresponding to a higher Re . With the end plates, they found that the critical transition occurred approximately at Re between 5×10^4 and 5.5×10^4 for $k/D=0.0065$, and at lower Re , between 4×10^4 and 4.5×10^4 , for $k/D = 0.01$.

Chapter 3

INSTRUMENTS AND APPARATUS

3.1 Introduction

The experiments were conducted in an open type wind tunnel. Several instruments were used to measure the velocity, vibration, turbulence intensity, and frequencies. Others were used for calibration, recording and monitoring. A general view of the apparatus and instruments is shown in Fig (3.1) and (3-2).

In this chapter a full description of all apparatus, instruments and measuring techniques used in the present work will be presented.

3.2 Apparatus

The apparatus consists of a low speed suction type wind tunnel and the experimental set-up which consists of the test cylinder with its stand and support, as well as, the interfering bodies and turbulence grids.

3.2.1 Wind Tunnel

All the measurements were carried out with a low-speed suction wind tunnel in the Fluid Mechanics Laboratory of the University of Jordan.

The range of wind velocity in the test-section is from 5 *m/sec* to 36 *m/sec* . The

turbulence level of the free stream at the working section is 0.35%, but it can be raised with the turbulence grids fitted upstream of the working section.

A schematic diagram of the different parts of the wind tunnel is shown in Fig(3-3). The air enters the wind tunnel through a nozzle to the test section. The test section was a straight duct made of 1cm thickness perspex and has a cross section of 30cm × 30cm . The fan is driven by a 5.6 kw 3-phase motor which rotates at constant speed of 2900 rpm. The maximum flow rate capacity is 3.24 m³/s. The air velocity is controlled by mean of a double butter fly valve. The schematic diagram shows the dimension of all parts of the wind tunnel.

3.2.2 Clamping and Position of the Test Cylinder

The experiments were conducted on an aluminum tube with circular cross section of outer diameter $D=21.5$ mm, wall thickness $t=0.5$ mm and length $l= 440$ mm. The cylinder was positioned in the wind tunnel horizontally; one end is fixed, while the other is free. This combination yields a mass per unit length 0.1662 kg/m without the accelerometer which is fixed at the free end. The stand with which the cylinder was fixed is rigid enough to be motionless during the experiments. The clamping of the cylinder is shown in Fig(3-4).

3.2.3 Interfering Bodies

Different sizes of circular cylinder were used as interfering bodies. The bodies were made of wood and covered by a sheet of plastic as shown in Fig(3-5). The relative dimension of the interfering bodies (d/D), with respect to the oscillating cylinder, are 0.5, 1.0, 1.5 and 2.0 . They are positioned horizontally in three arrangements; (1) tandem arrangement with gap spacing (g/D) in the range (1-6), (2) side by side arrangement with (g/D) in the range (1-4), (3) and finally the staggered arrangement for different positions. For

these arrangements the interfering body was held fixed between the walls of the wind tunnel, so that it is parallel to the test cylinder.

3.2.4 Turbulence Generating Grids

In order to raise the turbulence level of the free stream, turbulence grids were fitted upstream of the working section. The grids were made of wood with different cross section. The produced turbulence levels were used to investigate the effect free turbulence intensity on the flow-induced vibration of the test cylinder in different conditions; smooth or rough cylinder, with and without interfering bodies. The grids are shown in Fig(3-5), and the shapes, sizes and produced turbulence levels are tabulated in Table(3-1).

Table(3.1): Turbulence grids characteristics

Grid No	Grid shape	Grid size	Mesh size	blockage ratio	Turbulence level
no	-	-	-	0.0 %	0.35 %
1	square	0.5 cm	2.7 cm	17.0 %	3.25 %
2	circular	1.0 cm	5.0 cm	17.0 %	3.76 %
3	square	0.5 cm	6.0 cm	6.7 %	4.00 %
4	circular	1.0 cm	6.0 cm	13.3 %	4.40 %
5	circular	1.0 cm	7.5 cm	10.0 %	4.68 %

3.2.5 Standard Sand Papers

The sand papers were used to change the surface roughness of the test cylinder. Different sand papers, with known roughness heights, were used to satisfy this purpose. The sand papers were wrapped carefully so that the result cross section is circular. The sand papers roughness heights and relative heights with respect to the test cylinder (k/D) are tabulated in table(3-2).

Table(3.2): Sand papers roughness and relative heights

Grid No	$k(mm)$	k/D
40	0.500	0.0230
60	0.297	0.0138
70	0.254	0.0118

3.2.6 End Plates

Two metal sheets were used as end plates. The outer diameter of each one was 10cm. In order to fix the end plates on the cylinder, they were drilled at their centers with a diameter equals the diameter of the test cylinder.

Experiments were conducted to measure the amplitude vibration, flow velocity flow turbulence intensity and the oscillating cylinder frequency. For measuring the amplitude vibration in the transverse direction an accelerometer was used, while in the stream-wise direction a magnetic transducer was used. Hot wire and pitot tube were used for measuring the turbulence intensity and flow velocity. The signal was monitored by an oscilloscope and a frequency analyzer. These instruments and the techniques employed are discussed in the following sections.

3.3 Velocity and Turbulence Measurements

As mentioned before a hot-wire anemometer and a pitot-tube are used for velocity and turbulence measurements.

(i) Pitot-Tube :

The pitot static tube is a simple instrument used for the measurement of both static and stagnation pressures. The opening in the front of the probe senses the stagnation pressure, while the small holes around the outer periphery of the tube sense the static pressure. When Bernoulli's equation is applied, the velocity of stream can be found by:

$$U = \sqrt{2g(h_1 - h_2)/\rho} \quad (3.1)$$

where $(h_1 - h_2)$ is the deflection of manometer (mmH_2O), ρ is the stream density (kg/m_3), U is the velocity of the stream (m/sec).

For the experiments a subsonic probe was connected with micromanometer which gives the deflection in mmH_2O . The probe was positioned upstream the test cylinder so that it will not affect the leading flow to the cylinder. The opening of the probe was at the mid section.

(ii) Hot-Wire Anemometer:

The hot-wire manometer is a device that is often used to study rapidly varying flow conditions. In turbulence fluid flow, the fluid-velocity components exhibit a random oscillatory character, which depends on the average fluid velocity, fluid density, viscosity, and other variables. The hot-wire is very useful for turbulence measurements because it can respond to very rapid change in flow velocity. Two or more wires at one point in the flow can make simultaneous measurements of the fluctuating components, Holman(1978).

The sensor is a fine wire heated electrically and placed in the flow stream, and the early work of King (1914) has shown that the heat-transfer rate from the wire can be expressed in the form :

$$Q = (A + BU)(T_w - T_o) \quad (3.2)$$

where:

T_w = wire temperature.

T_o = free-stream temperature of fluid.

U = fluid velocity.

A, B = constants obtained from a calibration of the device.

The heat-transfer rate must also be given by:

$$Q = I^2 \times R_w = I^2 \times R_o [1 + \alpha(T_w - T_o)] \quad (3.3)$$

where ;

I = electric current.

R_w = resistance of the wire at the temperature T_w .

R_o = resistance of the wire at the reference temperature T_o .

α = temperature coefficient of resistance.

The heat transfer coefficient is given by:-

$$Nu = C + DU^n \quad (3.4)$$

from equations (3-1) to (3-4) it is found that

$$V^2 = A + BU^n \quad (3.5)$$

where;

V = D.C output of anemometer.

A, B, C, D are the calibration constants.

$n = 0.4 - 0.5$ for $0.1 \leq Re \leq 10^5$.

Using equation (3-5), the turbulence intensity can be determined as:

$$\frac{dU}{U} = \frac{2V dV}{n(V^2 - A)} \quad (3.6)$$

where;

dV = the Root Mean Square (RMS) of the anemometer output.

For measurement purpose, the hot wire is connected to a bridge circuit. Two different circuits are available for the measurement of the thermal loss. Named from their modes of operation they are called respectively, the Constant-temperature Anemometer and the Constant-current Anemometer.

The experiments were carried out using a DISA constant-temperature hot wire anemometry shown in Fig(3-6). It consists of a Wheatstone bridge and servo amplifier. The hot wire was connected with a probe type 55PO5 moving by a transverse

mechanism. The D.C voltage and RMS voltage were measured by the 55D30 DC and the voltmeter, respectively. The calibration and operation of the hot wire are discussed in the appendix.

3.4 Vibration Measurements

The amplitude of vibrations are measured in the transverse and streamwise directions:

(i) Transverse direction :

The amplitude vibration in the transverse direction was measured by an accelerator type (B&K 4371) fixed on the free end of the test cylinder as shown in Fig(3-3). The output signal of the accelerator was simultaneously fed to a portable vibration meter type (B&K 2511) and some times to a frequency analyzer type (B&K 2131). The output of the vibration meter could be taken as acceleration, velocity or displacement. A storage oscilloscope type (OS 4100) was used to monitor the output of the vibration meter. The signal from storage oscilloscope was recorded using an X-Y recorder type (WX 4402) . On the other hand, the signal from the frequency analyzer was recorded by a level recorder type (B&K 2307). The calibration and operation of the vibration meter are discussed in the appendix.

(ii) Streamwise direction :

A noncontact dynamic pickup type (B&K MM0002) was used to measure the streamwise vibration amplitude. The output signal was supplied to the frequency analyzer and a measuring amplifier type (B&K 2616). The output of the measuring amplifier is supplied to the oscilloscope to monitor the signal waveform. The reading of the measuring amplifier is in voltage output. At certain conditions the dynamic pickup and the measuring amplifier are calibrated with the accelerator and the vibration meter, so that the output voltage could be obtained as displacement.

3.5 Experimental Conditions

As mentioned before, the velocity range of the wind tunnel is (5 *m/sec*-36 *m/sec*), this will result in Reynolds number range of ($6.8 \times 10^3 - 4.9 \times 10^4$). The cylinder condition (i.e. length, mass per length, damping and clamping) results in a constant natural frequency (F) of 56 *Hz*, logarithmic decrement (δ) of 0.083 and damping factor K_s of 4.93 . For these results the reduced velocity (U/FD) is in the range (4.15 - 30.0).

The chosen interfering bodies were fixed between the walls of the tunnel at different gap spacings to investigate the effect of interference for different arrangements. The free stream turbulence intensity was changed in the range (0.35% - 4.68%) by using different turbulence grids. Test cylinder surface roughness was changed from smooth to about (k/D) of 0.023 . The end plates position was changed from small distance between them and the walls of the wind tunnel to a distance of 5 diameters.

3.6 Preliminary Tests

Before starting the experiments, the position of the test cylinder was chosen to be about 1.3 *m* far from the inlet of the test section.

The cylinder was clamped horizontally as a cantilever. The cylinder was fixed by a stand which is positioned vertically and has a cross-section of 12*cm* × 12*cm*. This was chosen to insure the motionless of the stand throughout the experiments. The wire of the accelerometer, mounted at the free end, was taken out from the fixed end of the cylinder so that the motion of cylinder will not affects it, and as a result to reduce the noise of the wire.

The natural frequency of the cylinder was measured by the impulse test as follows:-

1. A tunable filter (B&K1621) was connected in parallel with the vibration meter.

The signal of the accelerometer was fed to the vibration meter and monitored on

the storage oscilloscope and the frequency analyzer.

2. The oscillating cylinder was disturbed and the response was monitored on the oscilloscope and the frequency analyzer.
3. Step 2 was repeated for another frequency adjusted by the filter tuning. The natural frequency was the frequency at which the larger amplitude is obtained as shown in Fig(3-7) and (3-8).

Following this procedure a natural frequency of 56 *Hz* was obtained. This value was verified after determining the lock-in region. The frequency of vibration at the lock-in was measured by the frequency analyzer and the same value of 56 *Hz* was obtained. The structural damping was determined by using the logarithmic decrement equation.

$$\delta = \frac{1}{n} \ln \frac{x_o}{x_n} \quad (3.7)$$

where:

x_o = the amplitude of the first signal cycle.

x_n = the amplitude after n cycles.

Using Fig(3-7) it is found that $\delta = 0.083$. The stability damping factor (K_s) was determined by the equation:

$$K_s = \frac{2m\delta}{\rho D^2} \quad (3.8)$$

where;

ρ = density of air.

Applying the required values it was found that $K_s = 4.93$.

3.7 Experimental Procedures

3.7.1 Single Cylinder Measuring Procedure

1. The hot wire was calibrated as described in the appendix, then it was positioned at the determined location. The pitot tube was placed at its position and the manometer was adjusted to zero.
2. After fixing the accelerometer and the dynamic pickup, they are connected to the vibration meter and measuring amplifier, respectively. The outputs of the vibration meter and the measuring amplifier were connected to the oscilloscope and the frequency analyzer.
3. The fan was switched on and the flow was varied in the rang $(5-36)m/s$. After the steady state of the flow was obtained, 1.5 minutes were given before taking the reading of the vibration meter and measuring amplifier. This was repeated and the average of the readings was adopted. At each reading the signal was fed to the frequency analyzer to measure the frequency at which the largest amplitude occurred. The vibration signal monitored by the oscilloscope was recorded for certain reduced velocities.
4. The turbulence grids was located at the inlet of the test section. For this part, the pitot tube could not be used and the velocity will be measured by the hot wire only. For each grid, steps (1) to (3) were repeated.
5. The standard sand paper was wrapped around the cylinder. For each sand paper, steps (1) to (3) were repeated.

From time to time, the hot wire was recalibrated, the micromanometer was readjusted to zero, the calibration of the vibration meter and the measuring amplifier was tested.

3.7.2 Interference Arrangements Measuring Procedure

1. The instruments were calibrated and located as mentioned before.
2. One of the interfering bodies was located at certain distance (g/D) from the test cylinder which was mounted as for single cylinder. The same procedure for measuring the velocity and RMS of the amplitude vibration in the streamwise and transverse directions were followed.
3. The gap spacing (g/D) was changed in the range (1-6) and the same procedure of measurements were repeated.
4. The location of the interfering body was changed to the transverse direction (i.e. side-by-side arrangement). For each interfering body (d/D) the gap spacing was changed in the range (1-4) and the steps (1) and (2) were repeated.
5. Step (4) was repeated for the staggered arrangement.
6. For certain interfering bodies and gap interfering bodies and gap spacing, the freestream turbulence intensity was changed and the procedure was repeated.
7. The roughness of the test cylinder was increased and step (6) was repeated.

3.7.3 End Plates Measuring Procedure

1. The measuring instruments were warmed up and calibrated as mentioned before.
2. An end plate was fixed at each end of the cylinder inside the walls of the tunnel. The same procedure described before was followed.
3. The position of the end plate was changed so that the distance from the walls of the tunnel varied from very close to 5 diameters. For each time steps (1) and (2) were repeated.

3.8 Repeatability of Measurements

As mentioned before, the RMS of the vibration amplitude were repeated and averaged for each test. The averaged discrepancy was found to be about $\pm 5\%$.

On the other hand, the mean stream velocity and turbulence intensity were repeated from time to time. It was found that the repeatability is about $\pm 4\%$.

Chapter 4

DISCUSSION OF RESULTS

4.1 Introduction

The experiments were carried out to investigate the influence of interference, turbulence intensity and surface roughness on flow-induced vibration of cylindrical cantilever tube.

The response of a single cylinder will be discussed first using the results of the vibration dimensionless amplitude against the reduced velocity. The second part will show the dynamic response of the test cylinder for different turbulence intensities with and without interfering cylinders. The effect of surface roughness on the dynamic response of the test cylinder will be shown. Finally, the effect of the combinations of the factors, as well as, the end plates effects on the flow induced vibration of the test cylinder will be discussed.

4.2 Single Cylinder Results

The dynamic response of the test cylinder can be described by the variation of the RMS of the dimensionless amplitude (A/D), in transverse and streamwise directions, versus the reduced velocity (U/FD). After mounting the cylinder under the conditions described in chapter 3, the flow velocity was increased gradually and the vibration amplitude was recorded for different reduced velocity. The response is shown in Fig(4-1) for both the transverse and streamwise directions. Fig(4-1) shows that the vibration

amplitude is more significant in the transverse direction (lift direction) than that in the streamwise direction (drag direction). It is also shown that the lock-in region (i.e. the range of reduced velocity over which the frequency of fluid approaches the frequency of the vibration cylinder) starts at reduced velocity of 13.0. Before this reduced velocity the cylinder is almost stationary due to the weak vortex shedding. There is only one distinct resonance hump on the dynamic response curve which agrees with that found for vertical cantilever by Blevens (1977), Howell et al (1988), Humphries (1988) and Suiadosch et al (1990).

The largest amplitude vibration, for both the transverse and streamwise direction, occurs at $U/VD = 15.5$ at which the frequency of vibrating cylinder approaches its natural frequency as can be seen from Fig(4-2) where the maximum amplitude occurs when the vibrating frequency equal to the natural frequency (i.e. $f/F=1.0$). The lock-in region ceases for reduced velocity around 21.0. After this reduced velocity the cylinder reaches a steady oscillatory response as shown in Fig(4-1).

4.3 Effects of Interference

Flow interference between two circular cylinders in various arrangements causes continuous and discontinuous changes in vortex shedding. The resulting oscillations induced by the vortex shedding are strongly dependant on the arrangement of the two cylinders, Lakshmana (1987).

In order to see the influence of interfering body on the dynamic response of a single cylinder, the chosen interfering bodies were placed in tandem, side-by-side, and staggered arrangements. The velocity of the flow was increased gradually and the resulting dynamic response was represented graphically. These graphs will be used here to clarify the phenomena for each arrangement.

4.3.1 Interference Effects for Tandem Arrangement

Relative dimension $d/D = 0.5$:

The response of the vibrating cylinder with the presence of interfering body with relative dimension $(d/D) = 0.5$ in tandem arrangement is shown in Fig(4-3). When the reduced velocity is to the left of the lock-in region (i.e. less than 13.0), the influence of interfering body is negligible because for this range, the vortex shedding frequency will be lower than the natural frequency. As the velocity increases the effect of interference become more significant. At the lock-in region the cylinder is vibrating due to vortex excitation. For this condition there is a feedback mechanism between the body and the wake. The presence of interfering body in the wake influence the vortex shedding and the feed back mechanism, which is responsible for the observed increased in the vibration amplitudes. The amplitude decreases as the gap spacing (g/D) increases. When (g/D) is increased from 1.0 to 2.0 and 3.0, a significant reduction in the vibration amplitude is observed because there is suppression in the vortex formation due to the front cylinder. The shear layers leaving the test cylinder is attached on to the downstream cylinder and a near stagnant pool is formed in the gap between them. Fig(4-3) indicate also as (g/D) increases further to $g/D = 6.0$ the effect of interference on the vibration amplitude is negligible and the system tend to behave like a single cylinder. Note that there is a shift in the lock-in region for gap spacing (g/D) equal to 1.0, 2.0 and 3.0. This fact indicates that the presence of interfering body in wake can affect the frequency of vortex sheddings and as a result the lock-in region. For high reduced velocities (i.e. $U/VD > 19$), the interfering cylinder is seen to has a negligible influence on the vibration amplitude of the test cylinder. The vibrations in this case are due to the jet switching phenomena, which occurs when the vibration is produced by coupling and uncoupling of fluid jets behind the cylinder.

The streamwise amplitude for the same gap spacings is shown in Fig(4-4). It is shown that the amplitude is much smaller than that in the transverse direction as mentioned earlier. It is interesting to note there is a continuous reduction in the streamwise vibration amplitude as the gap spacing is increased.

Relative dimension $d/D = 1.0$:

Fig(4-5) shows the response of the cylinder with an interfering body of a relative dimension $d/D = 1.0$ (i.e. the same diameter as the cylinder). The response is shown for different values of (g/D) . It can be seen from Fig(4-5) that the influence of interference is more evident than that of $d/D = 0.5$. Also it is interesting to observe that after $U/FD = 19.0$ the amplitude will not return to that of a single cylinder. The vortex shedding from the front (i.e. downstream) cylinder becomes more coherence when (g/D) decreases. This explain the rise in the vibration amplitude at $g/D = 1.0$. For $g/D > 1.0$ a decrease in vibration amplitude occurs until $g/D = 4.0$ at which the amplitude is increased again due to the change in the vortex formation and shedding (i.e. the periodic replacement of vortex at the top and bottom of the wake). It is interesting to note that for $d/D = 1.0$, the shift of the maximum peak is significant. This implies that the influence of interference on the vortex shedding frequency increases as the relative dimension (d/D) increases.

Fig(4-6) shows that the change in the streamwise vibration amplitude is larger than the change in the transverse vibration amplitude. Unlike the dynamic response when $d/D = 0.5$, the maximum amplitude occurs at $U/FD = 19.0$ for $g/D = 1.0$ and 1.5 and at $U/FD = 17.0$ for $g/D = 3.0$ to 6.0 . Also it can be seen that the vibration is maximum at $g/D = 1.0$ and it decreases as (g/D) increases up to 4.0 where the vibration return to increase like that of transverse vibration amplitude. After $g/D = 4.0$, the vibration decreases but it still less than that for single cylinder.

Relative dimension $d/D = 1.5$:

The relative dimension (d/D) is increased to 1.5 and the resulting response is shown in Fig(4-7). As shown, the amplitude increases significantly for $g/D = 1.0$. It is seen that the reduced velocity for which the maximum peak occurs is increased to 22.0. As the gap spacing increases, the vibration amplitude decreases from that of $g/D = 1.0$ until $g/D = 4.0$ at which the change in the vortex formation and shedding occurs resulting in a significant increase in the dimensionless vibration amplitude in the vortex shedding region. It is seen that for $g/D = 1.5$ the system failed to reach a steady oscillation. Beyond $g/D = 3.0$, the response is characterized by a narrow lock-in region and a reduction in amplitude when the body become far away from the cylinder.

The vibration amplitude variation in the streamwise direction for this (d/D) is shown in Fig(4-8). The figure shows that the amplitude is lower than that for single cylinder except for close position (i.e. $g/D = 1.0$). This implies that the existence of interfering body beyond the cylinder can reduce the vibration to a very low value. It can be seen also that the reduced velocity at which the maximum peak occurs is reduced as the gap spacing increased.

Relative dimension $d/D = 2.0$:

At $d/D = 2.0$ an interesting response shown is observed in Fig(4-9), especially for $g/D = 1.0$. For the case of $d/D = 2.0$ it is evident that the fluid elastic instability occurs at U/VD about 27.0. As (g/D) increases to 2.0, the instability starts at lower U/VD . Further increase in (g/D) decreases the amplitude to a lower value. This reduction will continue until $g/D = 4.0$ and then increases as described for the other (d/D).

Fig(4-10) shows the variation of the streamwise amplitude. The main interesting point in this figure is the trend for $g/D = 1.5$ which is characterized by a very low amplitude. This result was found earlier for $d/D = 0.5$. As (g/D) increases the amplitude

increases either, but the maximum peak still less than that for single cylinder.

From the discussion presented in this section it becomes clear that the maximum peak amplitudes occur at $g/D = 1.0$ for all (d/D) investigated. In order to clarify this result, the variation of RMS vibration amplitude versus reduced velocity was plotted for the transverse and streamwise directions for various values of relative dimension (d/D) as shown in Fig(4-11). The same trend can be observed for the various dimensions of (d/D) , but with different vibration amplitude. As the relative dimension (d/D) increases the peak increases with an increase in the reduced velocity at which the peak occurs.

The effects of interference on the dimensionless vibration amplitude for the tandem arrangement at certain reduced velocities, gap spacing, and relative dimensions are shown in Fig(4-12) and (4-13). Fig(4-12) shows that the maximum amplitude is attained when the frequency of the vibrating cylinder approaches its natural frequency. In Fig(4-13), it can be seen that for $U/FD = 15.5$ the maximum vibration amplitudes are attained at large gap spacing and relative dimensions. For $U/FD = 19.0$ and 22.0 , the maximum amplitude occurs at small gap spacing even when the relative dimensions are large.

4.3.2 Interference Effects for Side-By-Side Arrangement

This set of experiments was carried out for (d/D) ratios of 0.5, 1.0, 1.5 and 2.0. The gap spacings (T/D) were 1.0, 2.0, and 4.0. For the interference $d/D = 0.5$, Fig(4-14-a) shows the response of the cylinder. It is clear that at $T/D = 1.0$ and $T/D = 2.0$ the same response is obtained. The oscillation at these spacing is slightly larger than single cylinder. This is caused by the increase of fluid-elastic excitation, Lakshmana (1987). As the transverse spacing between the axes of the cylinders is increased, the fluid-elastic instability becomes less. This is shown in the same figure for $T/D = 4.0$. It is noted that the reduction of transverse spacing not only increases the amplitude of oscillation, but

also decreases the critical reduced velocity at which the maximum peak occurs. Similar response is obtained for the interference $d/D = 1.0$ as shown in Fig(4-14-b). The main difference between them is the transverse spacing at which the fluid-elastic excitation occurs becomes small.

For larger relative dimensions (i.e. $d/D = 1.5$ and $d/D = 2.0$), the response of the oscillating cylinder seems to be different. Fig(4-15-a) shows that the vibration amplitude of the cylinder is reduced for different transverse spacing and $d/D = 1.5$. The maximum amplitude occurs at different reduced velocities. On the other hand, Fig(4-15-b) shows that for $d/D = 2.0$ the maximum amplitudes occurs at certain reduced velocities (i.e. $U/VD = 14.0$). The gap between the cylinders cause the flow to form a jet biased towards the narrow wake. This phenomena causes a reduction in the vibration amplitude which increases as the gap increases.

One may explain the obtained results by the fact that for $d/D = 0.5$, when the interfering cylinders are close, there is a strong gap below which biased towards the smaller cylinder. The wake behind the larger cylinder is sufficiently large. This result can also be pronounced for $d/D = 1.0$. For $d/D = 1.5$ or 2.0 and small (T/D) , the gap flow is seen to affect the wake of the test cylinder in a different manner.

4.3.3 Interference Effects for Staggered Arrangement

The interference in the staggered arrangement was studied by positioning the interfering cylinder downstream the test cylinder at particular values of the ratios (g/D) and (T/D) . Three positions are presented; (1) $g/D = 1.5$, $T/D = 3.0$, (2) $g/D = 2.0$, $T/D = 0.5$, and (3) $g/D = 0.5$, $T/D = 1.0$.

The first set of experiments were carried out for an interfering cylinder with relative dimensions of $d/D = 0.5$. The variation of the dimensionless amplitude (A_v/D) for the three locations are shown in Fig(4-16-a). The most interesting observation for this set

is the widening of the lock-in region for the first two locations. For the third position (i.e. $g/D = 0.5$ and $T/D = 1.0$) the interfering body is close to the oscillating cylinder resulting in significant oscillations. The second set of experiment was conducted for $d/D = 1.0$ (Fig(4-16-b)). As shown, the response of vibrating cylinder for the first two positions is almost similar to that of $d/D = 0.5$. At the third position, the oscillations become larger because the cylinders are close to each other. It can be seen that for these two sets, the oscillations decreases as the relative dimension (d/D) increases.

Similar response was obtained for the first two positions of the third set of experiments which was done for $d/D = 1.5$ and shown in Fig(4-17-a). The response for the third position shows that the lock-in region starts at reduced velocity (U/FD) of 11.0 and ceases at $U/FD = 21.0$. It can be noted that the maximum amplitude is the same as single cylinder. The fourth set of experiments was carried out for $d/D = 2.0$. Fig(4-17-b) shows the response for the three positions. For the first position, the response is similar to that of the other values of (d/D). The behaviour of cylinder for the third position shows a reduction in vibration amplitude from that shows earlier.

The streamwise RMS variation for the staggered arrangement is shown in Fig(4-18). For $d/D = 0.5$, the same maximum amplitude is attained for the first two positions. When the third position is applied a reduction in vibration is observed. This variation is also shown in Fig(4-18-b) for $d/D = 1.0$. As shown, the changes in vibration amplitudes are lower than that for $d/D = 0.5$. However, the maximum amplitude is lower than that for single cylinder for both cases.

Fig(4-19) and (4-20) show the variation of RMS amplitude versus gap spacing for tandem and side-by-side arrangements. As can be noted, the system behaves as a single cylinder after $g/D = 4.0$ or $T/d = 4.0$. For tandem arrangement, Fig(4-19) show that the maximum amplitude is attained at $g/D = 1.0$ followed by a reduction until $g/D = 2.0$, then it starts to increase from $g/D = 3.0$ to $g/D = 4.0$. The RMS amplitude

and its variation is not significant for side-by-side arrangement as shown in Fig(4-20). It is interesting note that for tandem arrangement, the maximum values of (A_v/D) occurs at $d/D = 2.0$ especially for close spacings of (T/D) while for side-by-side arrangement the maximum values of (A_v/D) occurs at $d/D = 0.5$ for a wide range of spacing.

For $U/FD = 15.5$ (i.e. the reduced velocity at the center of the lock-in region for single cylinder) the maximum amplitudes occur at $d/D = 0.5$ regardless of the arrangement type (Fig(4-21) and (4-22)). It is observed that the cylinder went into steady vibrations with a dimensionless amplitude of 0.013 for tandem arrangement and 0.009 for side-by-side arrangement. In Fig(4-21) the trends of the (A_v/D) curves for all (d/D) are similar except that of $d/D = 0.5$ where the vibration amplitudes has different trend. The reason for this is the formation of a single trapped vortex between the two cylinders under these conditions (i.e. $U/FD = 15.5$ and $d/D = 0.5$).

For higher reduced velocities (i.e. $U/FD = 19.0$ and 22.0), the vibration amplitude for tandem arrangement is increased especially for small gap spacings as shown in Fig(4-23) and (4-25). Different result is obtained for side-by-side arrangement; Fig(4-24) and (4-26) show that the vibration amplitude is decreased as U/FD increased. It is also noted that the effect of the relative dimension (d/D) becomes negligible for $U/FD = 22.0$.

4.4 Effects of Turbulence Intensity

The effect of free stream turbulence intensity was investigated through the use of different turbulence generating grids located at the entrance of the test section.

4.4.1 Turbulence Intensity Effects for Single Cylinder

Fig(4-27-a) shows a plot for the dimensionless amplitude (A_v/D) versus reduced velocity. It can be seen from this figure that the turbulence intensity has three main effects on

the transverse amplitude of the cylinder:

1. For low turbulence intensity (i.e. $TU = 0.35\%$) the cylinder behaviour is described earlier for single cylinder response.
2. For turbulence intensity $TU = 3.25\%$ and 4.0% , the lock-in region starts at $U/FD = 15.5$ and after that the system failed to reach a steady oscillatory response. The figure shows that the vibration amplitude for $TU = 4.0\%$ is larger than that for 3.25% . It must be noted that these intensities were generated by square cross sectional grids.
3. Increasing the turbulence intensity above 4.0% tends to produce almost the same response as single cylinder with higher amplitudes at high U/FD . For $TU = 4.68\%$ the oscillations become larger but after $U/FD = 21.0$ the same amplitudes observed for $TU = 4.4\%$ and $TU = 4.68\%$.

From the above observations it appears that the responses in turbulent flow are different from those in smooth flow and the former clearly depends on the turbulence intensity and hence, the generating grids. The increase in the turbulence modifies the flow patterns around the cylinder and hence the flow induced forces on it. As a result, the vibration amplitude increases due to the increases in growth rate of the shear layers, Miyata and Miyazaki (1988) .

Fig(4-27-a) also indicates that for $TU = 4.4\%$ and 4.68% the amplitude peak occurs almost at the same U/FD as single cylinder. This implies that the frequency of vortex shedding from the cylinder remains unchanged, while the energy of pulsations induced by this shedding builds up. This result agrees with that found by Sviadosch (1990) This is confirmed by the results obtained in Fig(4-29) which shows that the maximum amplitude for $TU = 4.68\%$ is attained when the vibrating cylinder frequency approaches its natural frequency . This result is pronounced for each TU .

The variation of streamwise RMS amplitude versus reduced velocity for different TU is shown in Fig(4-27-b). The main interesting point is the sharp increase of amplitude for $TU = 3.25\%$. This implies that for this TU , the drag forces increases at larger rate than that for the lift forces. The grid that was used to generate this TU consists of 10 rods of square cross section. As TU increases a reduction in the amplitude is observed. Except for $TU = 3.25\%$, the amplitude is lower than that for single cylinder.

The effect of turbulence intensity on flow-induced vibration of the cylinder for certain reduced velocities is shown in Fig(4-28). For $U/FD = 15.5$, the increase of TU behind 3.25% increases the vibration, while for $U/FD = 19.0$ and 22.0 different trends are attained as shown in the figure. In general, for high TU (i.e. $TU > 4.4\%$) the effect decreases as U/FD increases.

4.4.2 Turbulence Intensity Effects for Tandem and Side-By-Side Arrangement

Three turbulence grids were used to investigate the influence of turbulence intensity on the response of tandem and side-by-side arrangements. The gap spacing between the test cylinder and the interfering body was varied in the streamwise direction in the range $g/D = 1.0$ to 3.0, while in the transverse direction in the range $T/D = 1.0$ to 2.0. The study was carried out for two interfering bodies; $d/D = 1.0$ and $d/D = 2.0$.

Relative dimension $d/D = 1.0$:

1. Tandem Arrangement:

Fig(4-30-a) shows the response of the cylinder for $TU = 3.76\%$ and $d/D = 1.0$. As shown, two results can be observed for $g/D = 1.0$; the first is the vibration amplitude starts increasing sharply at $U/FD = 19$ and the maximum amplitude occurs at $U/FD = 23.5$. The second observation is the dimensionless amplitude reaches a value of $A_v/D = 0.0275$. Comparing this result with that at $TU = 0.35\%$

(Fig(4-5)), it is seen that the maximum amplitude increases as TU increases and reaches a higher value. For $g/D = 2.0$ it is seen that the lock-in region becomes wider for this TU than that at $TU = 0.35\%$. On the other hand, as (g/D) increases to 3.0 the vibration amplitude, compared with that at $TU = 0.35\%$, is increased. Increasing the TU to 4.0 %, the response shows a reduction in vibration amplitude even at $g/D = 1.0$ as shows in Fig(4-30-b). It must be noted here that the turbulence was generated by the third grid (i.e. square cross section). Further increase in TU shows almost the same response as $TU = 3.76\%$, but the maximum amplitude for $g/D = 1.0$ occurs at higher reduced velocity as shown in Fig(4-31-a) for $TU = 4.68\%$.

2. Side-by-side Arrangement:

For this arrangement, the experiments were carried out for gap spacing of $T/D = 1.0$ and 2.0. Similar to tandem arrangement, the TU used were 3.76 %, 4.0 %, and 4.68 % in addition to $TU = 0.35\%$.

The response for $d/D = 1.0$ and $TU = 3.76\%$ is shown in Fig(4-31-b). Comparing the result with that at $TU = 0.35\%$ reveals that a reduction in the vibration amplitude occurred. Fig(4-32) shows that the increase in TU produces further reduction in amplitude and a stable oscillatory response beyond $U/FD = 19.0$. For $TU = 4.68\%$ the amplitude is smaller than that at $TU = 0.35\%$ for both $T/D = 1.0$ and $T/D = 2.0$, but it is higher than that at $TU = 4.0\%$ as shown in Fig(4-32-b). In general, for this condition (i.e. $d/D = 1.0$) the increase in turbulence intensity will reduce the vibration amplitude.

The streamwise vibration amplitude has the same trend as the transverse which can be observed in Fig(4-33), (4-34), and (4-35) for tandem and side-by-side arrangements. The peak amplitude is attained at the same U/FD , while their values for $g/D = 2.0$

and 3.0 are lower than that for single cylinder.

Relative dimension $d/D = 2.0$:

1. Tandem Arrangement:

The same experiments were carried out for $d/D = 2.0$. The response for $TU = 3.76\%$ is shown in Fig(4-36-a). As can be seen for $g/D = 1.0$, the amplitude starts to increase sharply at the same value of U/FD as that at $TU = 0.35\%$, but it doesn't reach a steady behaviour which reached at $TU = 0.35\%$. For the other gap spacings, the response is similar to that of single cylinder, but the reduced velocity at which the lock-in region starts increases as (g/D) increases. However, wider lock-in region and higher amplitude at high reduced velocities can be observed. The TU was increased to 4.0 % and the response is shown in Fig(4-36-b). As shown, the same results obtained for $d/D = 1.0$ can be observed here with larger amplitudes, especially for $g/D = 1.0$. Further increase in TU to 4.68 % shows the same result as $TU = 3.76\%$ as shown in Fig(4-37-a).

2. Side-by-side Arrangement:

The results for $d/D = 2.0$ are shown in Fig(4-37-b), and (4-38). Unlike the results of $TU = 0.35\%$ which are characterized by a reduction in the amplitude, the results of $TU = 3.76\%$, 4.0% and 4.68% show an increase in amplitude especially at high reduced velocity. An interesting result can be seen in Fig(4-38-a) where the lock-in region is undistinguished. For $T/D = 1.0$ the amplitudes starts to increase at low reduced velocity and reaches steady oscillations of $A_v/D = 0.006$ for the remain range. On the other hand, for $T/D = 2.0$ the system failed to reach a steady oscillations, but the amplitude is larger. However, the response for $TU = 3.76\%$ and 4.68% are similar as shown in Fig(4-37-b) and (4-38-b).

Fig(4-39) to (4-41) show that the streamwise amplitude variation has the same trend

as the transverse one. However, the amplitude is lower than that for single cylinder for $U/FD < 19.0$ regardless of the TU . Unlike $d/D = 1.0$, the trends of the streamwise and transverse vibrations are different for $d/D = 2.0$; for $TU = 3.76\%$ the streamwise amplitude increases even beyond $U/FD = 16.0$ as shown in Fig(4-40-b). On the other hand, at $TU = 4.0\%$ not only the amplitude increases as U/FD increases but also the same value is attained for $T/D = 1.0$ and 2.0 as shown in Fig(4-41-a). The same result found for $TU = 3.76\%$ can also be observed for $TU = 4.68\%$ (Fig(4-41-b)).

4.5 Effects of Surface Roughness

The influence of surface roughness on flow-induced vibration was investigated by using some standard sand papers with different heights of (k/D).

4.5.1 Surface Roughness Effects for Single Cylinder

The variation of the RMS transverse dimensionless amplitude with the reduced velocity (U/FD) for single rough cylinder is shown in Fig(4-42-a). As shown the dimensionless surface roughness $k/D = 0.0118$ and $k/D = 0.0138$ have reduced the vibration amplitude to a very low value due to the roughness and the damping which is caused by the sand papers. It is interesting to note that the lock-in region disappeared in this case. The vibration amplitude for the higher roughness (i.e. $k/D = 0.023$) is slightly larger than the other surface roughnesses. After $U/FD = 13.0$ the RMS value of vibration amplitude is approximately constant. This indicate that the originated shedding activity disappeared just above this value of reduced velocity. Increasing the roughness to $k/D = 0.023$ tends to increase the vibration amplitude, but the lock-in region is still disappeared as show in Fig(4-42-a). The experiment was repeated several times to see if it was due to any experimental error or if it was occurred due to this particular roughness. The same behaviour was repeatedly observed. For this particular roughness, this may

be explained by the nonlinear induced negative aerodynamic damping which depends on the cylinder motion. This complex interaction with the nonlinear behaviour is not yet understood. The reduction of amplitude may be due to the retarded separation and narrowed wake which results in suppressing the vortices and hence reducing the fluctuating components of the aerodynamic forces resonable for the cylinder excitation as found by Zdravkovich (1977).

Not only the surface roughness reduces the transverse vibrations, but also the stream-wise one. This result can be seen in Fig(4-42-b) for different roughness height (i.e. roughness reduces the drag forces).

In order to summarize the effect of surface roughness on flow-induced vibration, Fig(4-43) was drawn to show the variation of RMS amplitude versus (k/D) for different values of U/FD (i.e. $U/FD = 15.5, 19.0$ and 22.0). As shown, the roughness of the surface reduces the vibration amplitude especially for $k/D = .0118$ and $.0138$.

4.5.2 Surface Roughness Effects for Tandem and Side-By-Side Arrangements

A standard sand paper with $k/D = 0.0118$ was chosen to investigate the effect of surface roughness on the tandem and side-by-side arrangement. The gap spacing for tandem arrangement was changed in steps $g/D = 1.0, 2.0$, and 3.0 , while for side-by-side arrangement $T/D = 1.0$, and 2.0 . The relative dimension of the interfering bodies were $d/D = 1.0$ and $d/D = 2.0$.

As shown in Fig(4-44) to (4-47) the existence of interfering body has negligible effect on the response of rough cylinder. The same behaviour for the effect of interference is observed for both single cylinder and rough cylinder, regardless of the gap spacing (g/D) or (T/D). Unlike $d/D = 1.0$, the vibration amplitude starts to rise at high reduced velocity when the gap spacing is small for $d/D = 2.0$ as shown in Fig(4-44-b).

These results can be pronounced for the streamwise direction as shown in Fig(4-46) and(4-47).

4.6 Effects of Turbulence Intensity, Surface Roughness on Tandem and Side-By-Side Arrangements

In order to investigate the effect of the three factors together on the flow induced vibration of the cylinder, a sand paper of relative height $k/D = 0.0118$ was used and the TU was changed for 0.35 % and 4.68 %. The experiments were conducted for $d/D = 1.0$ and $d/D = 2.0$.

For tandem arrangement, the response of the cylinder in the transverse direction can be seen in Fig(4-48). As shown, the trend is similar to that for single rough cylinder. This may indicates that the surface roughness is the main effect. In other word, the presence of interfering body and different TU will not affect the response of the rough cylinder even for small (g/D) and high TU .

Increasing the relative dimension of the interfering body to $d/D = 2.0$ shows different response at high reduced velocities and small (g/D) as can be seen in Fig(4-48-b). The same results can be observed for the side-by- side arrangement (Fig(4-49)), but there isn't significant difference between $d/D = 1.0$ and 2.0. Comparing the results obtained at $TU = 0.35\%$ with that at $TU = 4.68\%$ show that increasing the TU will reduce the vibration amplitude for $g/D = 1.0$ and $T/D = 1.0$.

The variation of RMS dimensionless amplitude in the streamwise direction is shown in Fig(4-50) and (4-51). For tandem arrangement, the effect is more clear for $d/D = 2.0$ than $d/D = 1.0$. Unlike the results obtained for tandem arrangement, the streamwise increases significantly at $T/D = 2.0$ for side-by-side arrangement as shown in Fig(4-51-b).

4.7 Effects of End Plates

Two circular end plates were investigated to eliminate the so-called end effects in an attempt to simulate a cantilever cylinder. The response of cylinder with and without end plates is shown in Fig(4-52).

It is shown that the damping of the system is increased due to the friction of the plates and the breathing flow from outside the tunnel. This damping, however, results in a decrease of amplitude vibration. As the plates slide far from the walls of tunnel, the amplitude increase because the effect of breathing flow is reduced. The response of cylinder will not be as that without end plate because the the effect of friction and damping will exist. However as the distance from the end plates is increased away from the wall, the dynamic response curve approaches that without end plates.

4.8 Effects of Experimental Conditions on the Response Signal Wave

Different wave forms are shown in Fig(4-53) to (4-56) for certain conditions and reduced velocities. As shown, the peak response of the lock-in region is characterized by a sinusoidal wave form, while around of this peak the beat phenomena is attained. The sinusoidal waveform occurs when the frequency of the vibrating cylinder coincides the natural frequency of the cylinder and the vortex shedding frequency. This result can also be found from Fig(4-53) and Fig(4-57-a) which show that the maximum amplitudes occur when the frequency of the vibrating cylinder approaches the natural frequency (i.e. $F = 56Hz$). Outside the lock-in region the occurrence of difference frequency accounts for the beat phenomena as shown in Fig(4-54) and (4-56). The frequency spectrum outside and around the lock-in region is shown in Fig(4-58).

Chapter 5

CONCLUSIONS AND RECOMMENDATIONS

5.1 Conclusions

This section is devoted to assess the important points which have emerged from the present investigation. These can be summarized as follows:

5.1.1 Single Cylinder

1. Flow-induced vibration is more significant in the transverse direction than that in the streamwise direction.
2. The cylinder displacement in the lift (transverse) direction becomes important for $13.0 < U/FD < 21.0$.
3. Three parts characterized the dynamic response of the cylinder; (i) low vibration amplitude, $U/FD < 13.0$, (ii) large amplitude in the lock-in region, $13.0 < U/FD < 21.0$ and (iii) steady oscillatory response, $U/FD > 21.0$.
4. There is only one lock-in region for the dynamic response in both the lift and the drag directions.

5.1.2 Effects of Interference

- Tandem arrangement

1. The oscillatory amplitude depends on both the relative dimension (d/D) and gap spacing (g/D). As (d/D) increases, the peak amplitude increases and its dynamic response curve is shifted away from the vibrating cylinder.
2. The interference effects are very much influenced by the reduced velocity.
3. The interference effect ceases at gap spacing (g/D) around 6.0 for which the system dynamic response is similar to that of a single cylinder.
4. The streamwise vibration amplitude is much lower than the transverse amplitude.
5. The trend of variation for both the streamwise and the transverse amplitude is similar, but the streamwise amplitude is smaller than that for single cylinder except for close position.

- Side-by-side and staggered arrangements

1. The peak vibration amplitude is lower than that for tandem arrangement even for small gap spacing.
2. For side-by-side arrangement, the effect of interference is significant only when $d/D > 1.0$ and for staggered arrangement when $d/D = 0.5$.
3. The magnitude and position of the peak amplitude and the minimum amplitude are found to depend on both the gap spacing and the relative dimension.

5.1.3 Effects of Turbulence Intensity

1. The effect of turbulence on the flow induced vibration depend on its intensity and hence the type of generating grids.

2. For single cylinder, the increase of turbulence intensity increases the vibration amplitude in the transverse direction and decreases it in the streamwise direction except for $TU = 3.25\%$.
3. For two cylinders in tandem, the increase of TU to 3.76% and 4.68% increases the vibration amplitude in the transverse direction slightly, but for TU of 4.0% a reduction in the amplitude is attained. In the streamwise direction, the vibration amplitude is reduced for close positions and increases for larger gap spacings.
4. Increasing the free stream turbulence intensity for two cylinders in side-by-side arrangement decreases the vibration amplitude in the transverse direction for small relative dimension (i.e. $d/D = 1.0$) and increases it for larger (d/D) (i.e. $d/D = 2.0$).

5.1.4 Effects of Surface Roughness

1. When the cylinder is rough, the vibrating amplitude becomes small in the vortex shedding region, and the lock-in region disappeared. The vibration amplitude in the transverse direction is larger than that for smooth cylinder for high (k/D) only (i.e. $k/D = 0.023$). In the streamwise direction, the roughness decreases the drag forces and hence the vibrating amplitude.
2. The presence of an interfering body in tandem downstream the rough cylinder results in an increase in the vibration amplitude in the transverse direction for close locations downstream the test cylinder and large relative dimension (i.e. $d/D = 2.0$). The same result is pronounced for side-by-side arrangement, but the increase in (A/D) is smaller than that for tandem arrangement trend attained with exception of the conditions ($d/D = 2.0$, $T/D = 2.0$) where there is an increase in the drag forces and hence an increase in the vibration amplitude.

3. The streamwise vibration amplitude increases for the conditions ($d/D = 2.0$, $T/D = 2.0$) when the free stream turbulence intensity is increased. For the other conditions (i.e. for the other combinations of (d/D) and (T/D)) insignificant effect is found when the TU is increased.

5.2 Recommendations

The literature survey in chapter 2 together with the present experimental investigation suggest that there are areas which need further experimental and theoretical investigations to understand the phenomena of flow-induced vibration. Some of these areas are mentioned in this section as follows:-

1. Flow visualization studies are needed to help explaining the nature of the phenomena under various experimental conditions. In addition, further measurements, especially in the wake region, are required for a better understanding of the observed response of the test cylinder.
2. Circular interfering bodies were used in the present work, so different geometries may be investigated, such as rectangular cylinders.
3. Experiments on the effect of flexible interfering bodies may help in the understanding of the effect of galloping.
4. Since limited ranges of free stream turbulence intensity and Reynolds number were investigated, higher levels of TU with a wider range of Re need to be explored.
5. Measurements of the response amplitude using strain gages (Piezo-electric crystal) at the clamping end, may be investigated to compare with that of measuring a single point at the free end.

6. Different properties of the cylinder are required to be investigated such as clamping (i.e. different natural frequencies), geometry, dimension and arrangement.
7. Studing the effect of injection on the dynamic response of the test cylinder clamped as a cantilever.
8. Investigating the effect of end plates geometry for different flow conditions on the dynamic response of a cantilever test cylinder.

REFERENCES

1. ALBRECHT T, BARNES F. H., BAXENDALE A. J. and GRANT I" Vortex Shedding for Two Cylinders in Tandem" J. of Wind Eng. and Ind. Aerodynamics, vol. 28, pp. 201-208, 1988.
2. ARNOLD E. "Aircraft structure for engineering students" T.H.G McGson, 1972.
3. BEDOOR B. O. Effect of flow history on the flow induced vibrations of rough interfering bodies" M.sc Thesis, University of Jordan, 1989.
4. BERGER E. "On a mechanism of vortex excited oscillations of a cylinder" J. of Wind Eng. and Ind. Aerodynamics, vol. 28, pp. 301-310, 1988.
5. BLEVINS R. D. "Flow-induced vibration", Van Nostrand Reynolds, New York, 1977.
6. BOKAIAN A " Interference galloping of upstream member of a pair of circular cylinders " J. of Sound and Vibration, 117(3), pp. 433-446, 1987.
7. BOKAIAN A " Galloping of a circular cylinder in the wake of another " J. of Sound and Vibration, 128(1), pp. 71-85, 1989.
8. FARELL C. and BLESSMANN J. "On critical flow around smooth circular cylinders" J. of Fluid Mech., vol. 136, pp. 375-391, 1983.

9. FARELL C. and FEDENICK S. K. "Effect of end plates on the flow around rough cylinders" *J. of Wing Eng. and Ind. Aerodynamics*, vol. 28, pp. 219-230, 1988.
10. GERICH D. and ECKELMANN "Influence of end plates and free ends on the shedding frequency of circular cylinders" *J. of Fluid Mech.* vol. 122 , pp. 109-121, 1982.
11. CHEN S. S. and JENDRZEJCZYK J. A. "Dynamic response of a circular cylinder subjected to liquid cross flow" *Trans. of the ASME, J. of Pressure Vessel Technology*, vol. 101, pp. 106-112, 1979.
12. GOWDA B.H.L. and PRABHU D.R." Interference effects on the flow- induced vibrations of a circular cylinder." *J Sound and Vibration*, Vol.122, part 3, pp. 487-502, 1987.
13. GOWDA B.H.L. and DESHKVLKARNI K.P." Interference effects on the flow- induced vibrations of a circular cylinders in side-by-side and staggered arrangement " *J. of Sound and Vibration*, Vol.122, part 3, pp. 465-478, 1988.
14. GRAHAM J. M. R. "The effect of end-plates on the two- dimensionality of a vortex wake" *The Aeronautical Quarterly*, pp. 237-247, August 1969.
15. GRIFFIN et al " The vortex-excited resonant vibrations of circular cylinder" *J. of Sound and Vibration* 39(2), pp. 235-249, 1973.
16. GRIFFIN O.M. and RAMBERG S.E. "The vortex-stress wakes of vibration cylinders" *J. of Fluid Mechanics*, part 3, vol. 66, pp. 553-576, 1974.
17. GRIFFIN O. M. , SKOP R.A. and KOOPMANN G. H. "The vortex- excited resonant vibrations of circular cylinder" *J. of Sound and Vibration*, vol. 31, pp. 235-249, 1973.

18. GUVEN O. , FARELL C. and PATEL V.C. " Surface-roughness effects on the mean flow past circular cylinders" J. of Fluid mech, Vol. 125, part 4 pp. 673-701.
19. HOWELL J. F. and Novak M. " Vortex shedding from circular cylinders in turbulent flow" Wind Eng. , Proceedings of the fifth interational conference, Fort Collins, Colorado, USA ,Vol.2, pp. 619-631 July 1979.
20. HUMPHRIES J. A., AINSWORTH D. P. and WALKER D. H. "Vortex shedding measurements from a cylinder in uniform and shear flow" International Symposium on Flow-Induced Vibration and Noise, vol.1, pp. 39- 50, 1988.
21. JUBRAN B. HAMDAN M. N. and BEDOOR B. O. "Roughness and turbulence intensity effects on the induced flow oscillation of a single cylinder" Accepted J. Applied Scientific Research, 1991.
22. LAKSHIMANA B. H. and DESHKULKARNI K. P. "Interference effects on the flow-induced vibrations of a circular cylinder in side-by-side and staggered arrangement J. of Sound and Vibration, vol. 122, part 3, pp. 465- 478, 1988.
23. LAKSHIMANA B. H. and PRABHU D. R. "Interference effects on the flow-induced vibration of a circular cylinder" J. of Sound and Vibration, vol. 112, part 3, pp. 478-503, 1987.
24. MIYATA T. and MIYAZAKI M. " Turbulence effects on aerodynamic response of rectangular bluff cylinders " Wind Eng. Proceeding of fifth international conference, Fort Collins, Colorado, USA, Vol.2, pp. 939-949, July 1979.
25. PERRY A. E., CHONG M. S. and LIM T. T. "The vortex-shedding process behind two-dimensional bluff bodied" J. Fluid Med., vol. 116, pp. 77-90, 1982.

26. ROGER KING" A review of vortex shedding research and its application, " Ocean Eng. Vol. 4, pp. 141-171. Pergamon Press 1977.
27. SAKAMOTO H and HANU H " Effect of free-stream turbulence on characteristics of Fluctuating forces acting on two square prisms in tandem arrangement" Trans of the ASME, J. of Fluids Eng. Vol. 110, pp.140-146, June 1988.
28. SHIRAKASHI M, ISHIDA Y and WAKIYA S "Higher velocity resonance of circular cylinders in cross-flow" Trans. of the ASME, J. of Fluid Eng. , vol. 107, pp 392-396, September 1985.
29. SHIRAKASHI M, MIZUGUCHI K. and BAE H. M. "Flow-induced excitation of an elastically-supported cylinder caused by another located downstream in cruciform arrangement" J. of Fluid and Structures, vol.3, pp 595-607, 1989.
30. SKOP R. A. and GRIFFIN O.M. "On a theory for the vortex-excited oscillations of flexible cylindrical structures" J. of Sound and Vibrations, vol. 41, part 3, pp. 263-274, 1975.
31. SVIADOSCH V. " Vibrations of smooth and finned tubes in a cross flow of viscous fluid at different turbulence levels" Vibration control of Mechanical, structural, and Fluid-Structural Systems, Vol.202, pp. 69-74, 1990.
32. YENG H. C. and WEAVER D. C. "The effect of approach flow direction on the flow induced vibration of a triangular tube arrays" Trans. of the ASME, J. of Vibration, Acoustics, Stress and Reliability in Design, vol. 105, pp. 76-82, 1983.
33. ZDRAVKOVICH M. M. "Review of flow interference between two circular cylinders in various arrangements" Tran. of the ASME, J. of Fluids Eng. , pp. 619-633, December 1977.

34. ZDRITAVKOVICH M.M. "Aerodynamics of two parallel circular cylinders of finite height at simulated high reynolds numbers " J. of Wind Eng. and Industrial Aerodynamics, Vol.6, pp. 59-71, 1980.
35. ZDRAVKOVICH M. M. "Classification of flow-induced oscillations of two parallel circular cylinders in various arrangements" ASME flow induced vibrations Symposium ed. M. P. paidonsis et al, vol. 2, pp. 1-18, 1984.
36. ZDRAVKOVICH M. M. " Flow induced oscillations of two interfering circular cylinders " J. of Sound and Vibration, Vol.101, part 4, pp. 511- 521, 1985.
37. ZDRAVKOVICH M. M. "The effects of interference between circular cylinders in cross flow " J. of Fluid and Structures, Vol.1, pp. 239-261, 1987.
38. ZDRAVKOVICH M. M. "Review of interference induced oscillations in flow past two parallel circular cylinders in various arrangements" J. of Wind Eng. and Ind. Aerodynamics, vol. 28, pp. 183-200, 1988.

Appendix A

Operation and Calibration of The Measuring Instruments

A.1 Introduction

The general operation instruction for the measuring instruments can be found in the instruction manual. In this chapter, the calibration and operation procedure will be summarized with some explanations for the instructions which are not clear in the manual.

A.2 Calibration of the "VIBRATION METER" (B&K 2511)

The vibration meter was used with the accelerometer Type 4371 which has a unified charge sensitivity of $1\mu\text{c}/\text{ms}^{-2}$.

On the rear and front panel set:

EXT. FILTER: "Out"

HIGH FREQ. CUT OFF: "15 kHz"

INT-EXT POWER: "internal Battery"

METER FUNCTION: "RMS"- "1s"

ACC.-VEL.-DISP.: "Acc." "3Hz"

RANGE I-II: Extreme clockwise setting

BATTERY: "On"

- Check the "Battery" by pressing the CHECK push-button
- Set the RANGE to "Ref" and using the small screwdriver, adjust the CAL potentiometer to procedure a pointer deflection of 10 after fitting the instrument with vibration scale (SA 0183).
- Using the ACC.-VEL.-DISP. knob, select the "ACC.-3kHz", "Vel.-10Hz" and "Disp.-10Hz" settings in turn and wait to obtain a stable meter indication with each setting.

A.3 Calibration of the "MEASURING AMPLIFIER" (B&K 2610)

- Set control switches and Knobs on the 2610 as follows:

REF: "50 mv RMS"

INPUT GAIN: click-stop "Cal" position

INPUT SECTION GAIN: extreme clockwise position

OUTPUT SECTION GAIN: extreme clockwise position

AVERAGING TIME: "Fast"

POWER: "On"

DETECTOR: "RMS"-"NORMAL"

FILTER: All three FILTER switches set to "OFF"

- Set the INPUT SELECTOR GAIN knob anticlockwise until the INPUT SELECTOR GAIN LED lights and using a small screwdriver provided, turn the SENS.

ADJ potentiometer of the appropriate INPUT on the 2610 to obtain a reference indication of 50mv on the meter scale, after fitting the 2610 with vibration scale (SA 0250).

- Once correctly, set the REF. switch to "OFF" and step the INPUT SECTION GAIN knob to its extreme clockwise position, ready for measurements.

A.4 Calibration and operation of the "HOT-WIRE" (DISA) anemometry

A.4.1 Operation procedure

1. Initial Setting of Controls

SQUARE WAVE: "OFF"

HF FILTER: "1"

VOLTS: "1"

FUNCTION: "STD. BY"

PROBE TYPE: depending on probe type"

GAIN: "1"

Decade resistance: "00.000"

2. Terminate the probe cable, which has been plugged into the PROBE, in a reliable short-circuit.
3. Turn the FUNCTION switch to RES. MEAS position and set the ZERO OHMS potentiometer so that the meter needle covers the red mid-scale mark.
4. Replace the short-circuit with the probe to be used.
5. Alter the decade resistance setting so that the meter needle again covers the red scale mark.

6. Reduce the decade resistance setting by the probe-lead resistance. This resistance can be found by measuring it if it was broken before or 0.6 ohms if it is used for the first time. The indicated value is the sensor resistance.
7. Adjust the ZERO OHMS potentiometer so that the meter needle return to the red mark.
8. Find the sensor hot resistance using the equation:

$$R = R_o(1 + a)$$

where;

a is the overheating ratio = $\frac{R-R_o}{R_o}$ and usually taken 0.8,

R_o is the sensor cold resistance at ambient temperature.

The decade resistance should be set at the calculated R .

9. Turn the FUNCTION switch to OPERATE, the probe will be heated, and the anemometer is in operation. Adjust the meter range switch to the suitable range. The resulting reading of the voltmeter will be around 2.9V.

This procedure must be repeated for any damage of the probe.

A.4.2 Calibration procedure

The calibration is carried out by using the calibration equipment type 55D90 shown in Fig(A-1).

1. Using the disk calculator shown in the figure determine the reference nozzle pressure as described on the calculator noting that the barometric pressure in mbar.
2. Choose the suitable nozzle as follows:

- (a) Set the pointer corresponding to a velocity of 40 m/s to one of the nozzle areas. This is the reference nozzle.
 - (b) Note the closest nozzle to the maximum calibration velocity required. The chosen nozzle is the calibration nozzle.
 - (c) Check that the maximum flow rate of 300 l/min. is not exceeded.
 - (d) Repeat the previous three steps until the largest calibration nozzle that can be used, for the required velocity range, has been found.
3. Adjust the primary pressure scale by aligning the pointer corresponding to 40 m/s with the reference nozzle area. The scale will be in the range 6-10 bar.¹
 4. Read the primary pressure corresponding to the maximum calibration velocity.

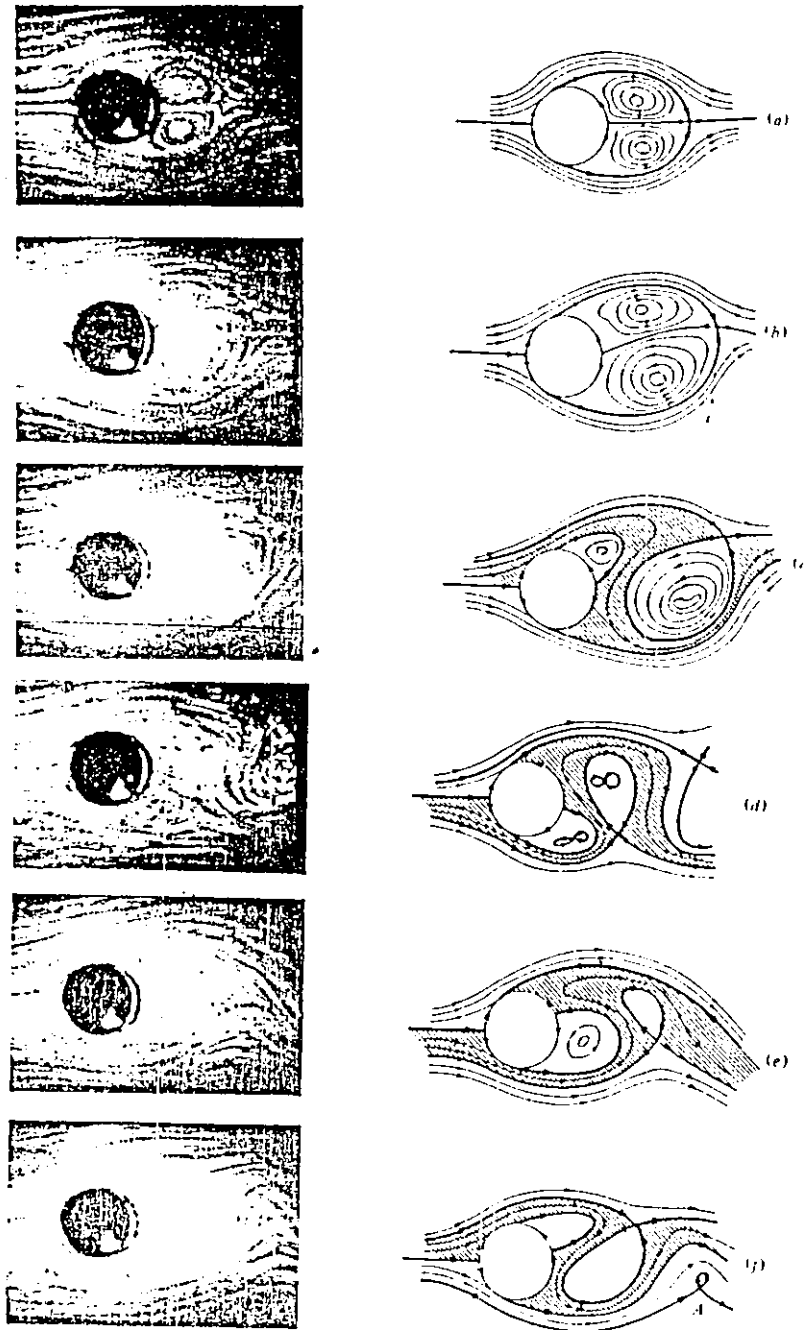
The calibration equipments are now ready for plotting the calibration curve. For this purpose the practical procedure is summarized as follows:

1. Insert the chosen nozzle and the probe in their position on the nozzle unit.
2. Connect the pressure control unit with the compressor and follow the instruction on the unit.
3. Record the readings of pressure from the pressure converter and the voltages V from the digital voltmeter.
4. Use the disk calculator to convert the values of pressure in the previous step into velocity values U . Check that the largest voltage gives the maximum velocity. If not, some thing wrong was done , and repeat the calibration.

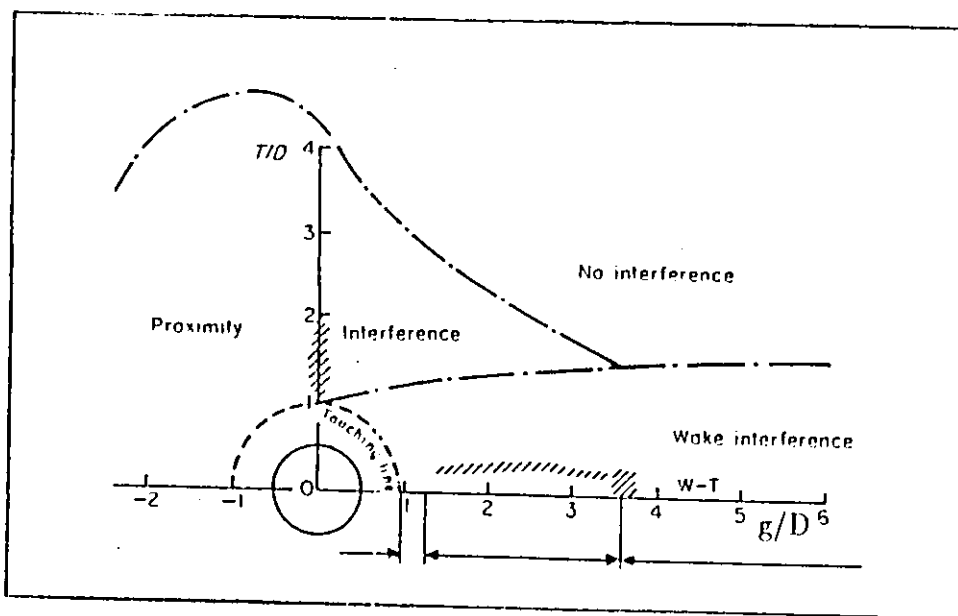
¹See the manual for more details

5. Plot the relation between V^2 and $U^{1/2}$ and find the resulting values of the intercept A and the slope B as shown in Fig(A-2).
6. Apply the values of A and B in the equation $V^2 = A + BU^{1/2}$

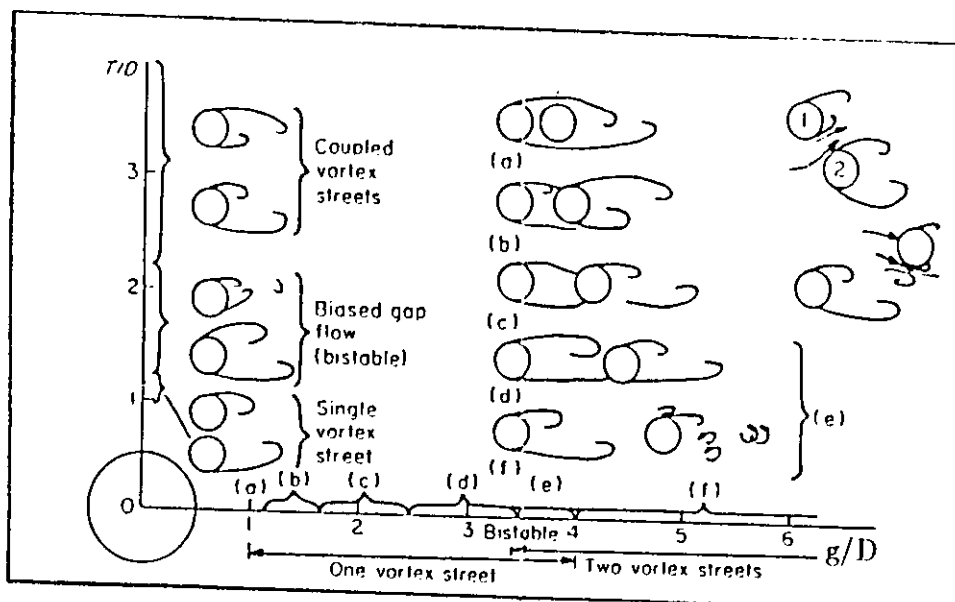
The hot-wire is calibrated now and the previous equation can be used to convert the resulting voltages V through the experiments into free stream velocities U . Note that the procedure of calibration must be repeated from time to time depending on the changes of the atmospheric pressure and the ambient temperature.



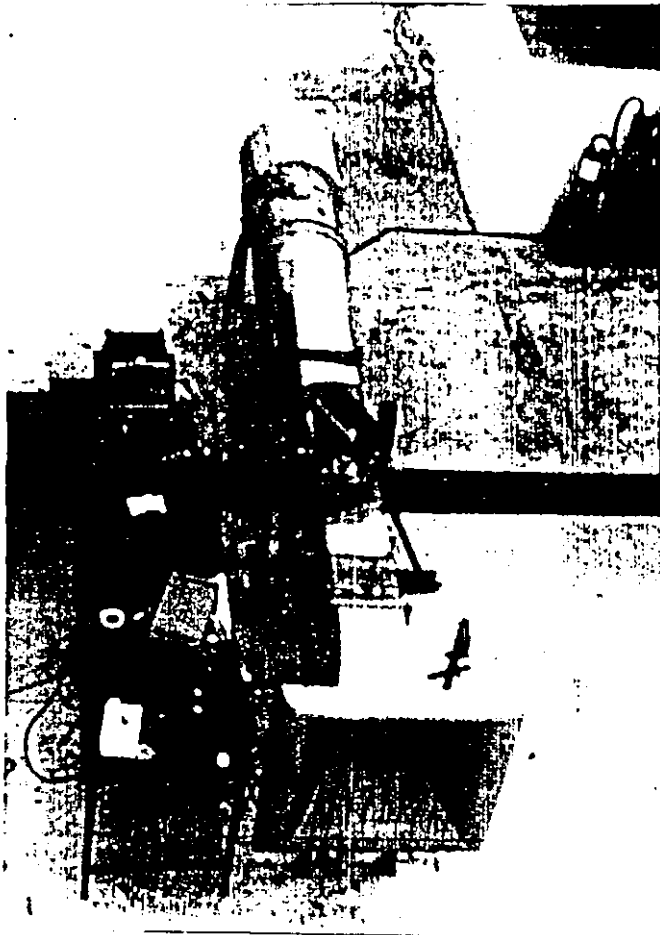
Fig(1-1). Flow in the near wake of a cylinder starting from rest sequence of events begins at (a) and continue to (f), Perry et al (1982).



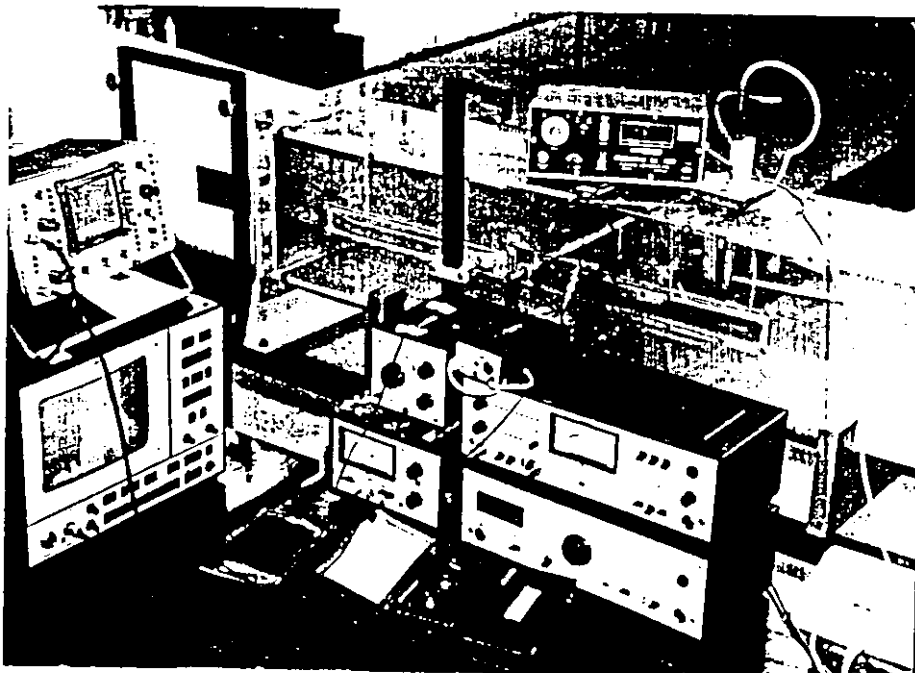
Fig(1-2). Definition of regions of flow interference for two-pipe arrangement, Zdravkovich (1987).



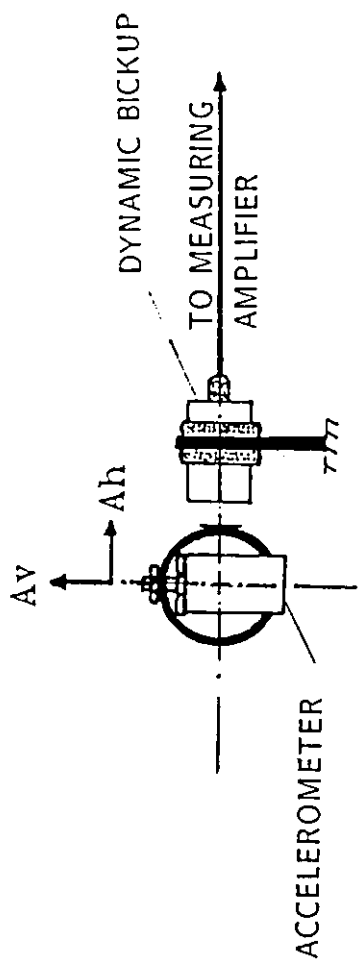
Fig(1-3). Interference flow regimes for side-by-side, tandem and staggered arrangements of two pipes. For tandem regims: (a) single slender body; (b) alternate reattachment; (c) quasi-steady reattachment; (d) intermittent shedding; (e) discontinuous jump; (f) binary vortex street, Zdravkovich (1987).



Fig(3-1). General view of
the wind tunnel.

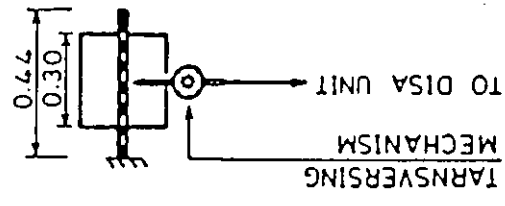
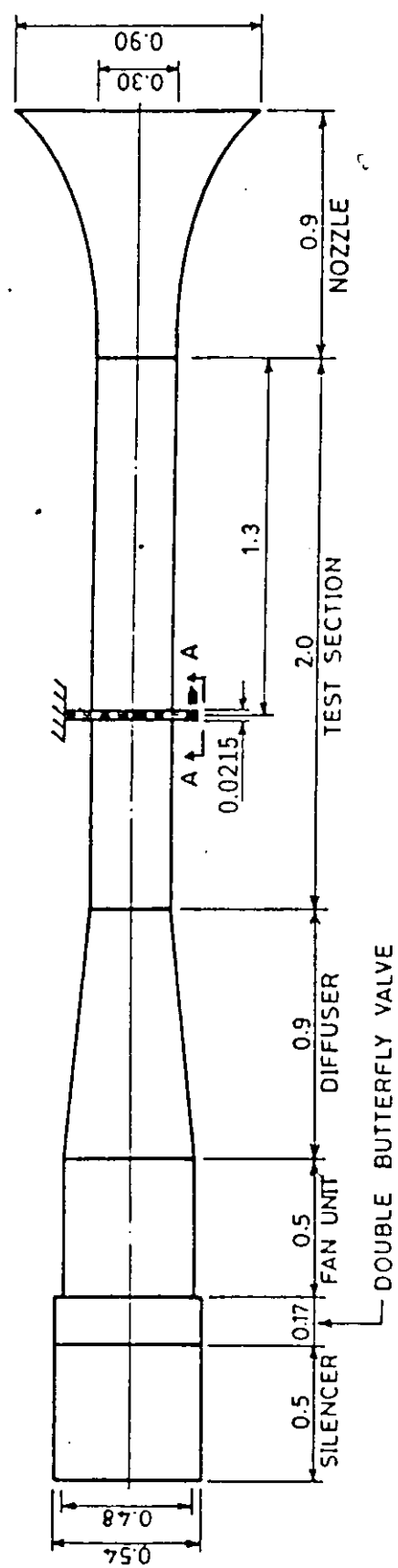


Fig(3-2). General view of the instruments and test section.

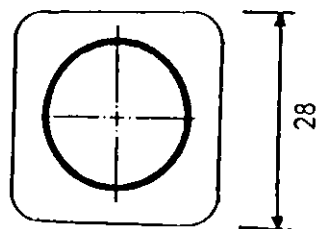
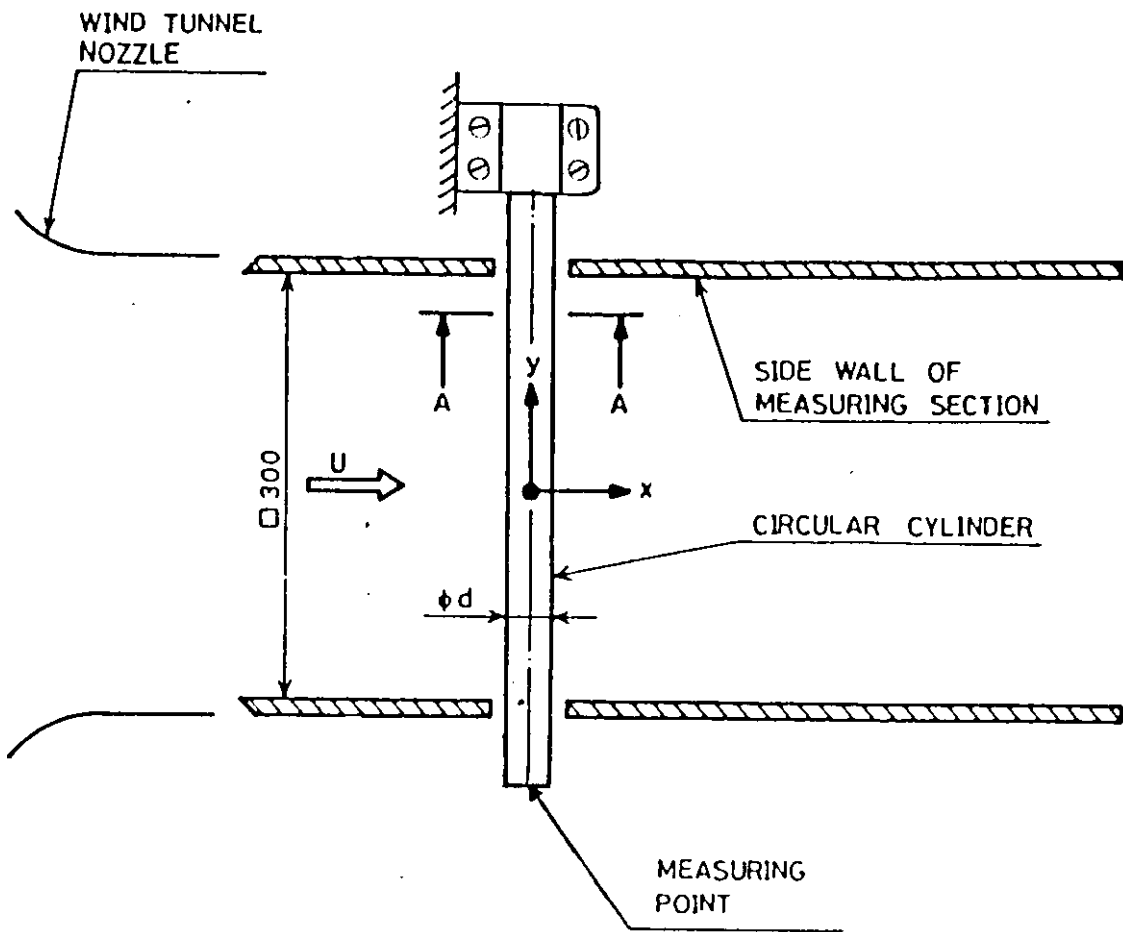


NOTE :-
 * ALL DIMENSIONS ARE IN METER.
 * DRAWING NOT TO SCALE

SECTION A-A



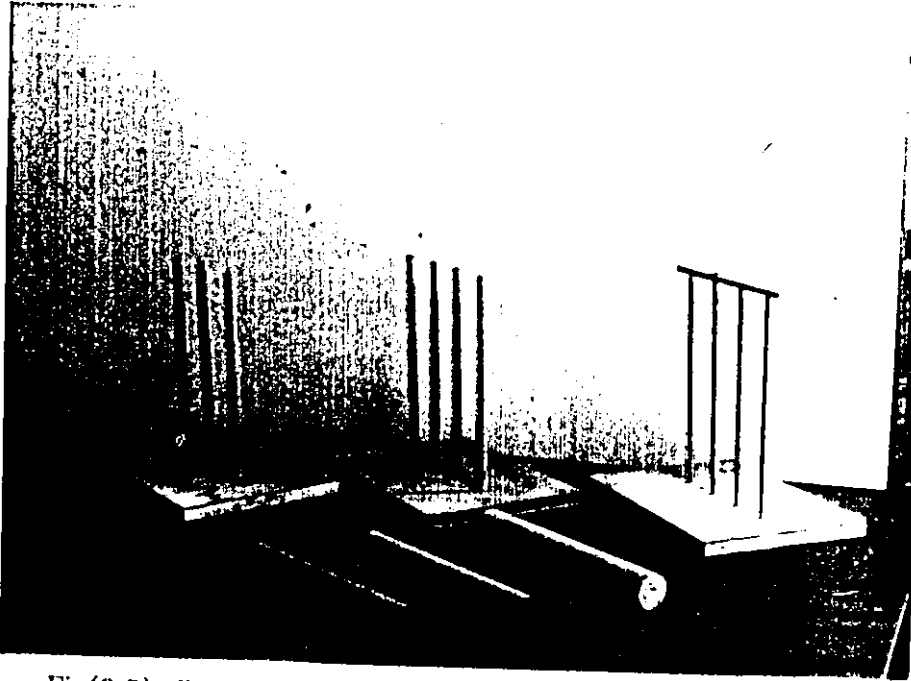
Fig(3-3). Schematic diagram of the different parts of the tunnel and the experimental rig.



SECTION A-A

NOTE : ALL DIMENSIONS ARE IN (mm)

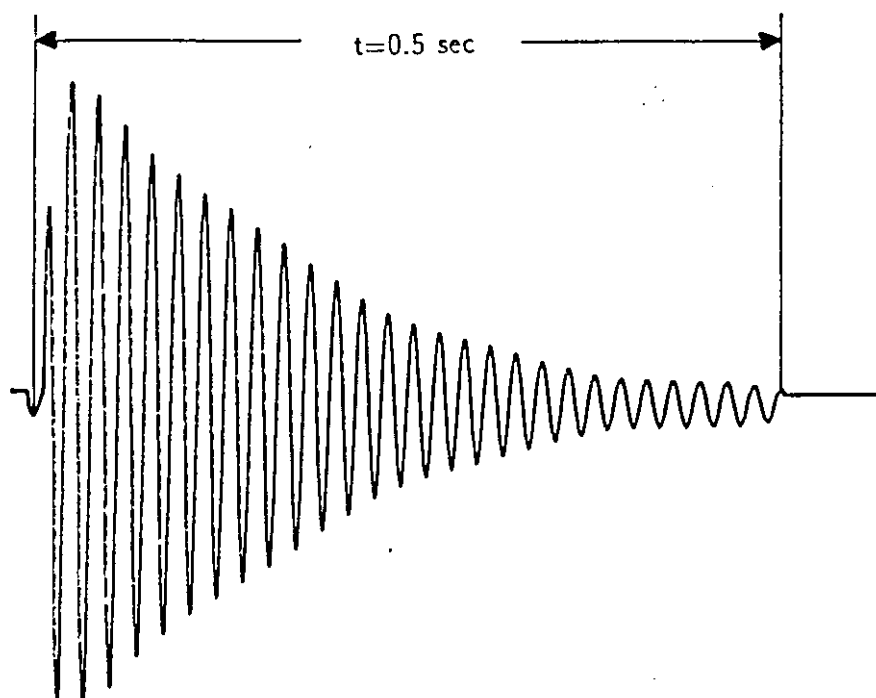
Fig(3-4). The cylinder clamping in the tunnel.



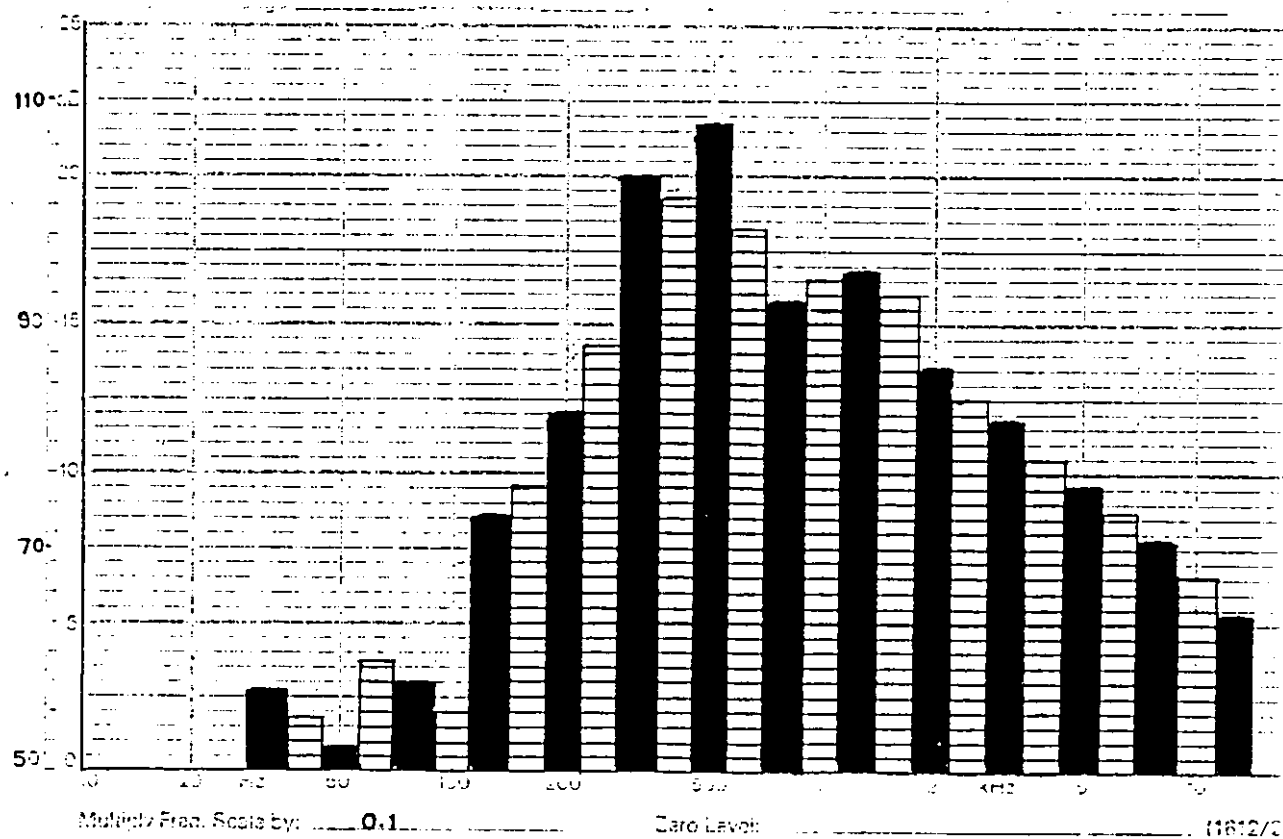
Fig(3-5). Turbulence generating grids and interfering bodies.



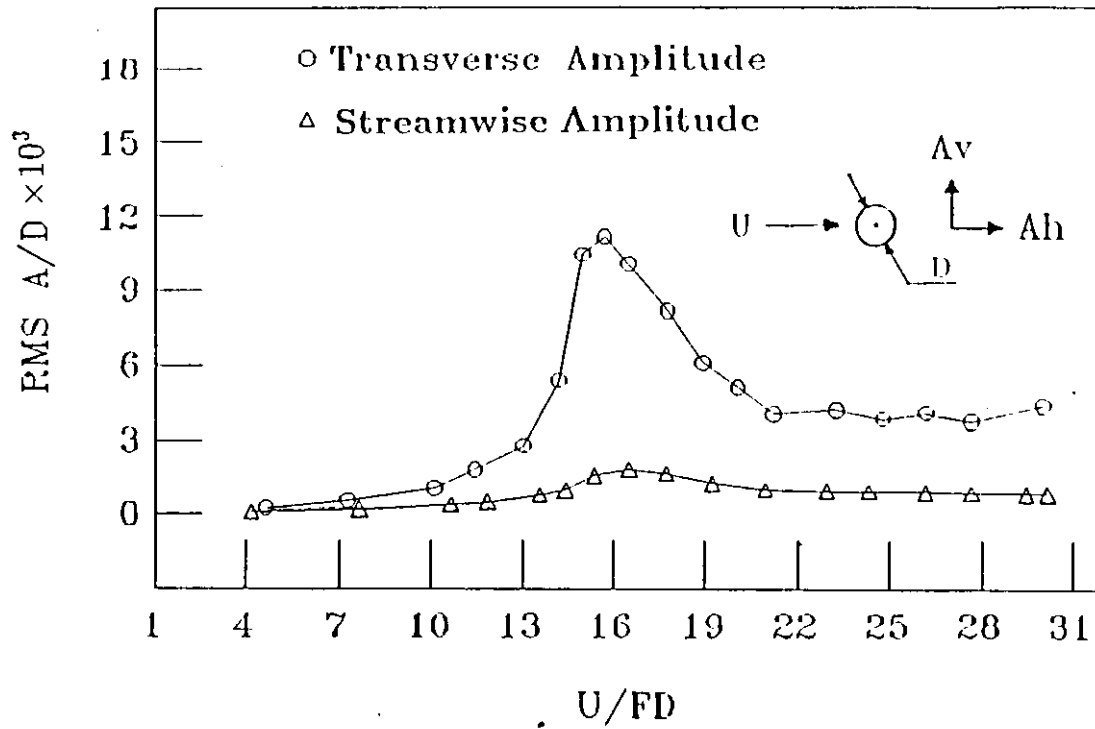
Fig(3-6). DISA Hot-wire Anemometry.



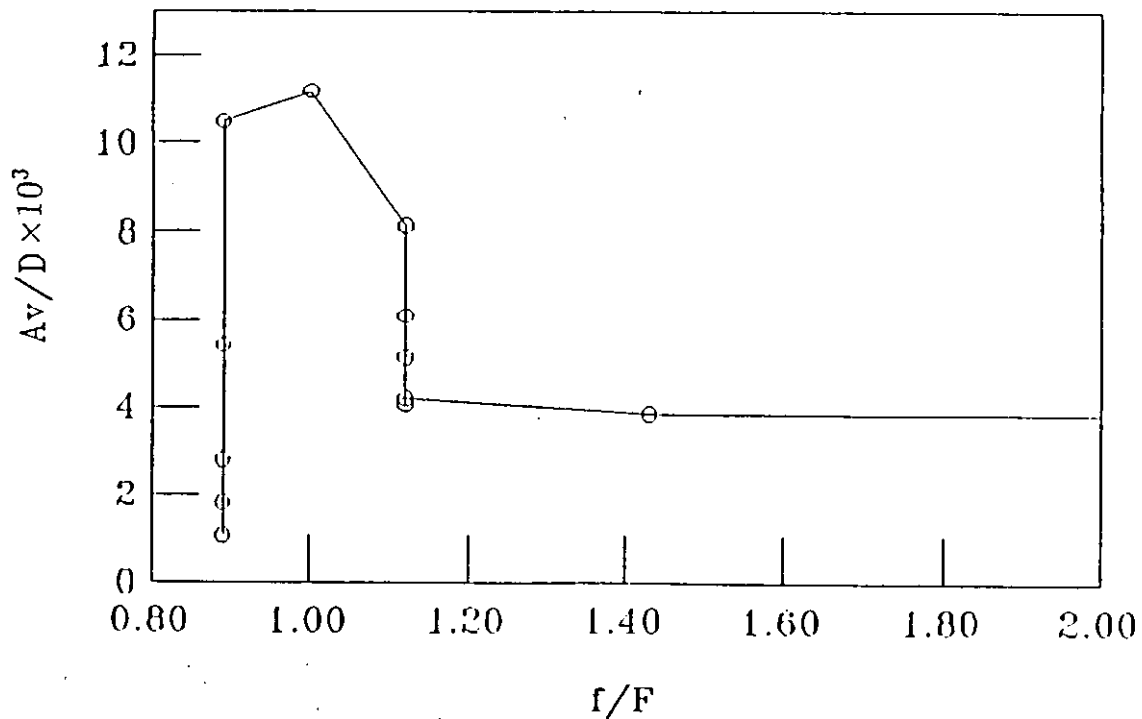
Fig(3-7). Signal wave form for the impulse test; $F=56$ Hz, $\delta=0.083$ and $K_c=4.93$.



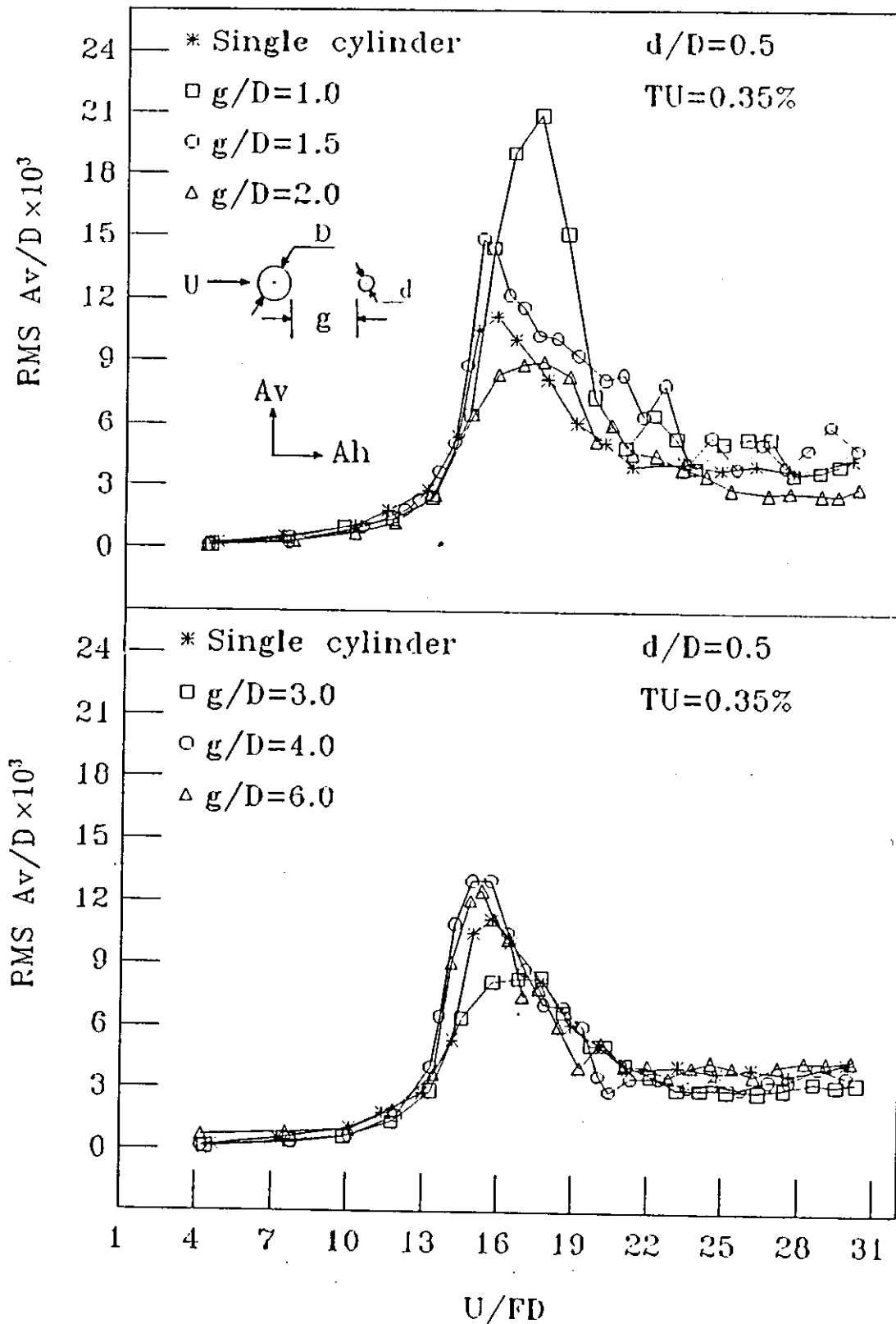
Fig(3-8). Frequency spectrum of the impulse test.



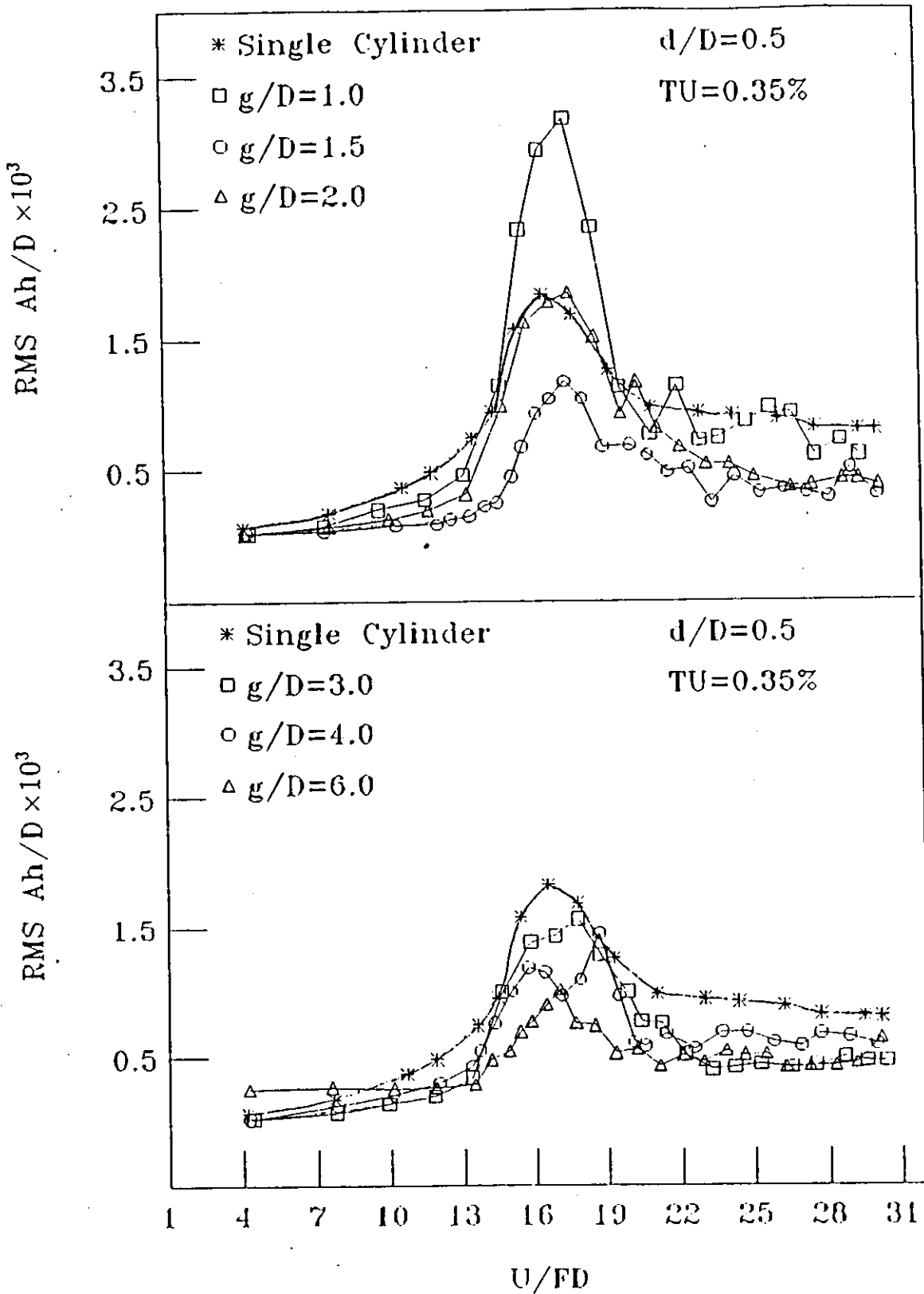
Fig(4-1). RMS vibration amplitude in the transverse and streamwise directions with reduced velocity for single cylinder.



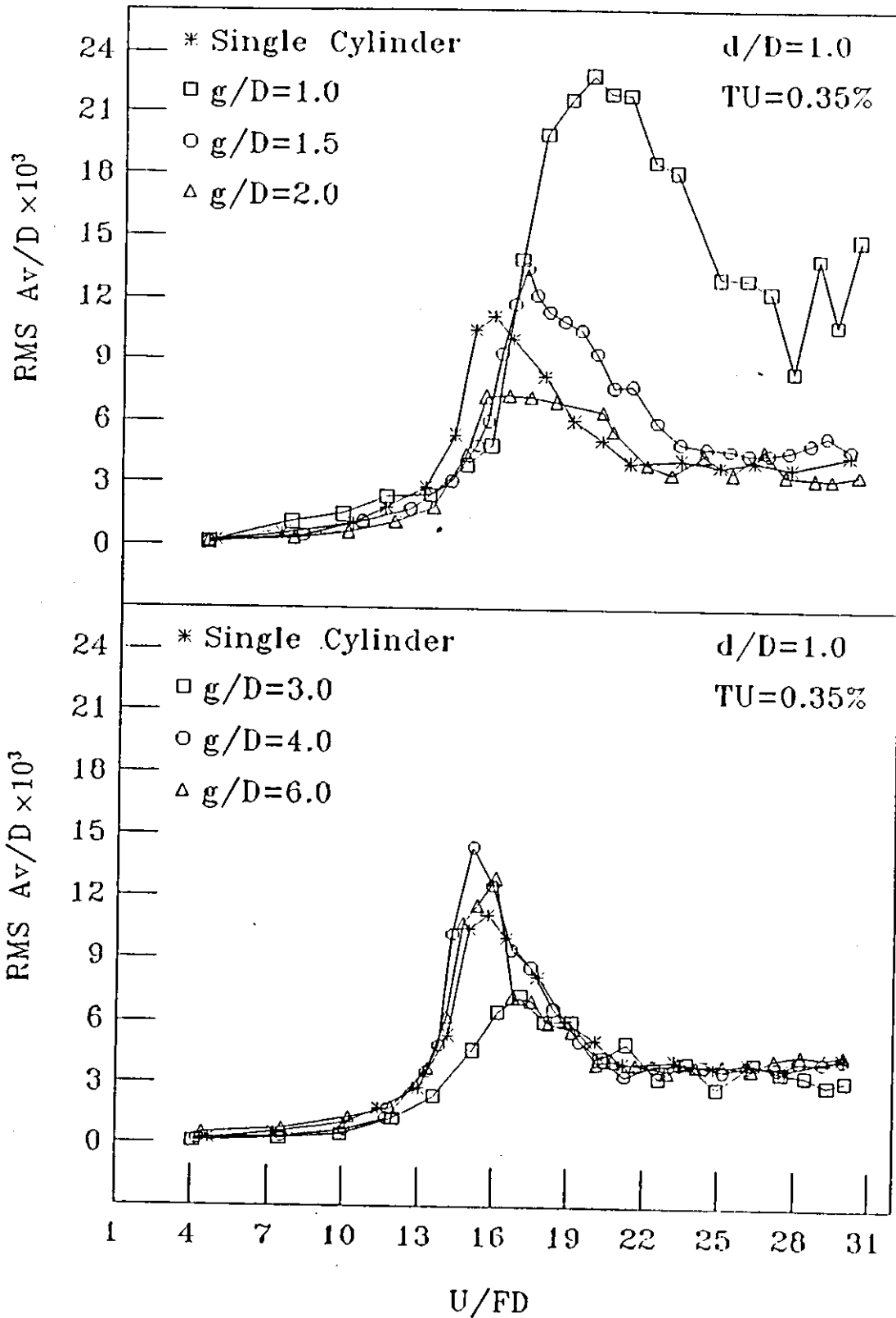
Fig(4-2). RMS vibration amplitude in the transverse direction with reduced frequency for single cylinder.



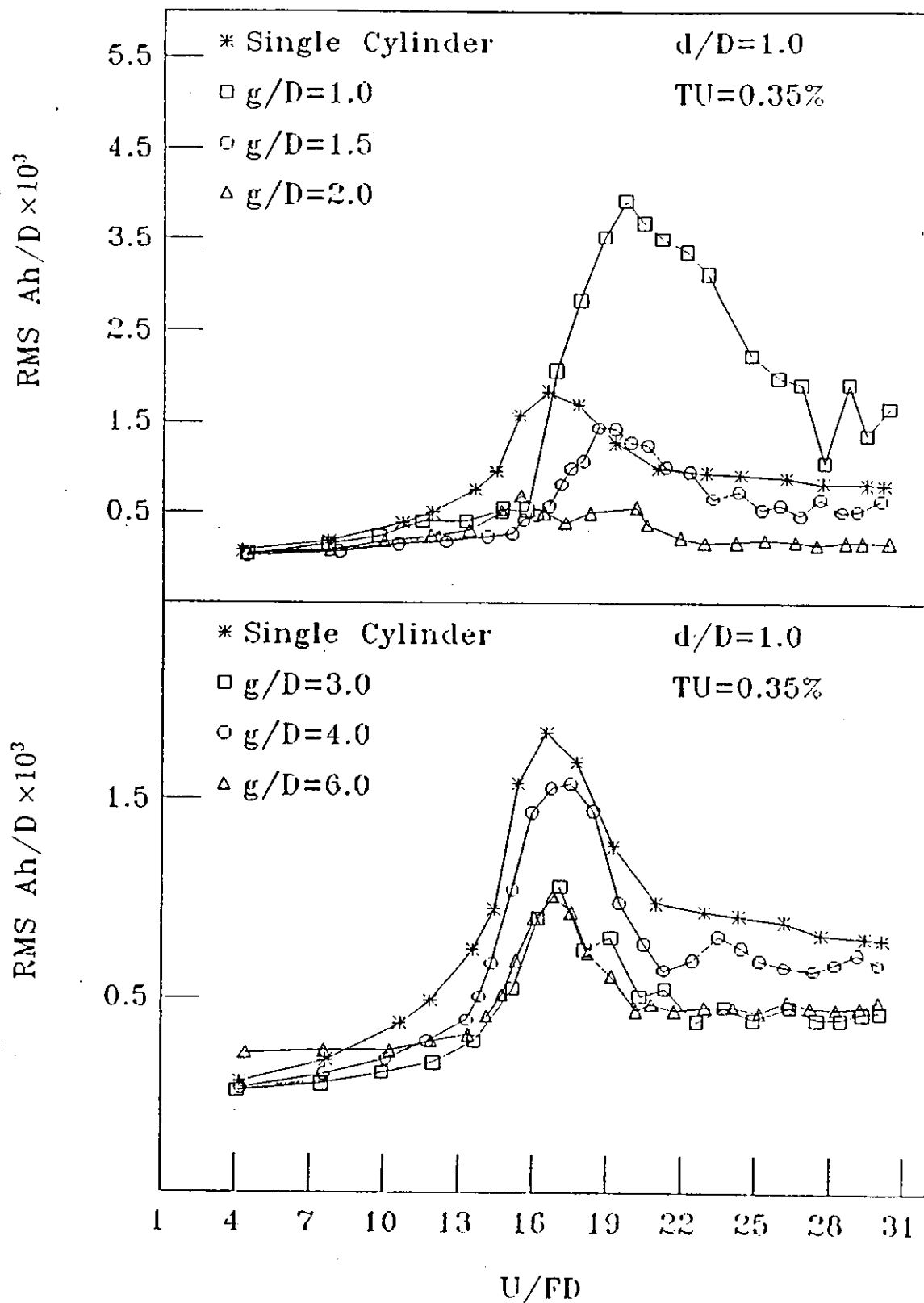
Fig(4-3). Interference effect in transverse direction for tandem arrangement; $d/D = 0.5, TU = 0.35\%$



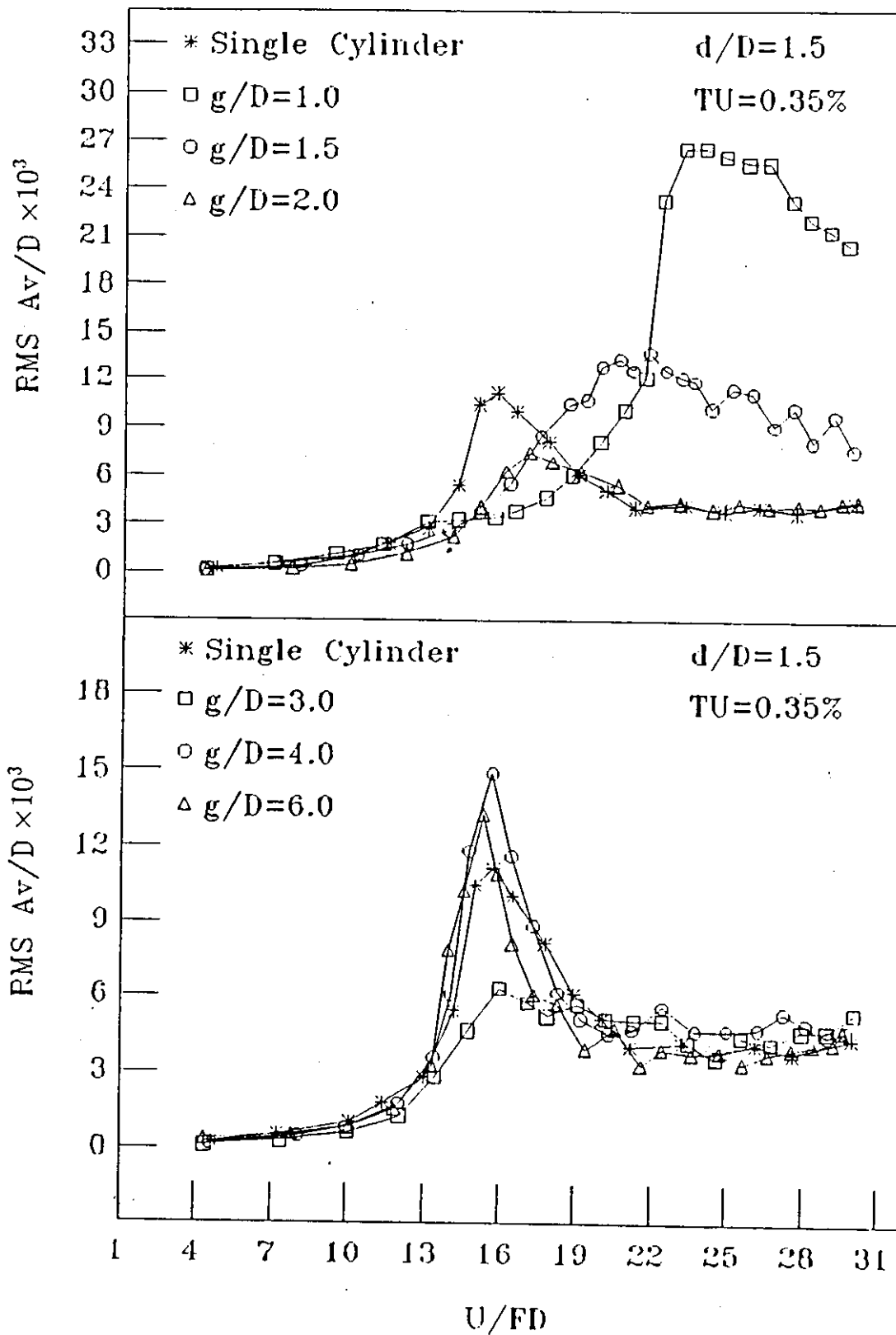
Fig(4-4). Interference effect in streamwise direction for tandem arrangement; $d/D = 0.5, TU = 0.35\%$



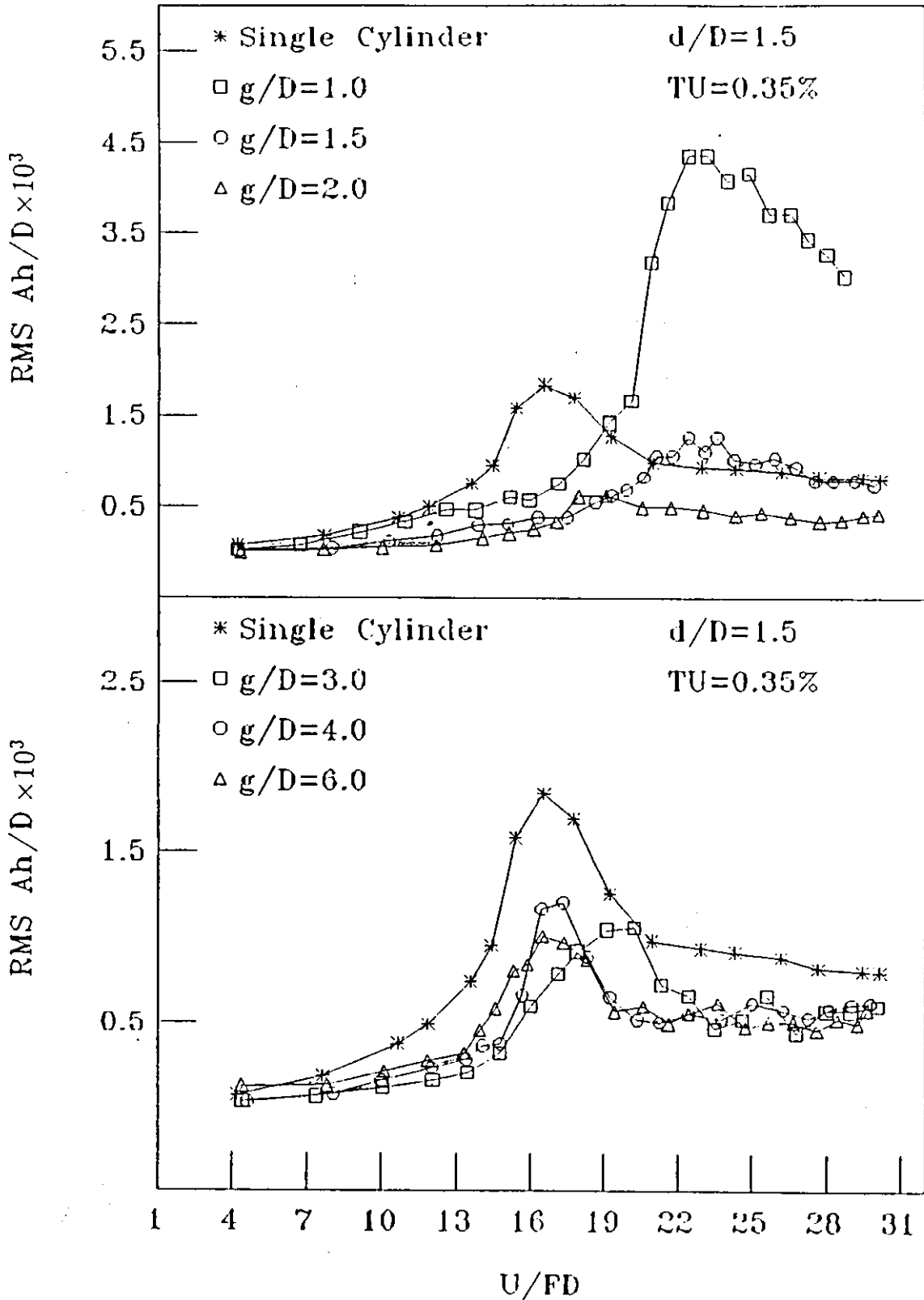
Fig(4-5). Interference effect in transverse direction for tandem arrangement; $d/D = 1.0$, $TU = 0.35\%$



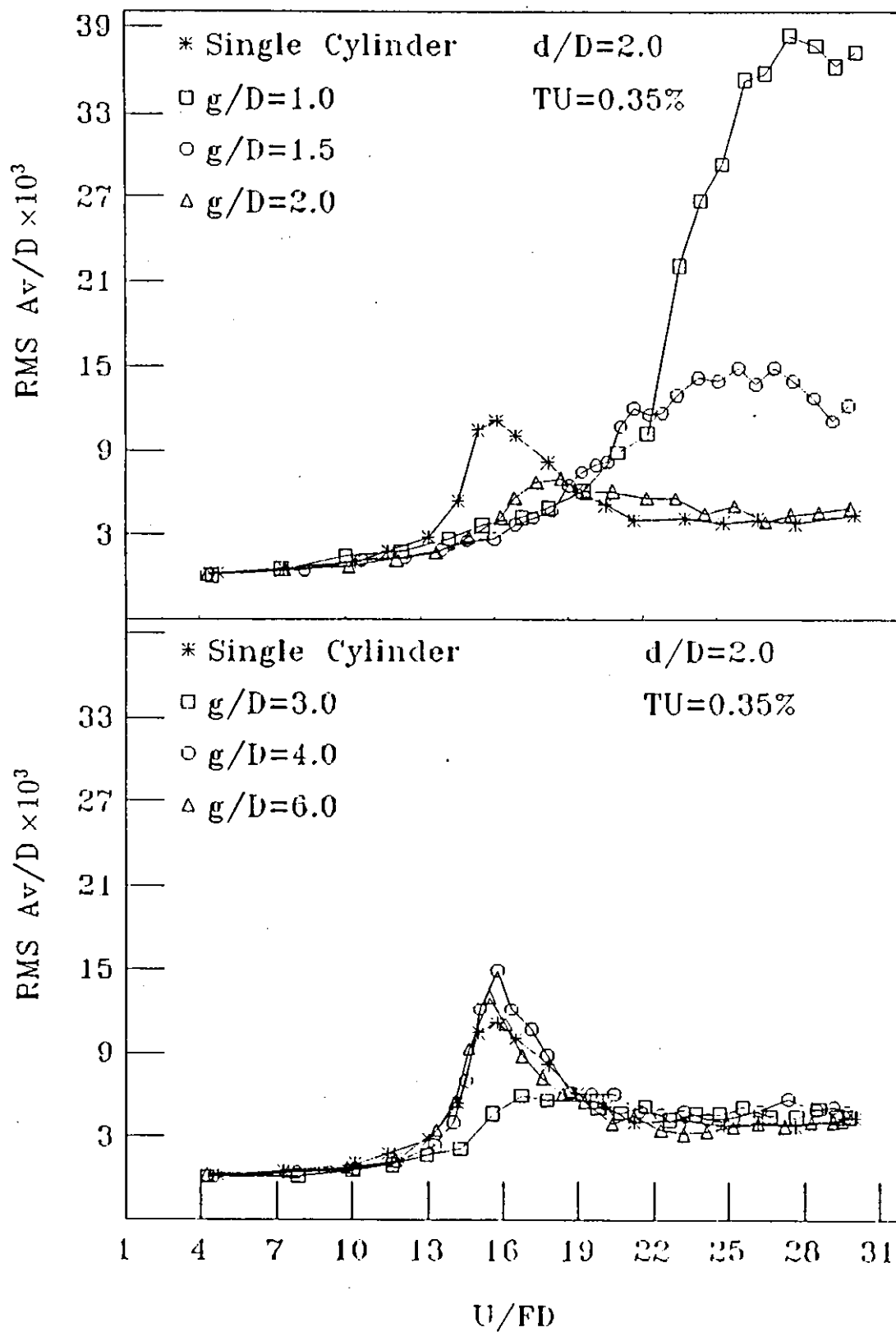
Fig(4-6). Interference effect in streamwise direction for tandem arrangement; $d/D = 1.0$, $TU = 0.35\%$



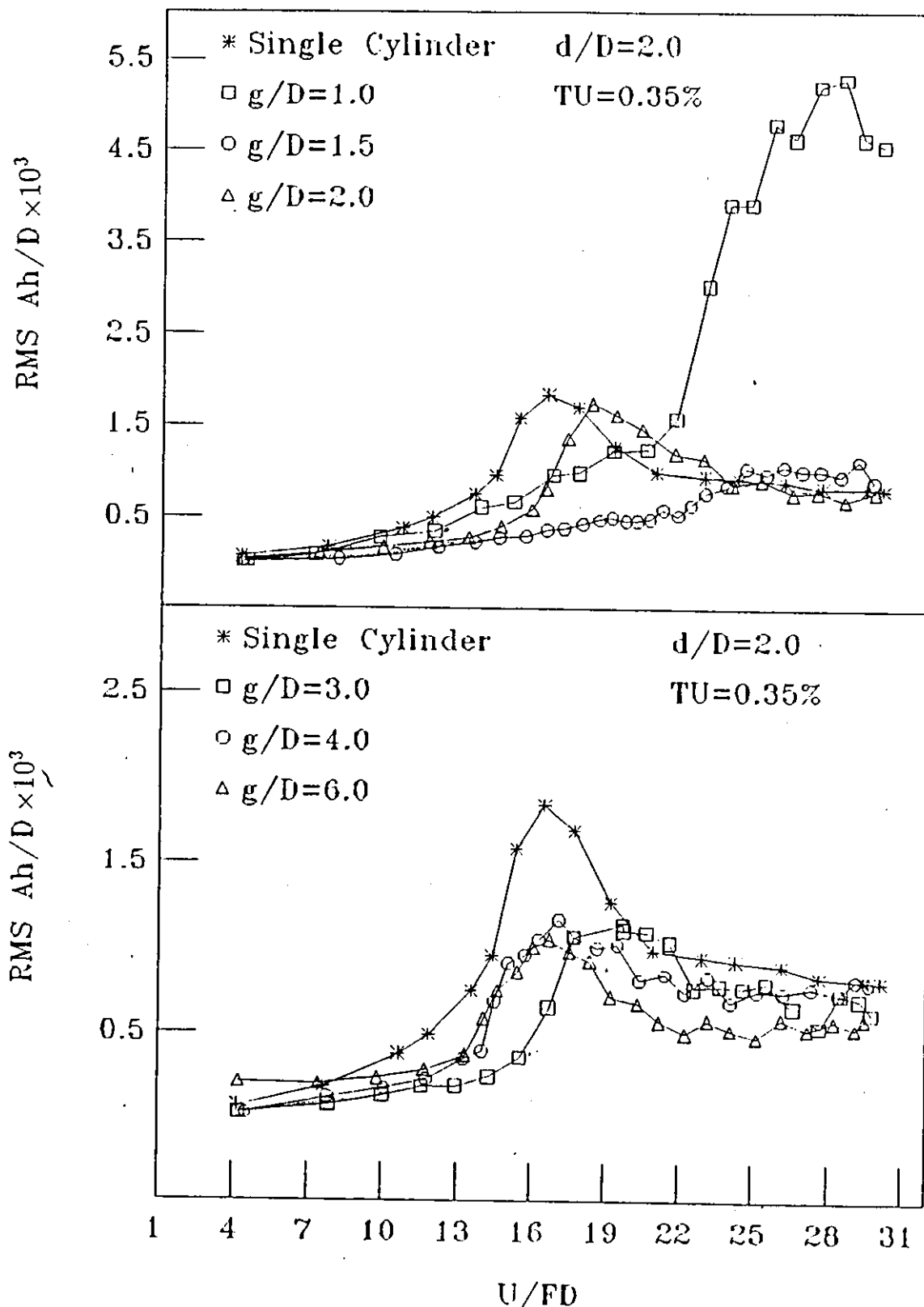
Fig(4-7). Interference effect in transverse direction for tandem arrangement; $d/D = 1.5, TU = 0.35\%$



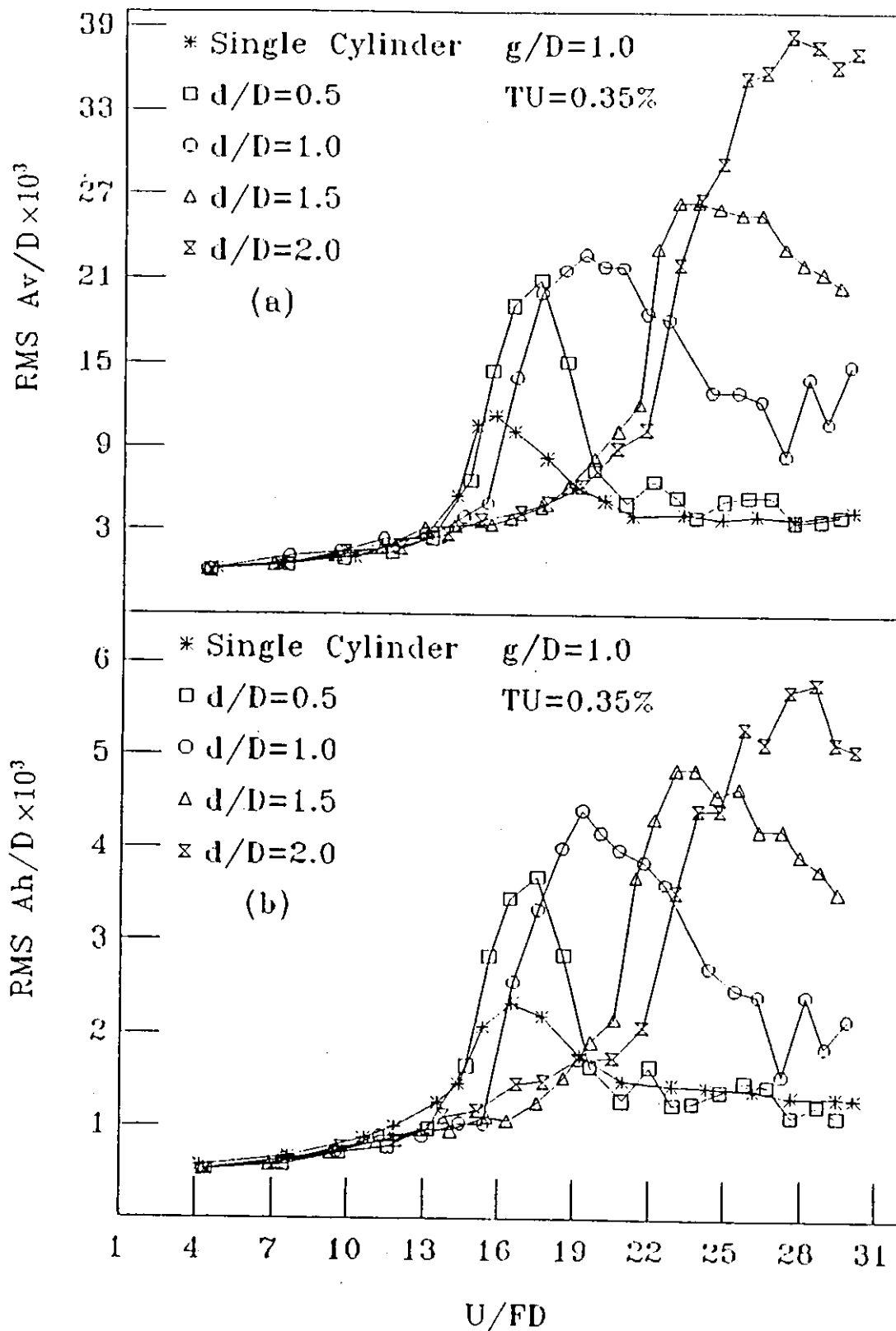
Fig(4-8). Interference effect in streamwise direction for tandem arrangement; $d/D = 1.5, TU = 0.35\%$



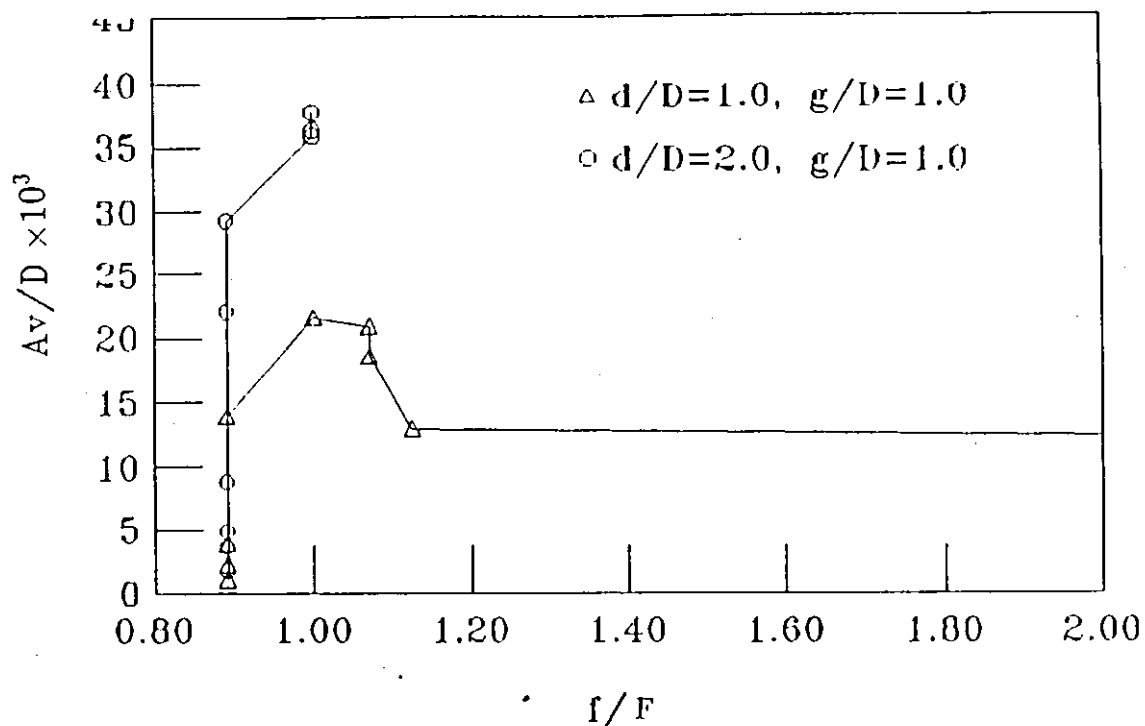
Fig(4-9). Interference effect in transverse direction for tandem arrangement; $d/D = 2.0$, $TU = 0.35\%$



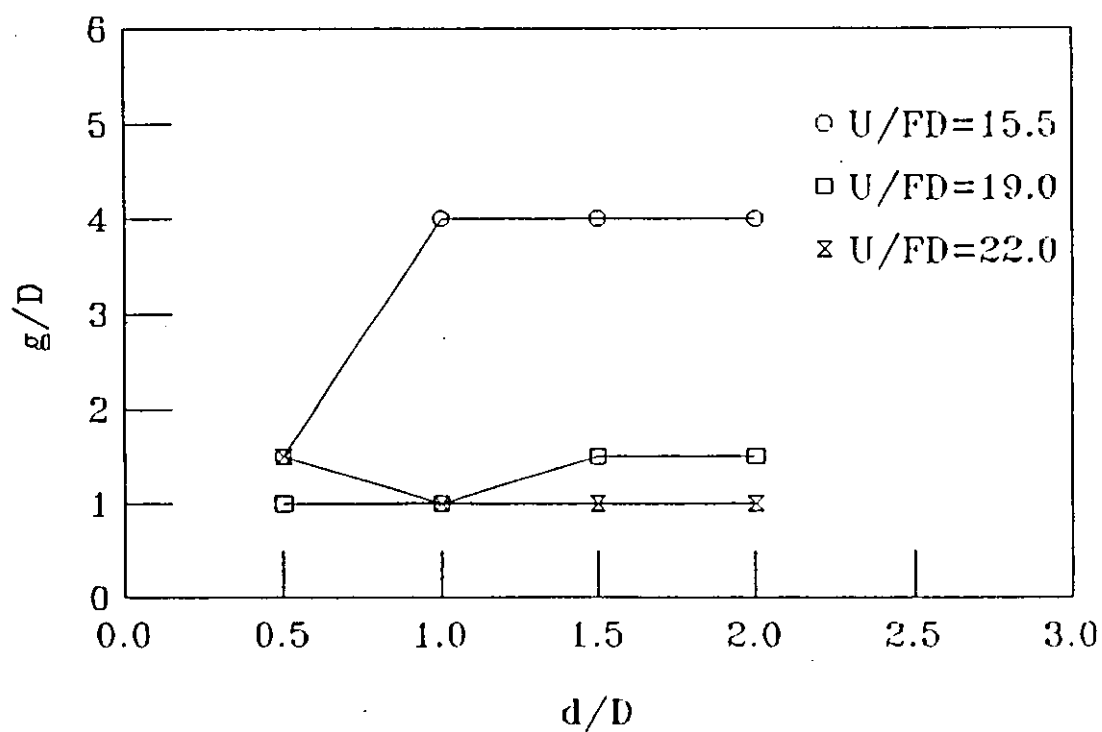
Fig(4-10). Interference effect in streamwise direction for tandem arrangement; $d/D = 2.0, TU = 0.35\%$



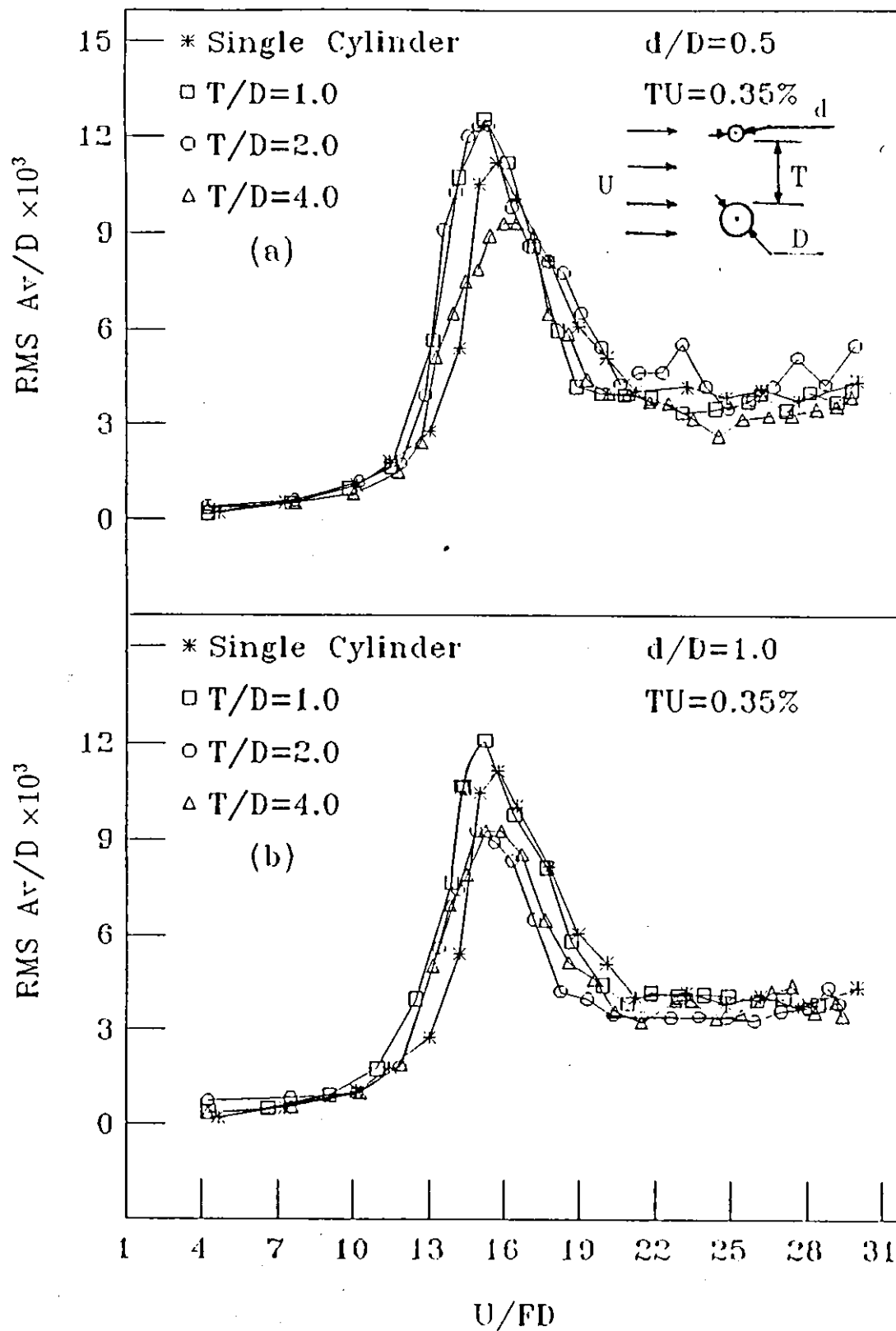
Fig(4-11). Interference effect in transverse direction for tandem arrangement; $g/D = 1.0$, $TU = 0.35\%$



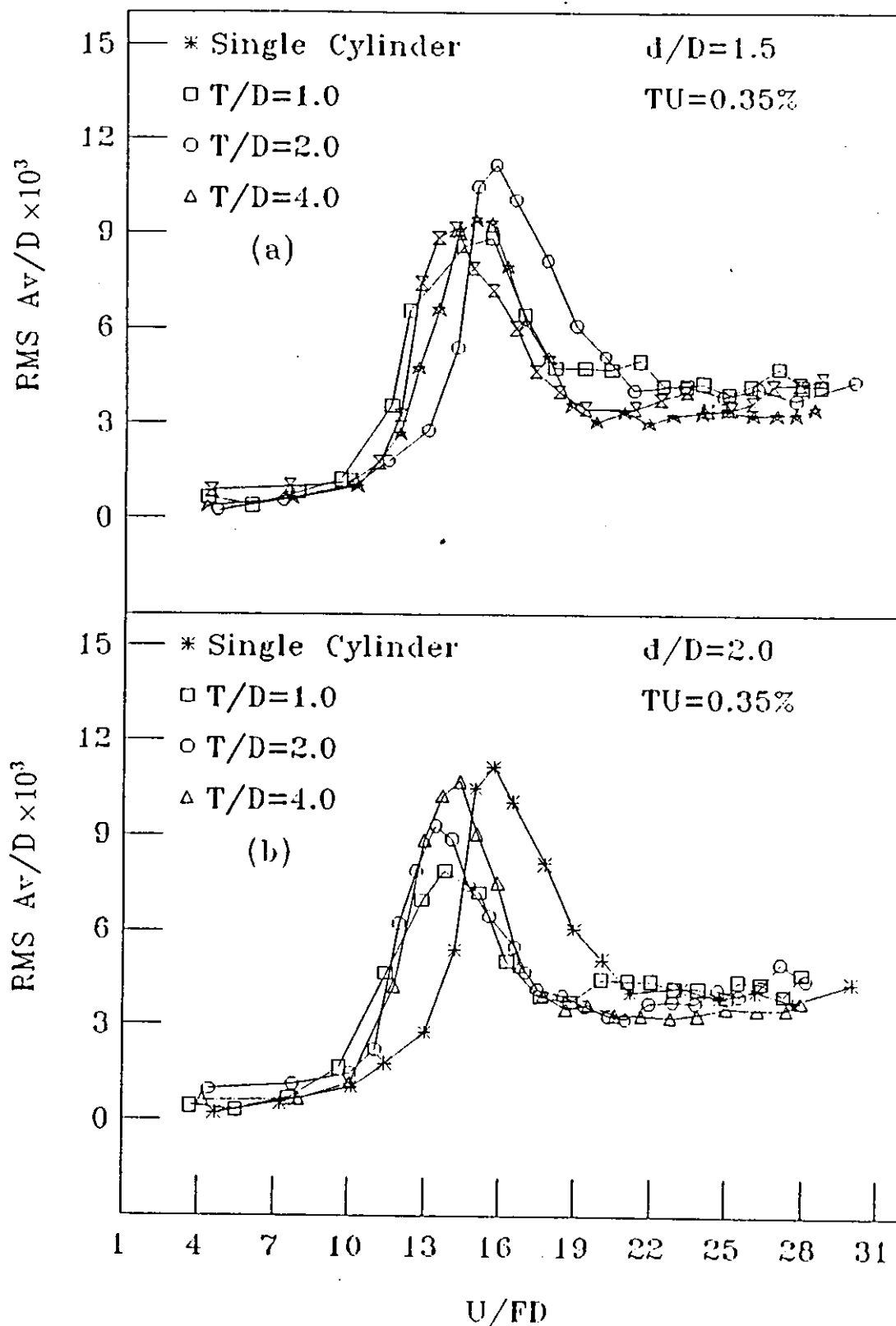
Fig(4-12). RMS vibration amplitude in the transverse direction with reduced frequency for tandem arrangement.



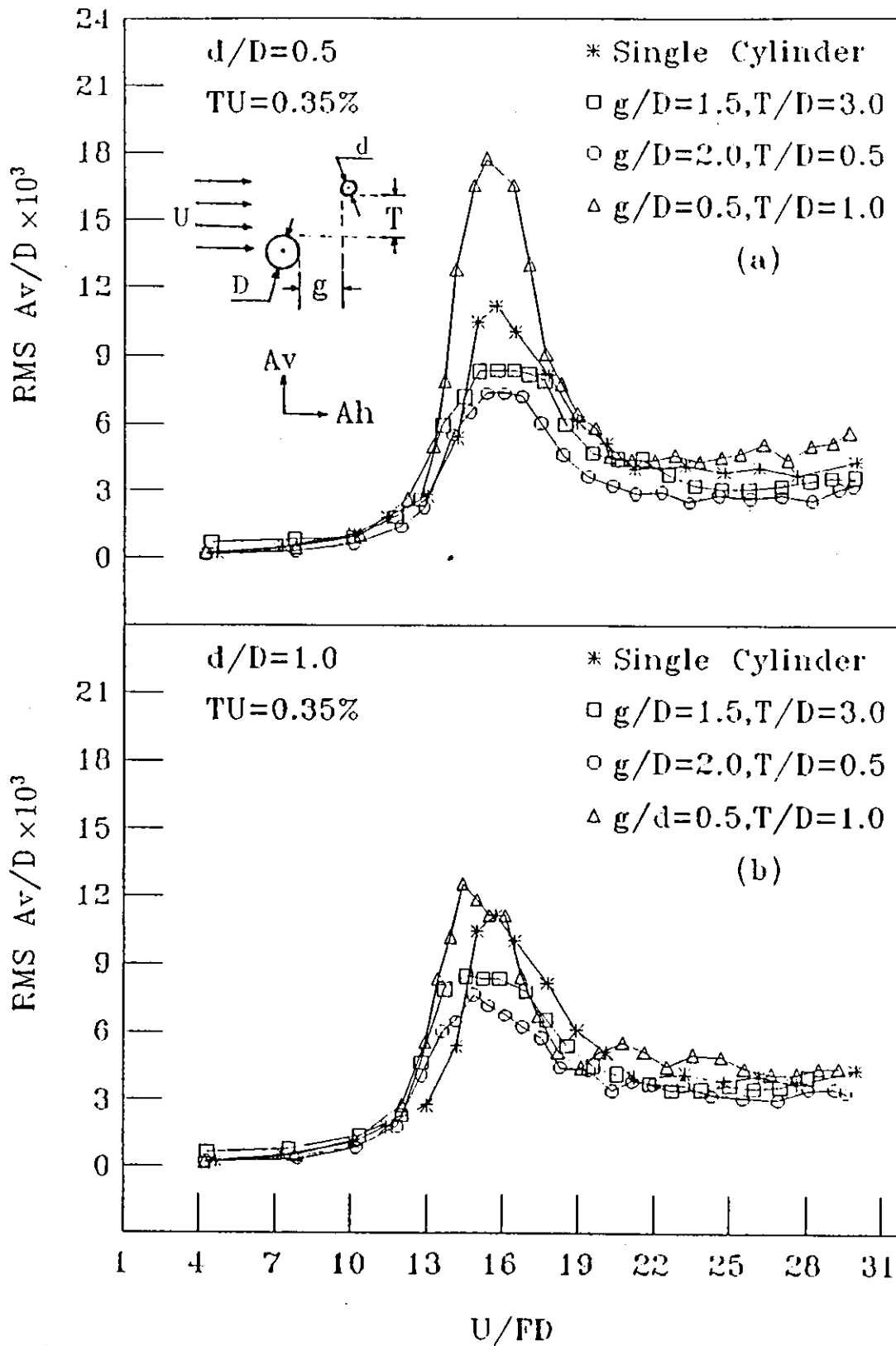
Fig(4-13). Position of the major peak in transverse direction for different reduced velocities.



Fig(4-14). Interference effect in transverse direction for side-by-side arrangement;
 (a) $d/D = 0.5$, (b) $d/D = 1.0$

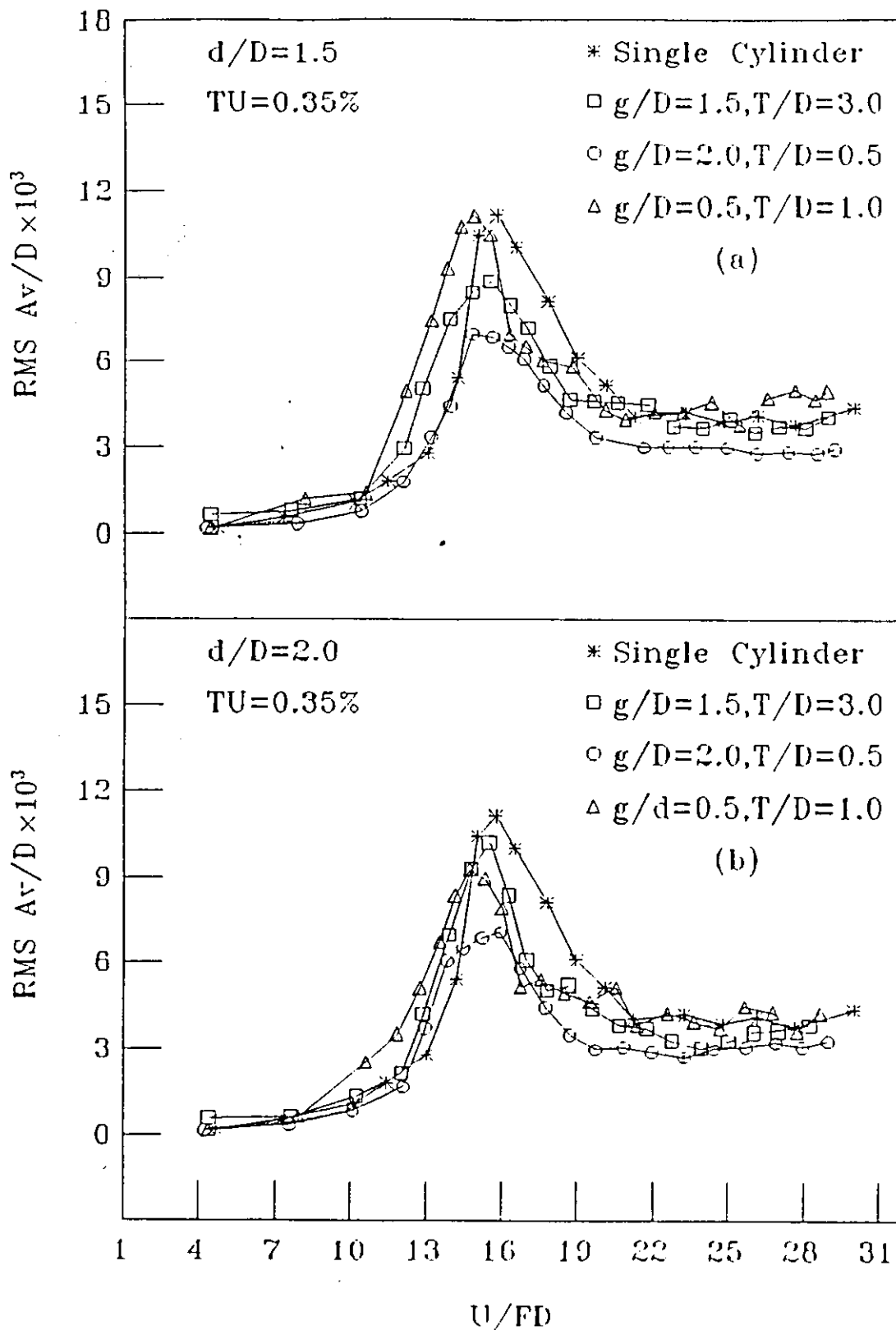


Fig(4-15). Interference effect in transverse direction for side-by-side arrangement;
 (a) $d/D = 1.5$, (b) $d/D = 2.0$

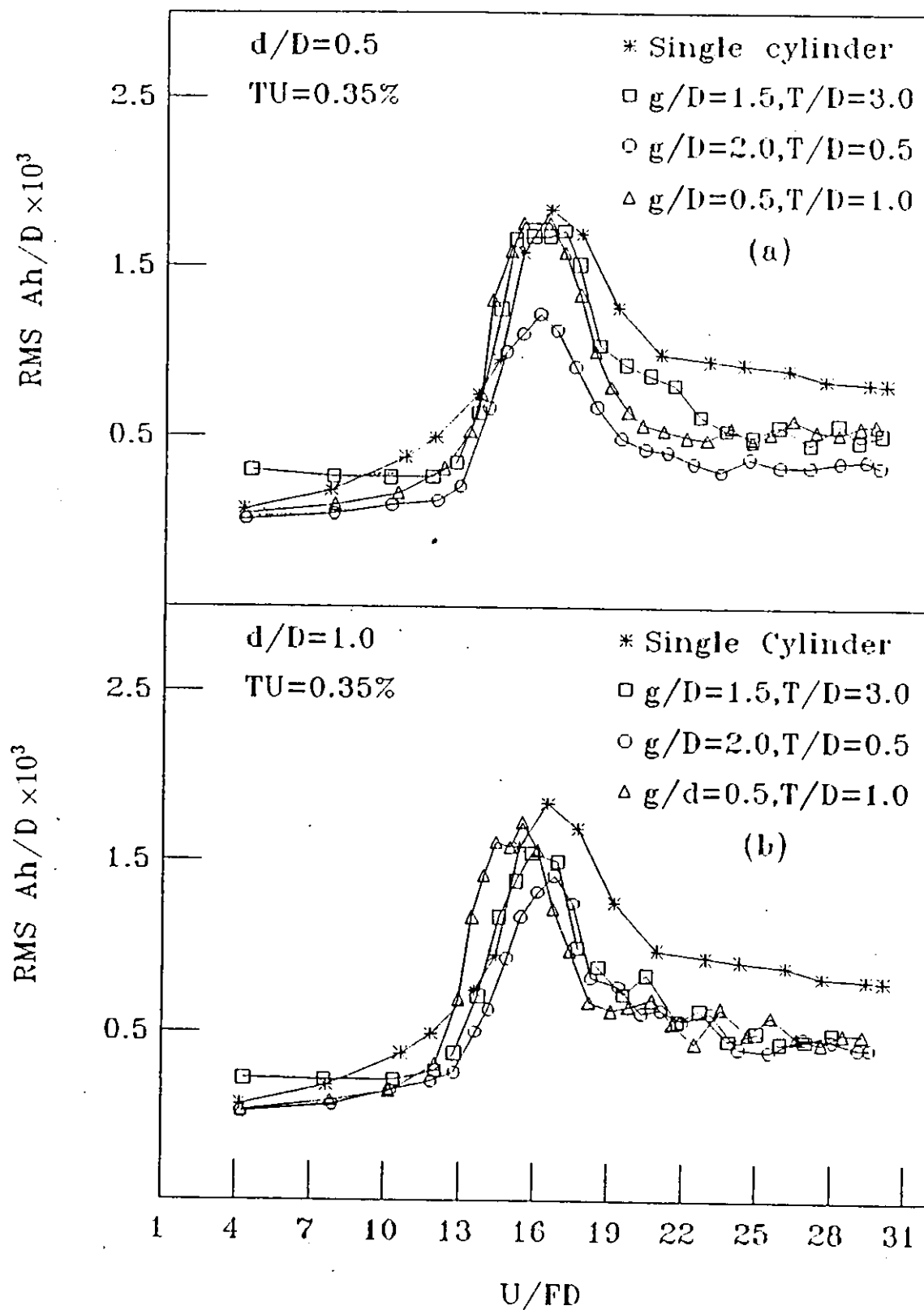


Fig(4-16).: Interference effect in transverse direction for staggered arrangement;

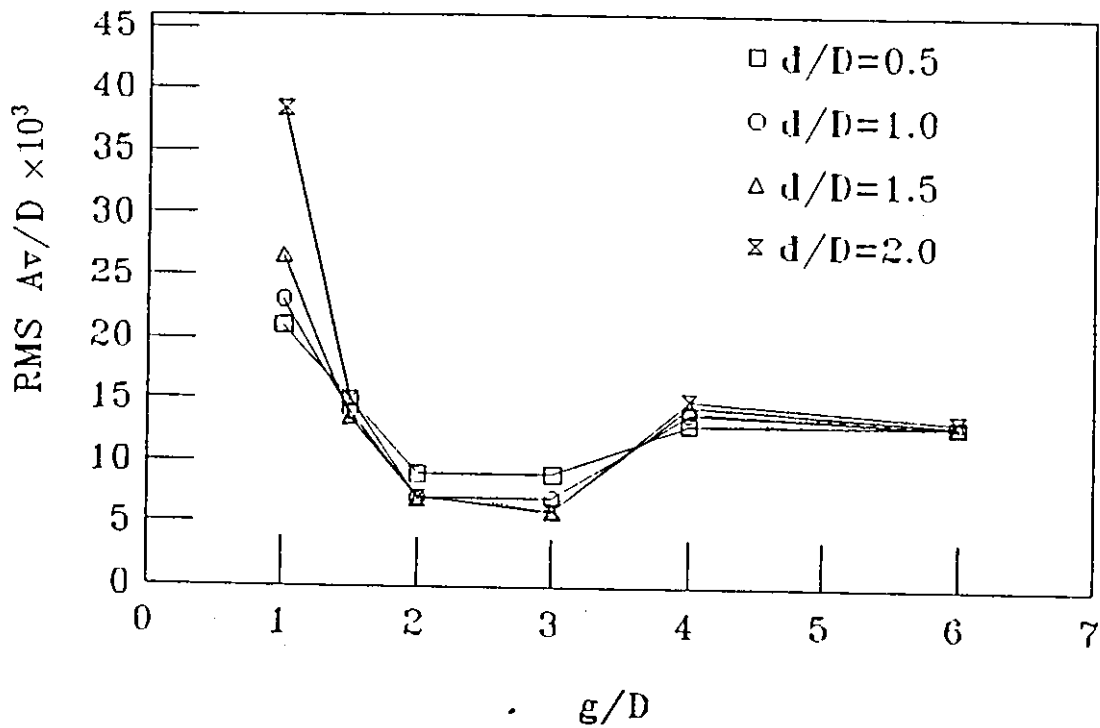
(a) $d/D = 0.5$, (b) $d/D = 1.0$



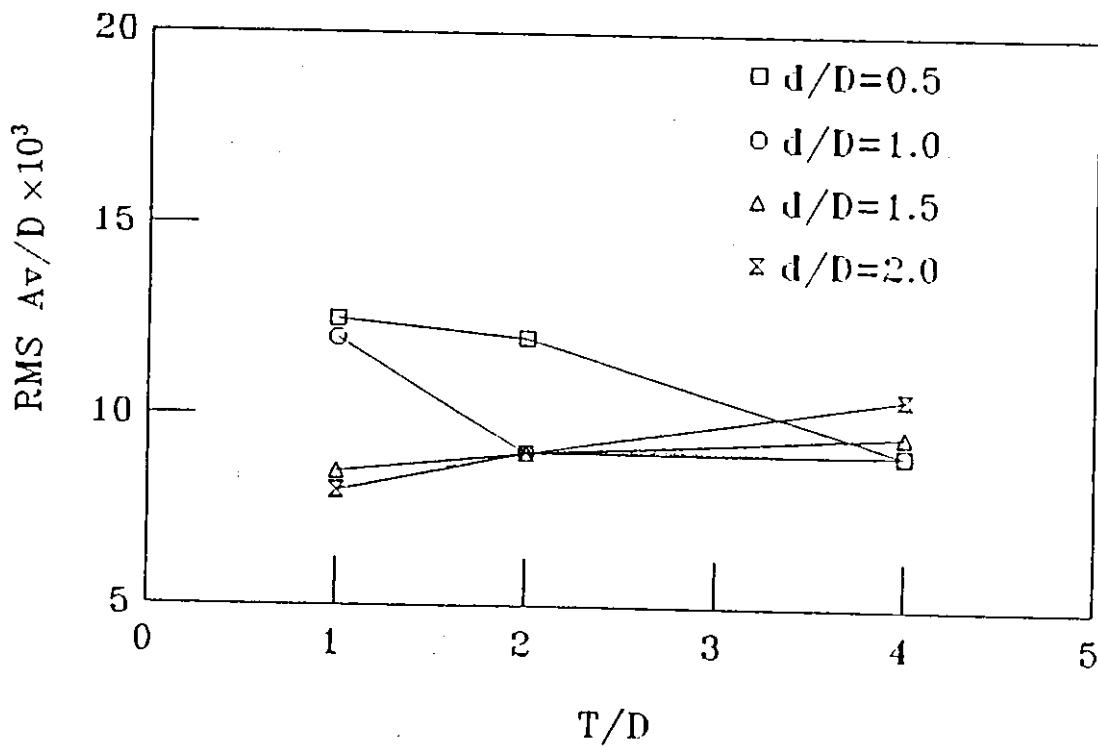
Fig(4-17). Interference effect in transverse direction for side-by-side arrangement;
 (a) $d/D = 1.5$, (b) $d/D = 2.0$



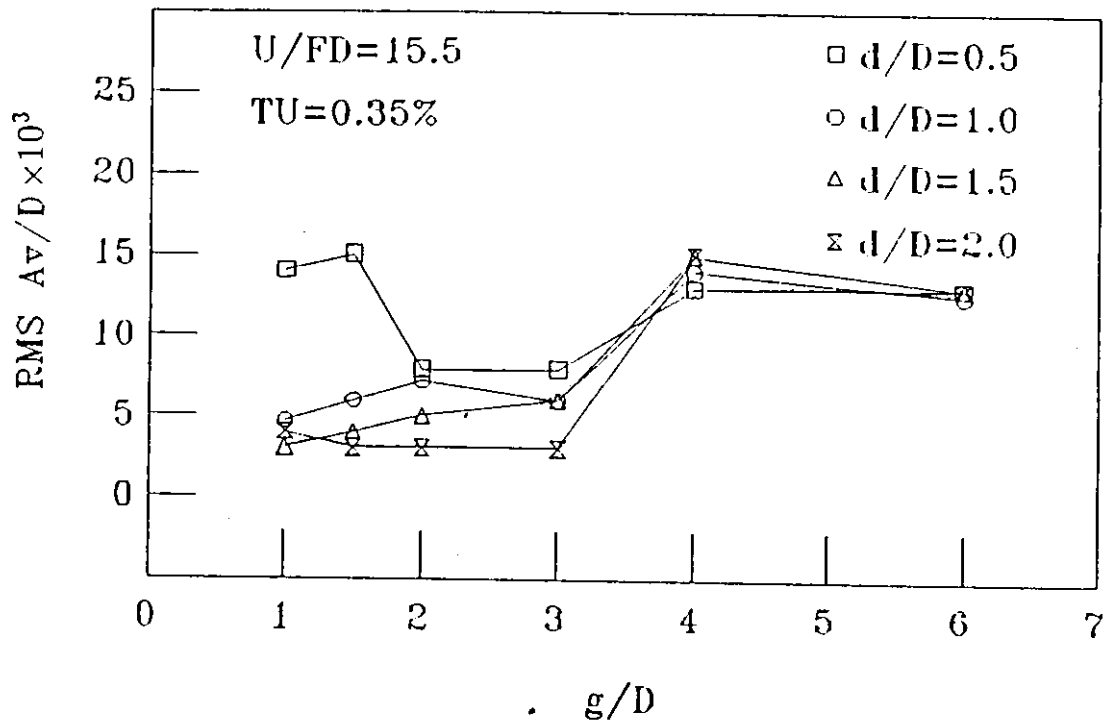
Fig(4-18). Interference effect in streamwise direction for staggered arrangement;
 (a) $d/D = 0.5$, (b) $d/D = 1.0$



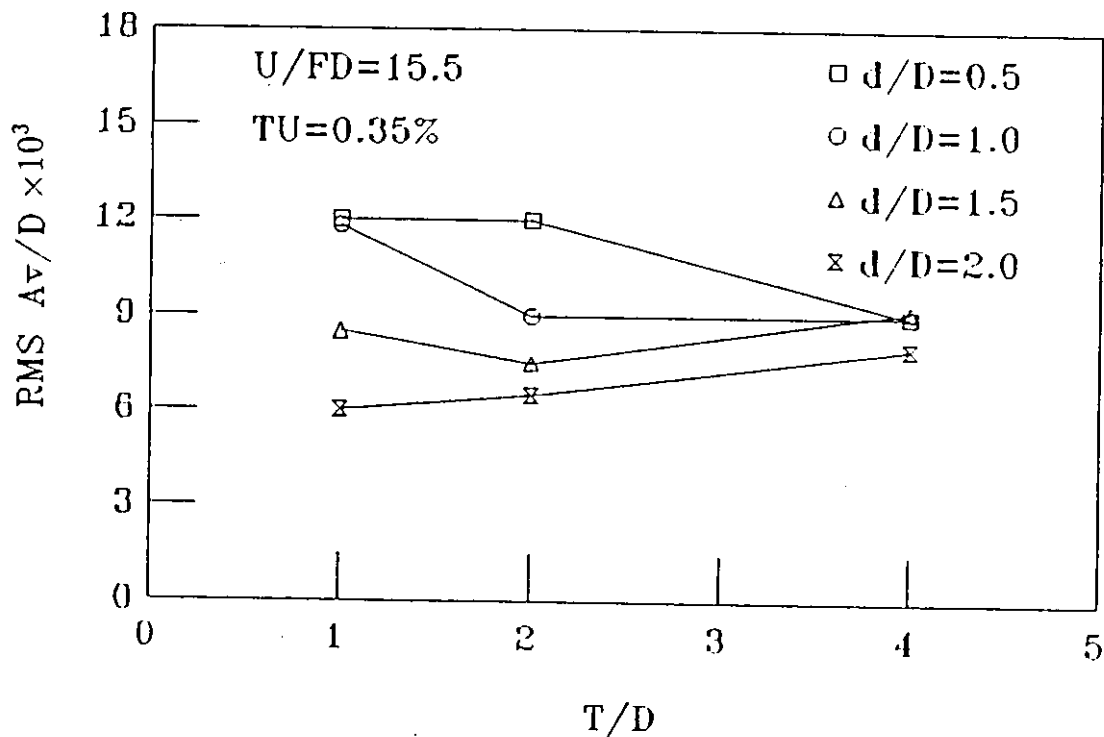
Fig(4-19). RMS vibration amplitude with gap spacing for tandem arrangement.



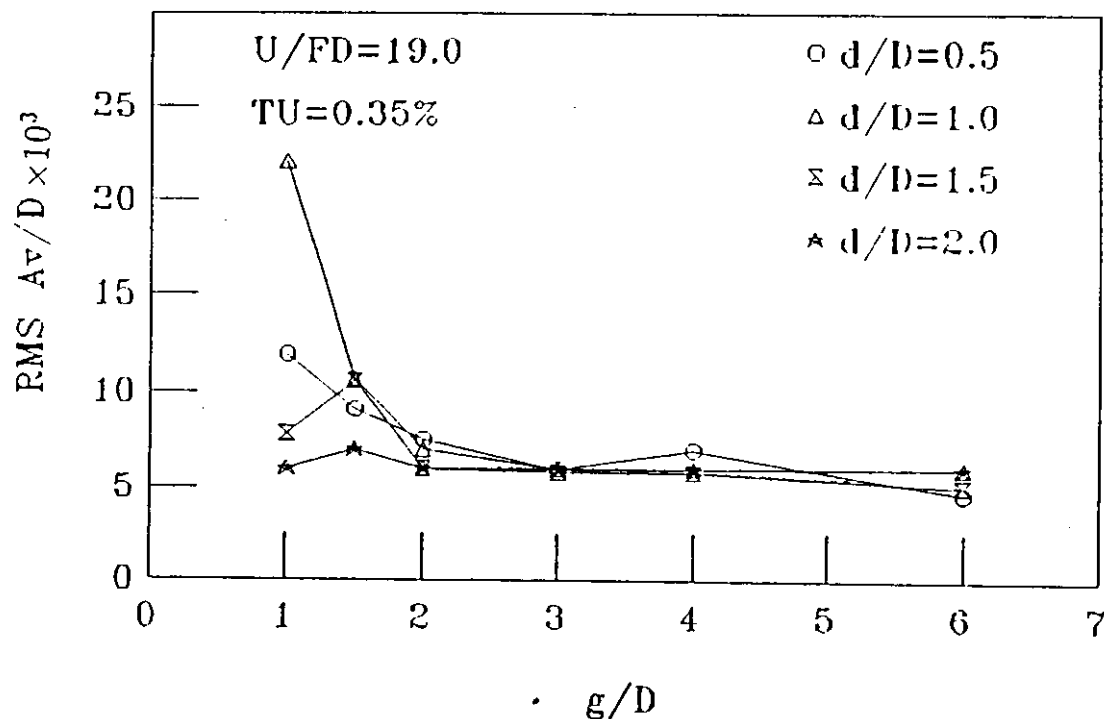
Fig(4-20). RMS vibration amplitude with gap spacing for side-by-side arrangement.



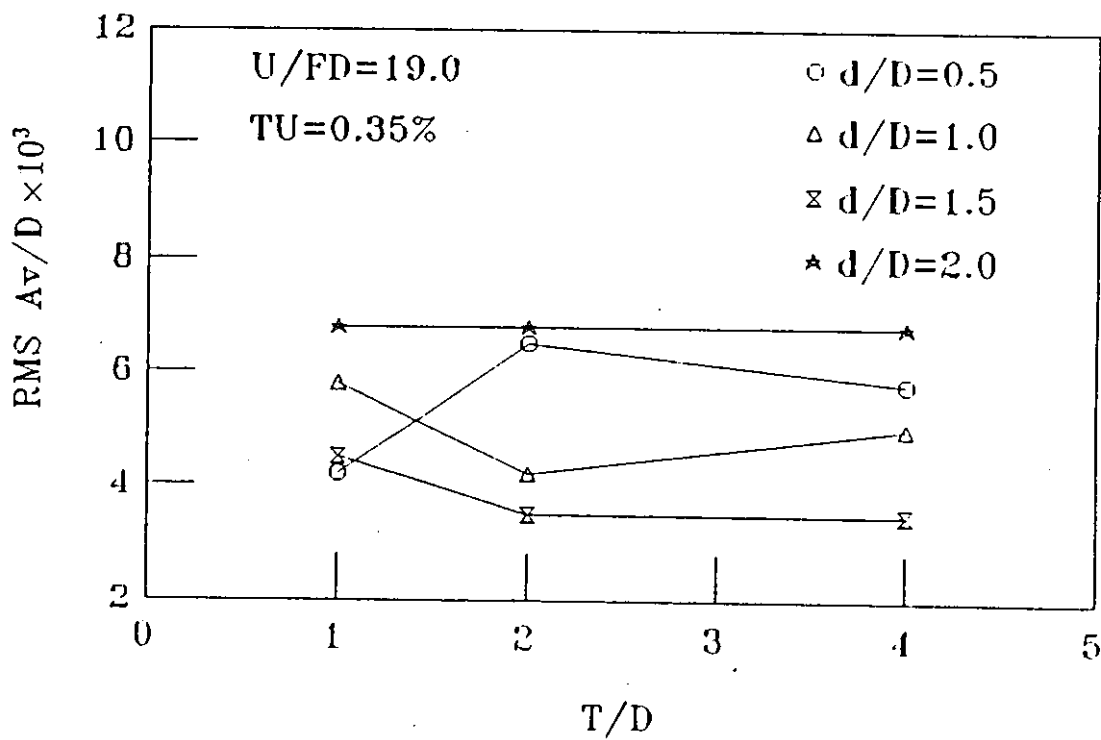
Fig(4-21). Variation of transverse vibration amplitude versus gap spacing for tandem arrangement; $U/FD = 15.5$.



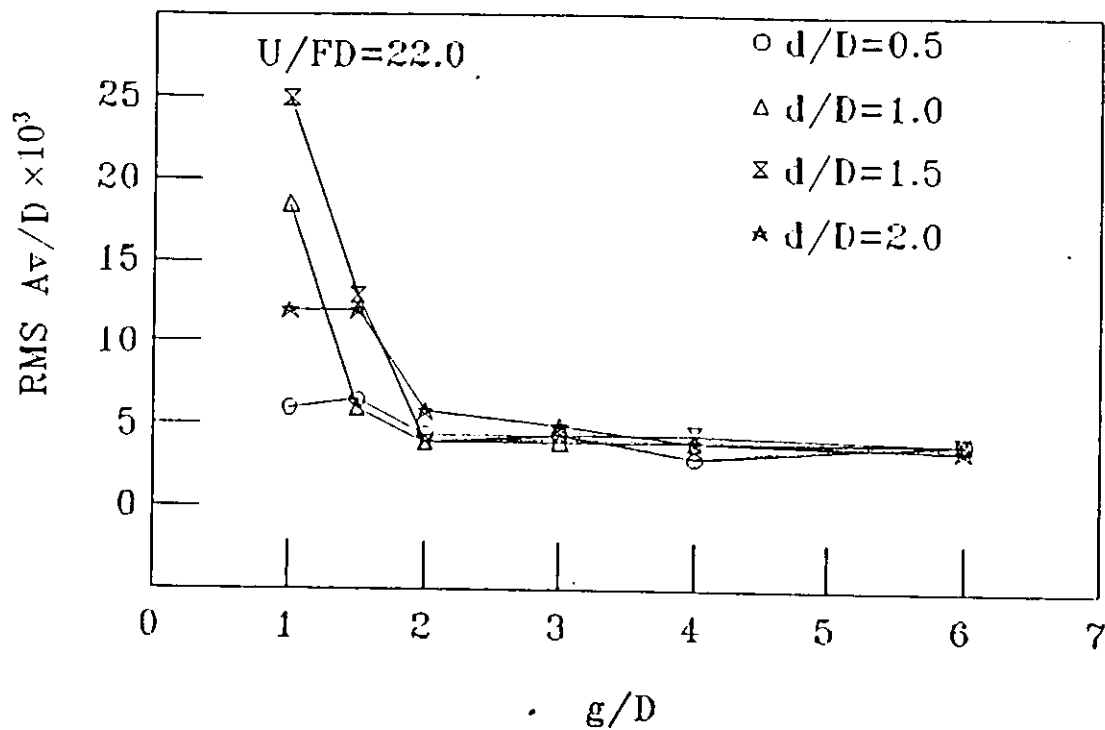
Fig(4-22). Variation of transverse vibration amplitude versus gap spacing for side-by-side arrangement; $U/FD = 15.5$.



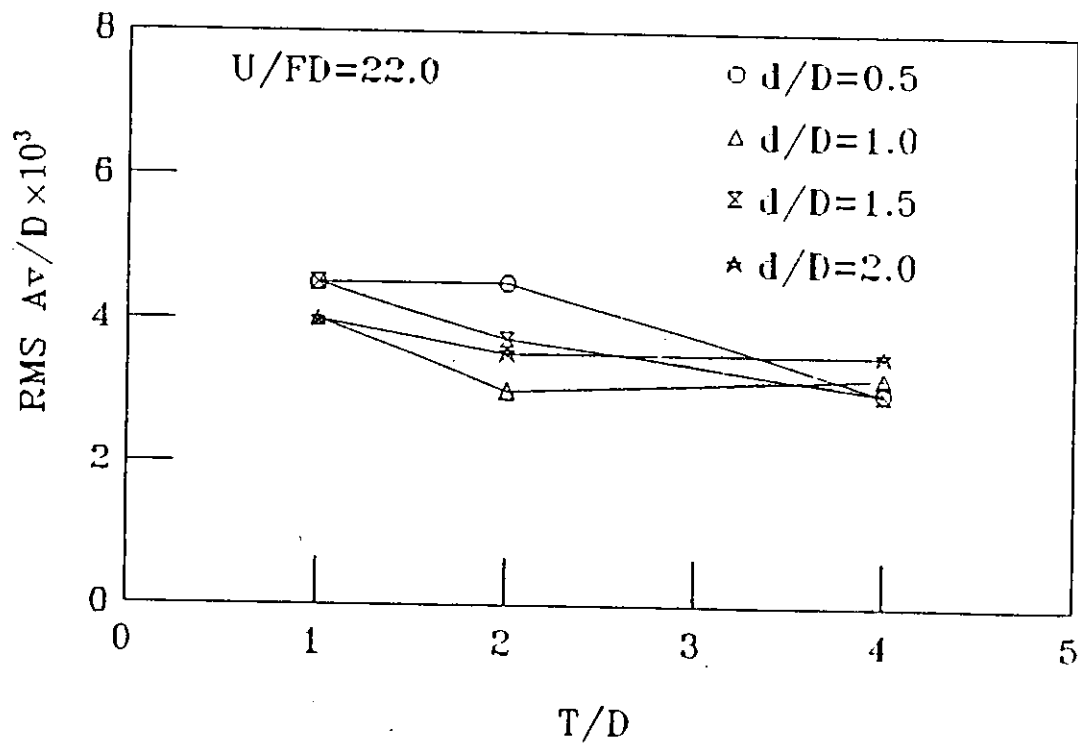
Fig(4-23). Variation of transverse vibration amplitude versus gap spacing for tandem arrangement; $U/FD = 19.0$.



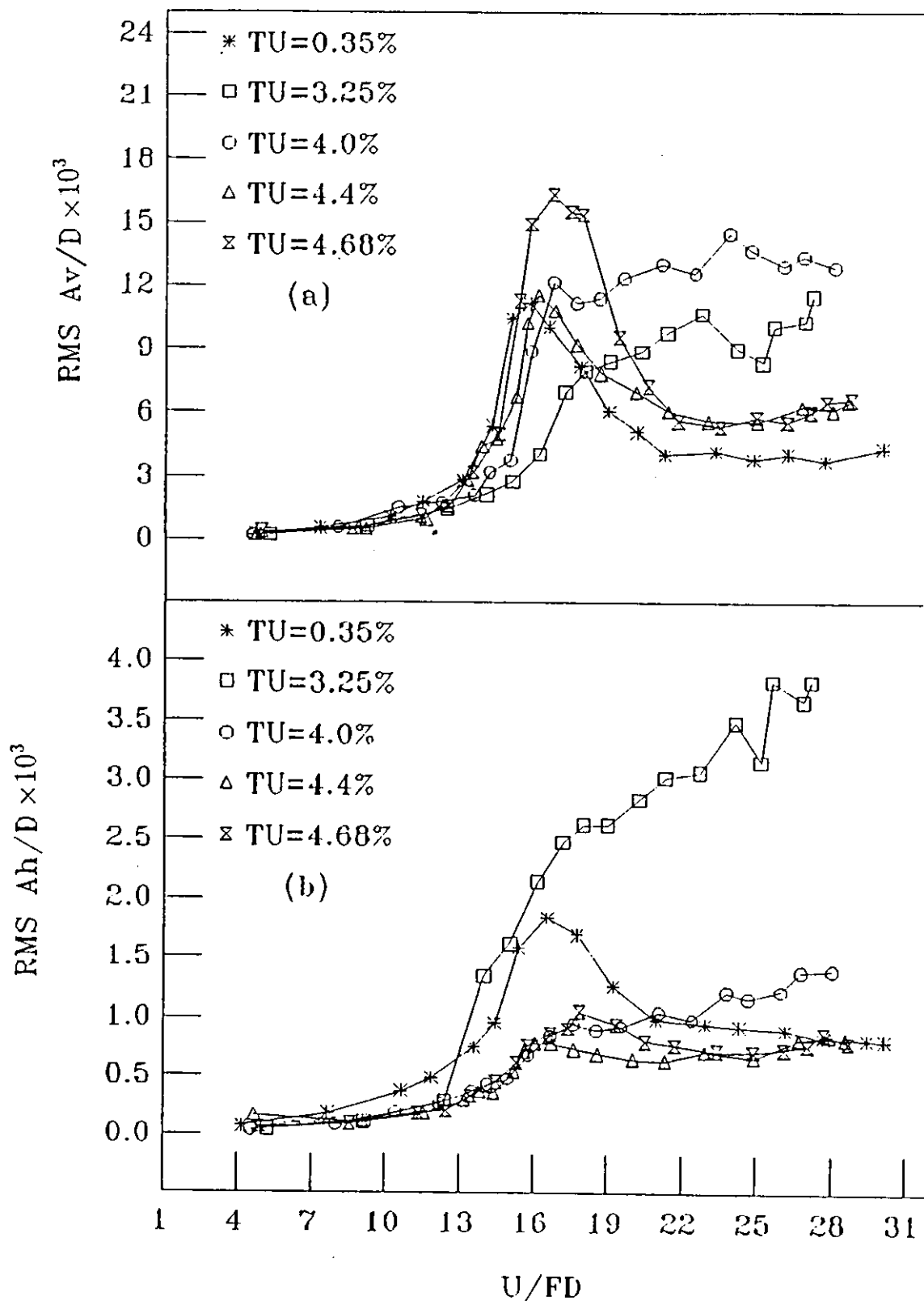
Fig(4-24). Variation of transverse vibration amplitude versus gap spacing for side-by-side arrangement; $U/FD = 19.0$.



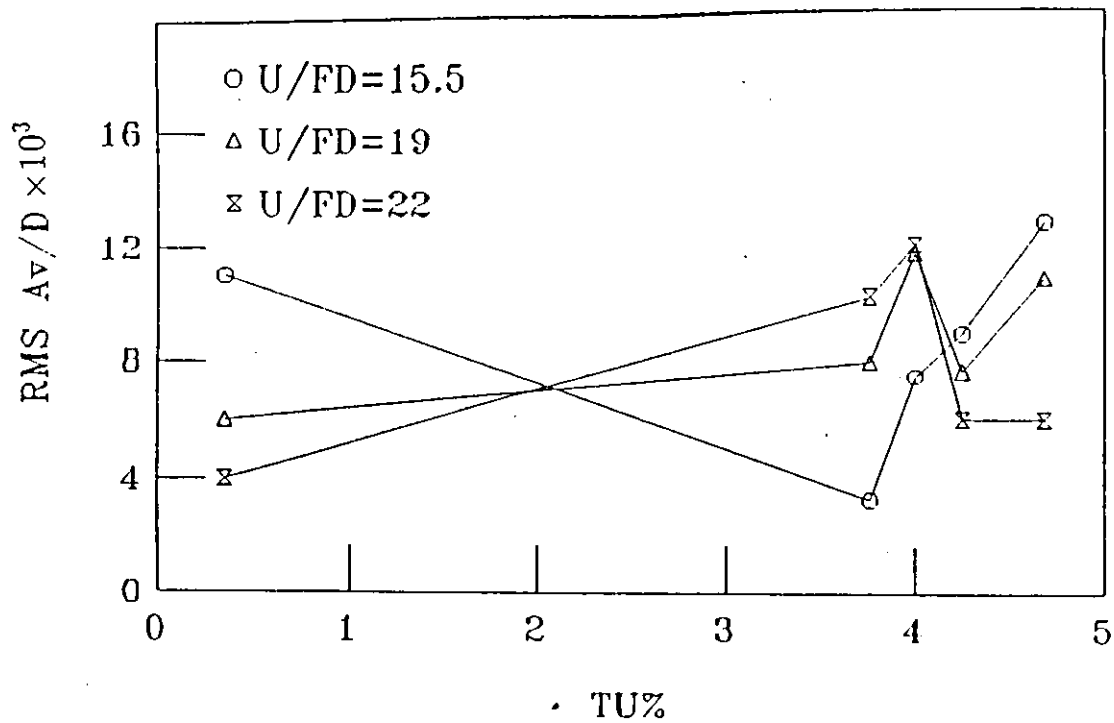
Fig(4-25). Variation of transverse vibration amplitude versus gap spacing for tandem arrangement; $U/FD = 22.0$.



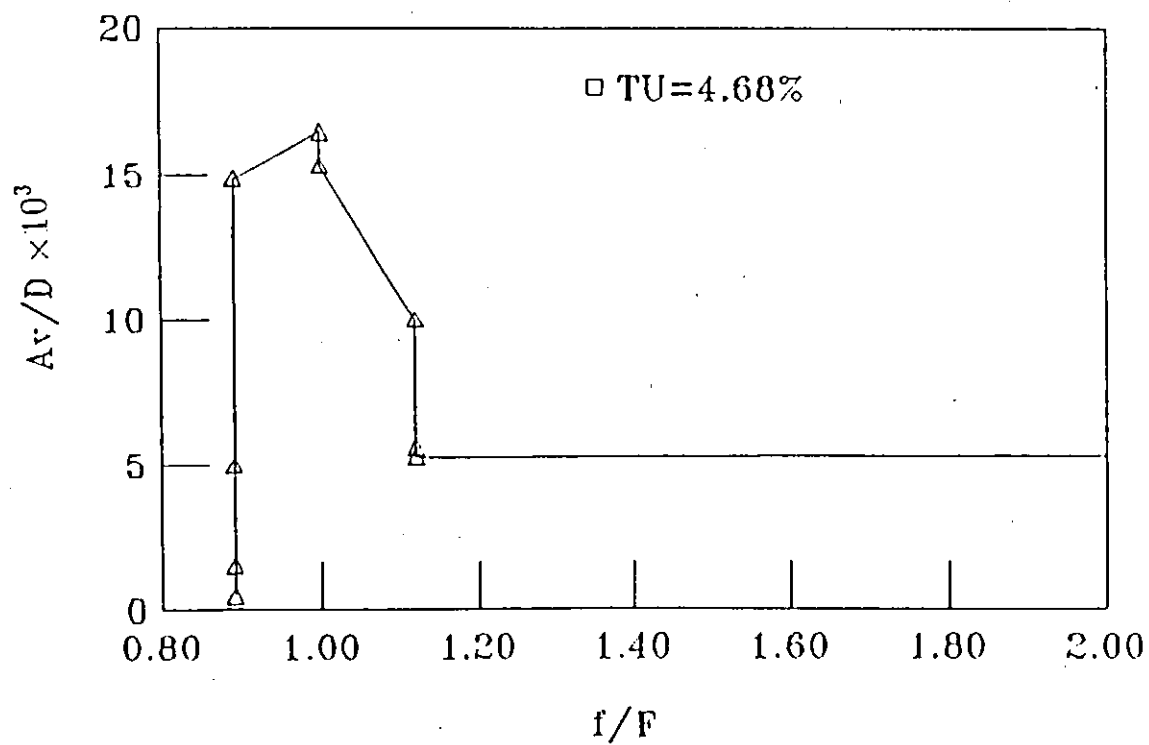
Fig(4-26). Variation of transverse vibration amplitude versus gap spacing for side-by-side arrangement; $U/FD = 22.0$.



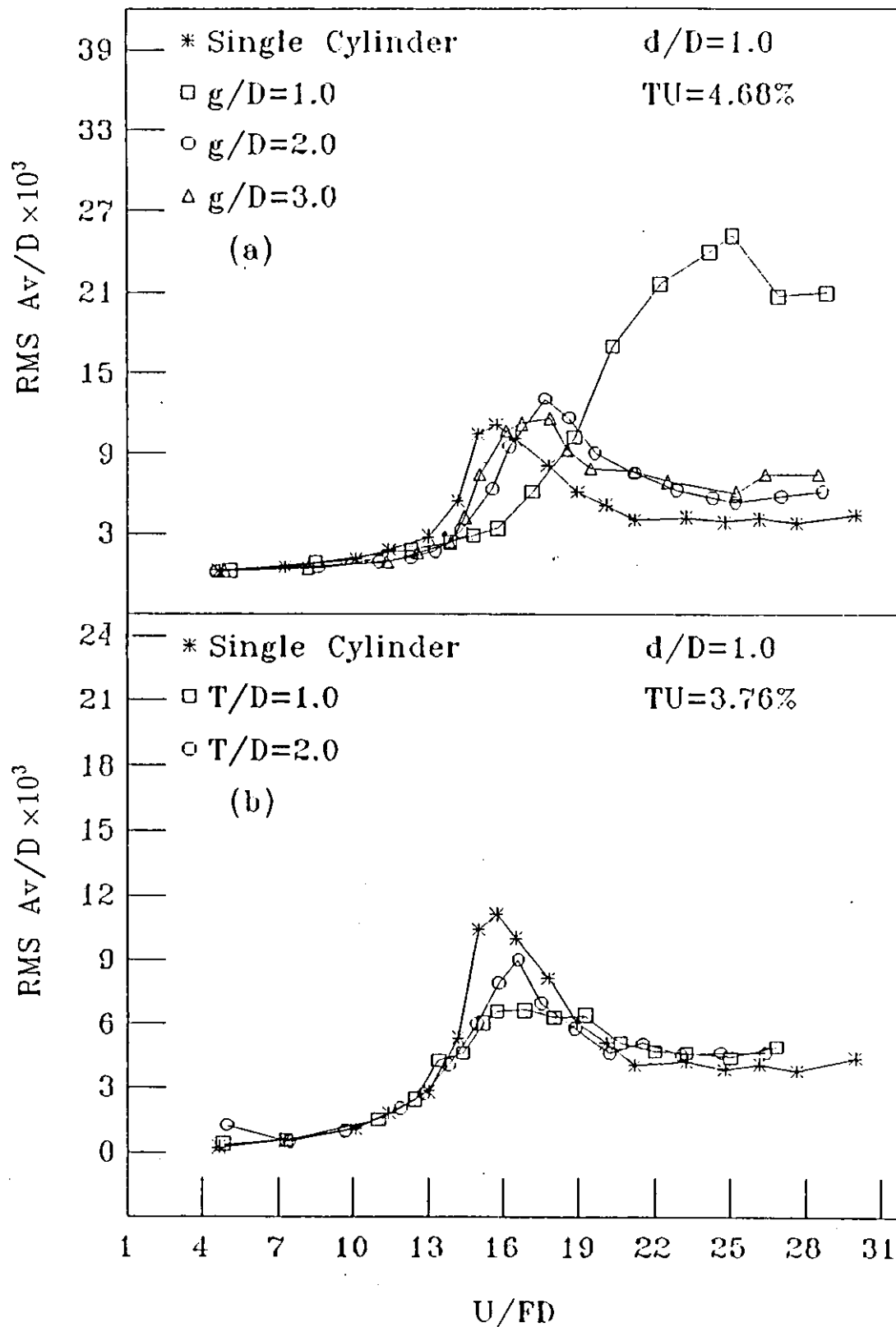
Fig(4-27). Effect of turbulence intensity on the flow-induced vibration of single cylinder; (a) transverse direction, (b) streamwise direction.



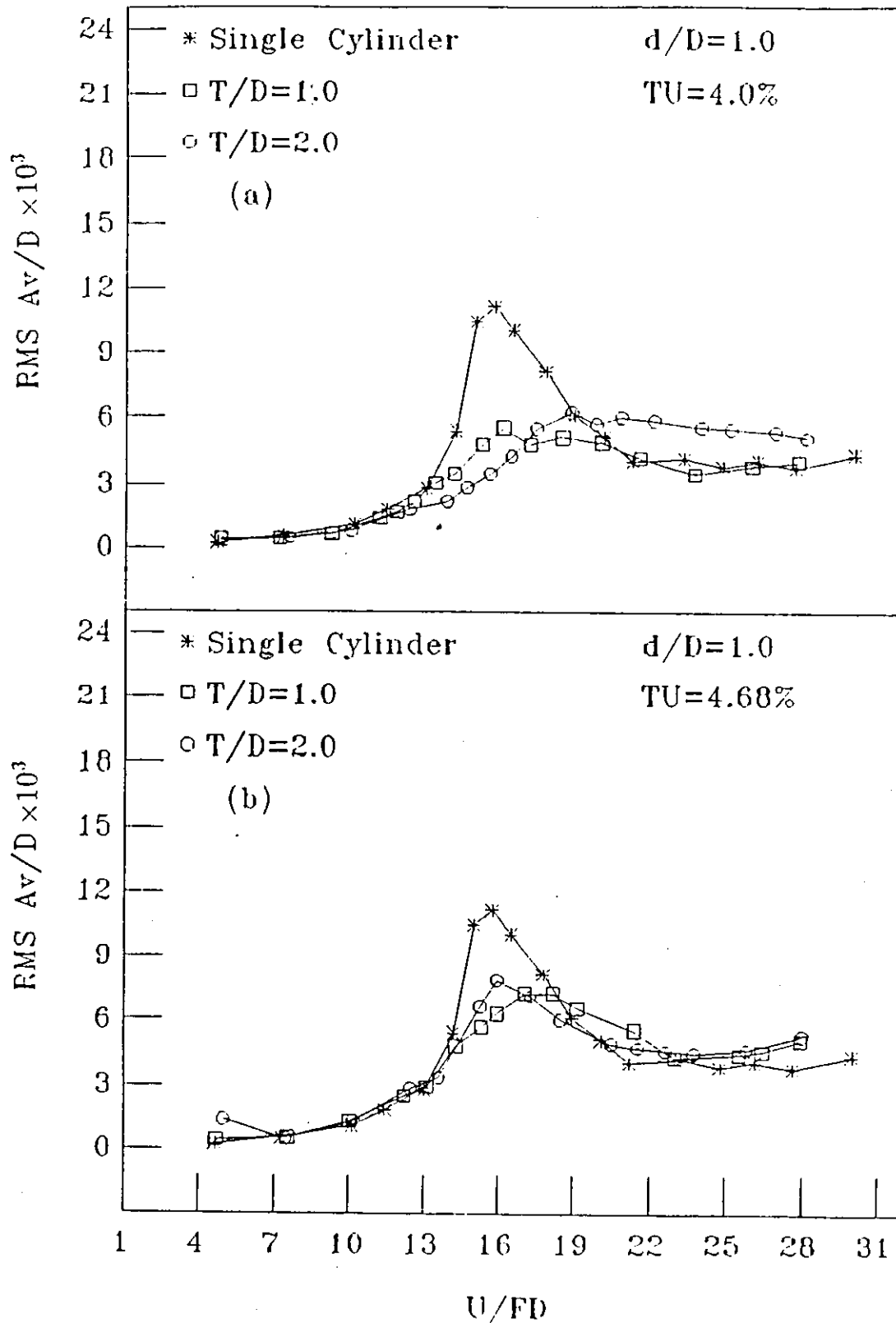
Fig(4-28). RMS vibration amplitude with turbulence intensity for single cylinder.



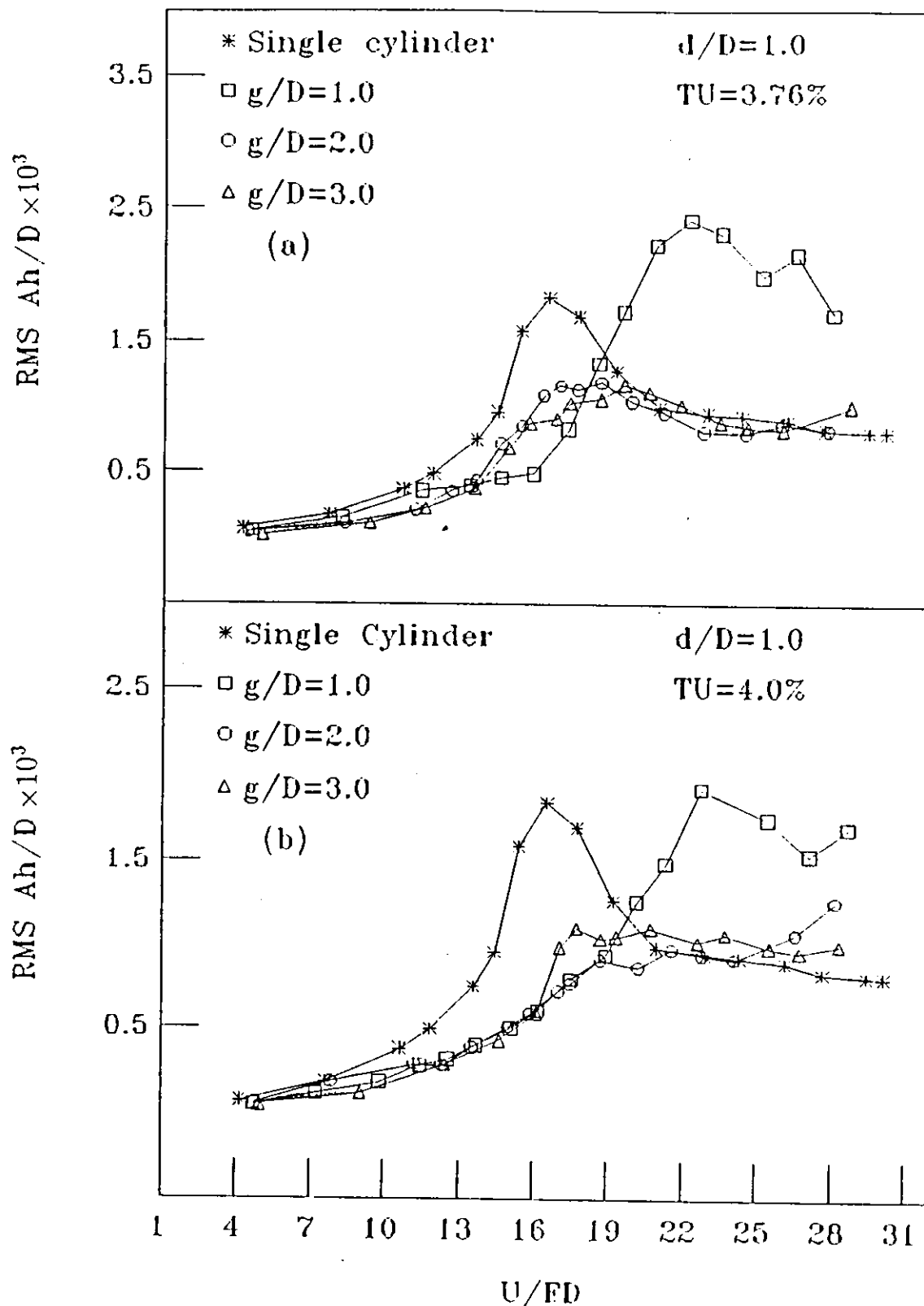
Fig(4-29). RMS vibration amplitude in the transverse direction with reduced frequency for single cylinder.



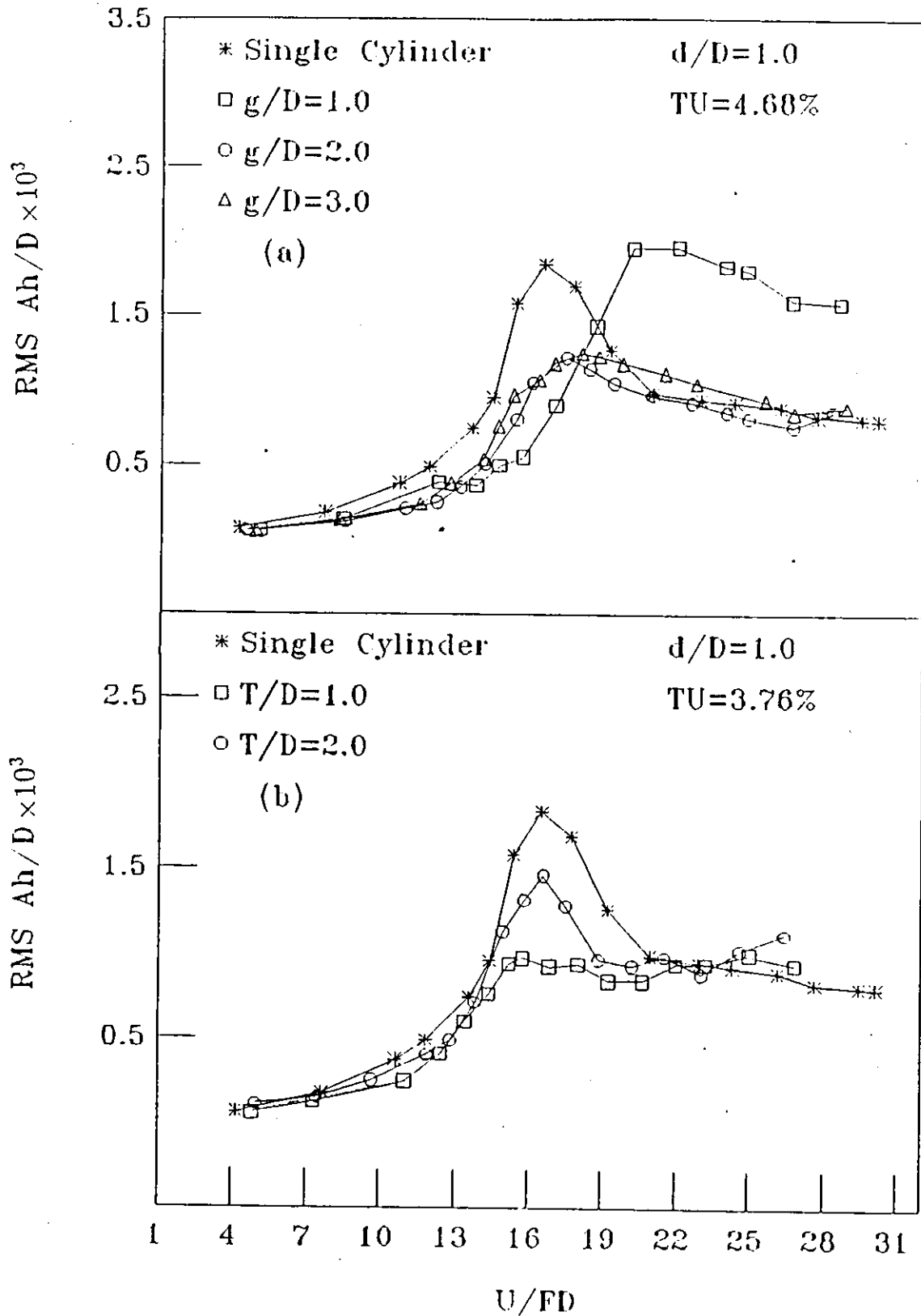
Fig(4-31). Effect of turbulence intensity in the transverse direction; $d/D = 1.0$, (a) tandem arrangement, (b) side-by-side arrangement.



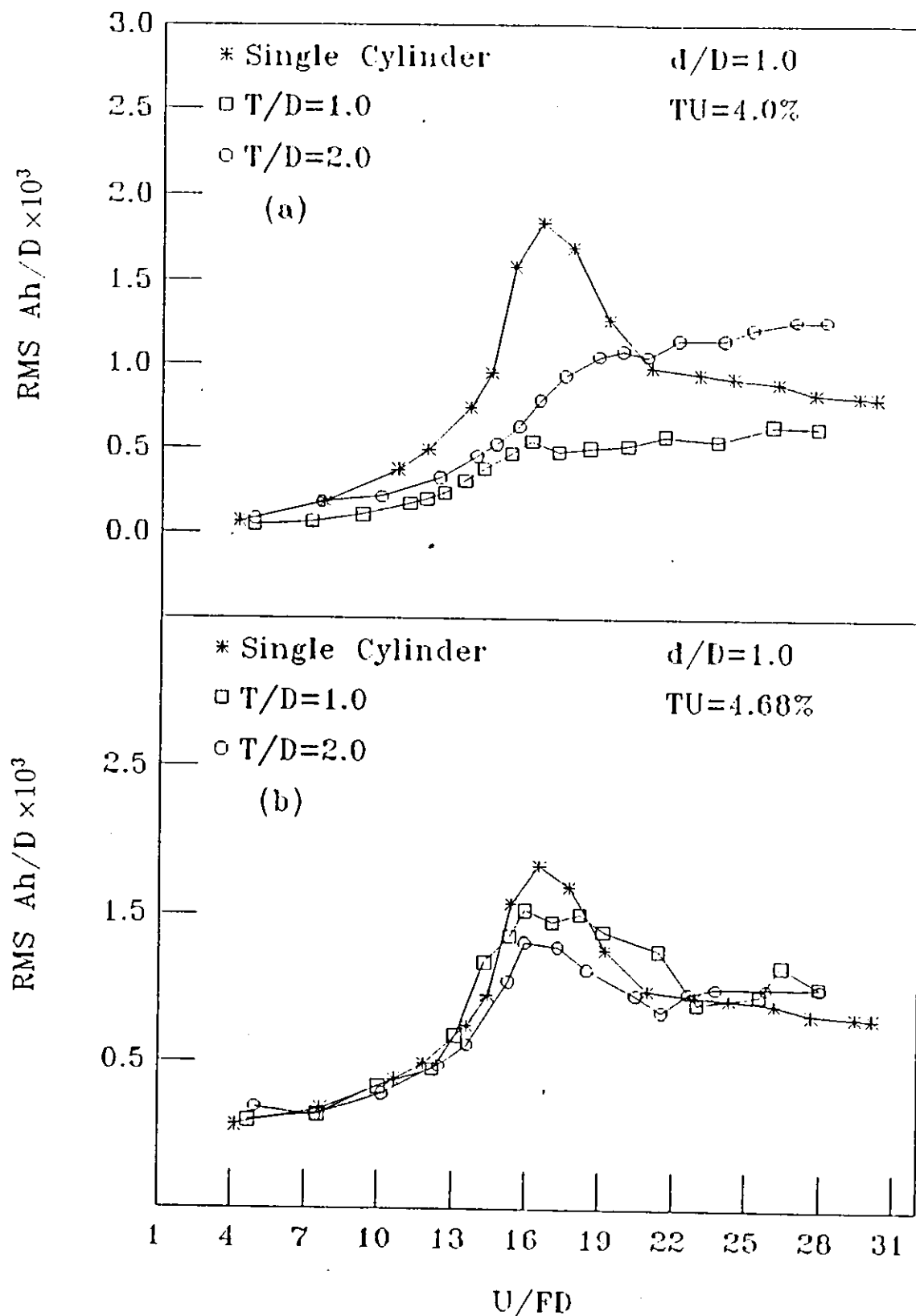
Fig(4-32). Effect of turbulence intensity in the transverse direction for side-by-side arrangement; $d/D = 1.0$, (a) $TU = 4.0\%$, (b) $TU = 4.68\%$.



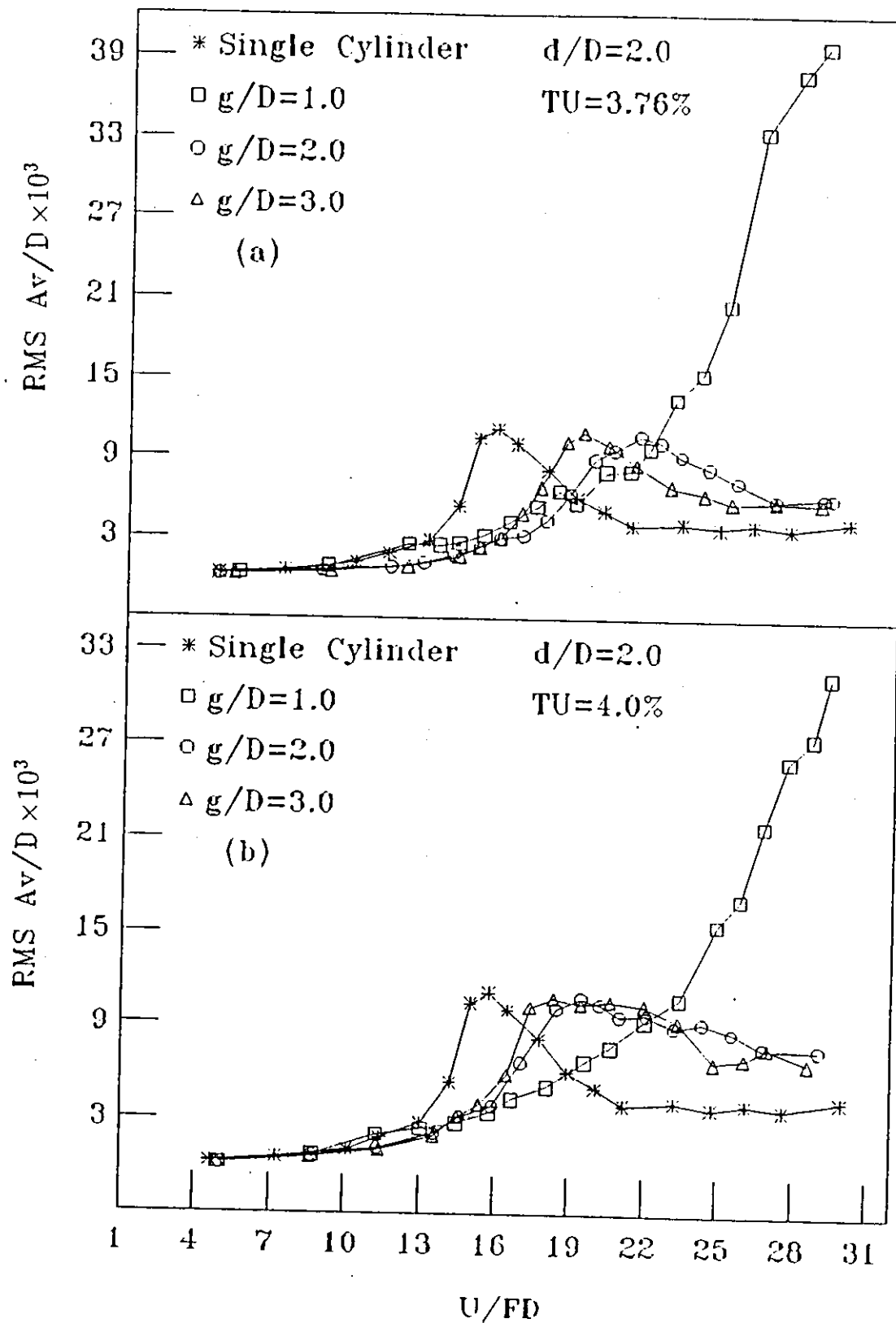
Fig(4-33). Effect of turbulence intensity in the streamwise direction for tandem arrangement; $d/D = 1.0$, (a) $TU = 3.76\%$, (b) $TU = 4.0\%$.



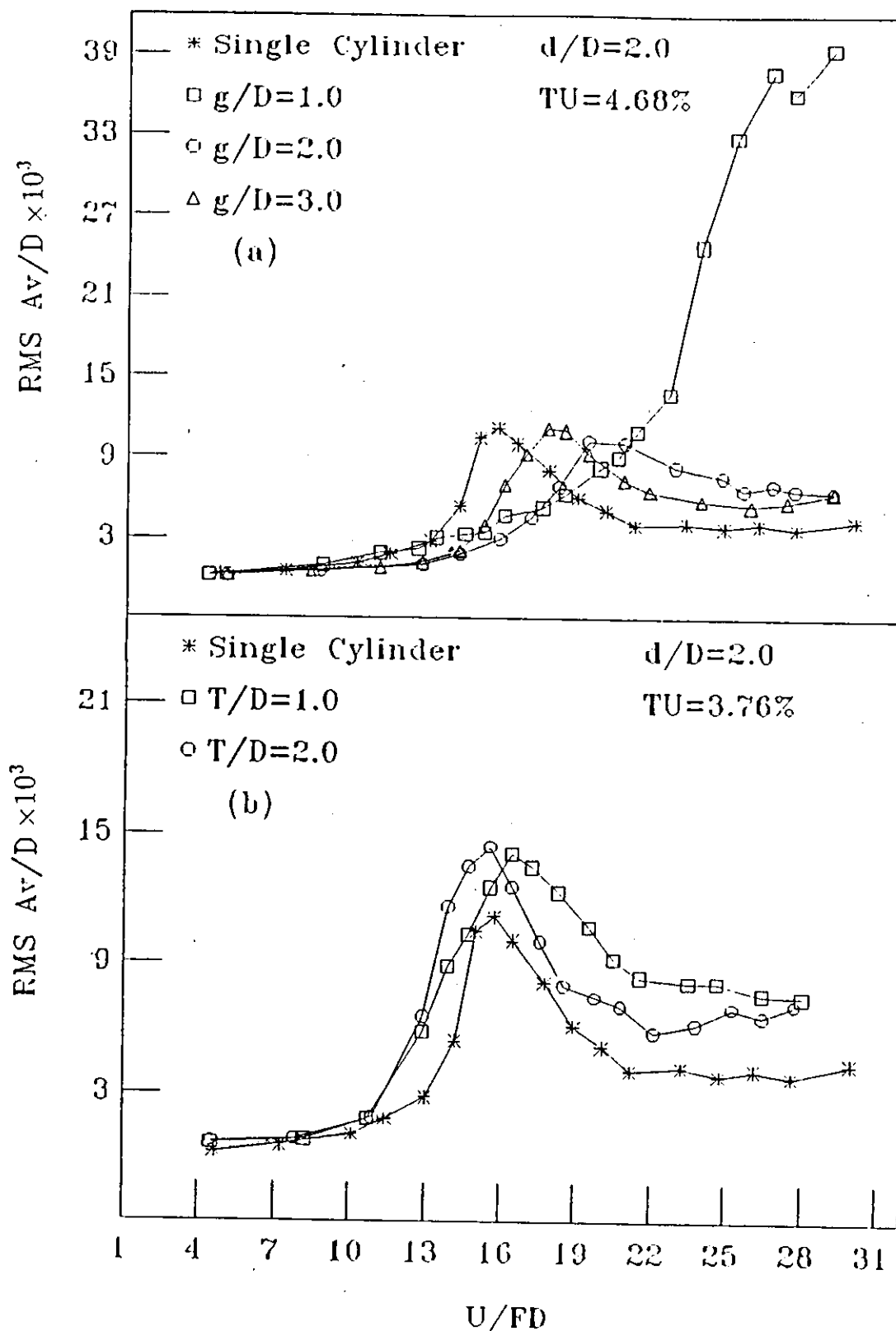
Fig(4-34). Effect of turbulence intensity in the streamwise direction; $d/D = 1.0$,
 (a) tandem arrangement $TU = 4.68\%$, (b) side-by-side arrangement $TU = 3.76\%$.



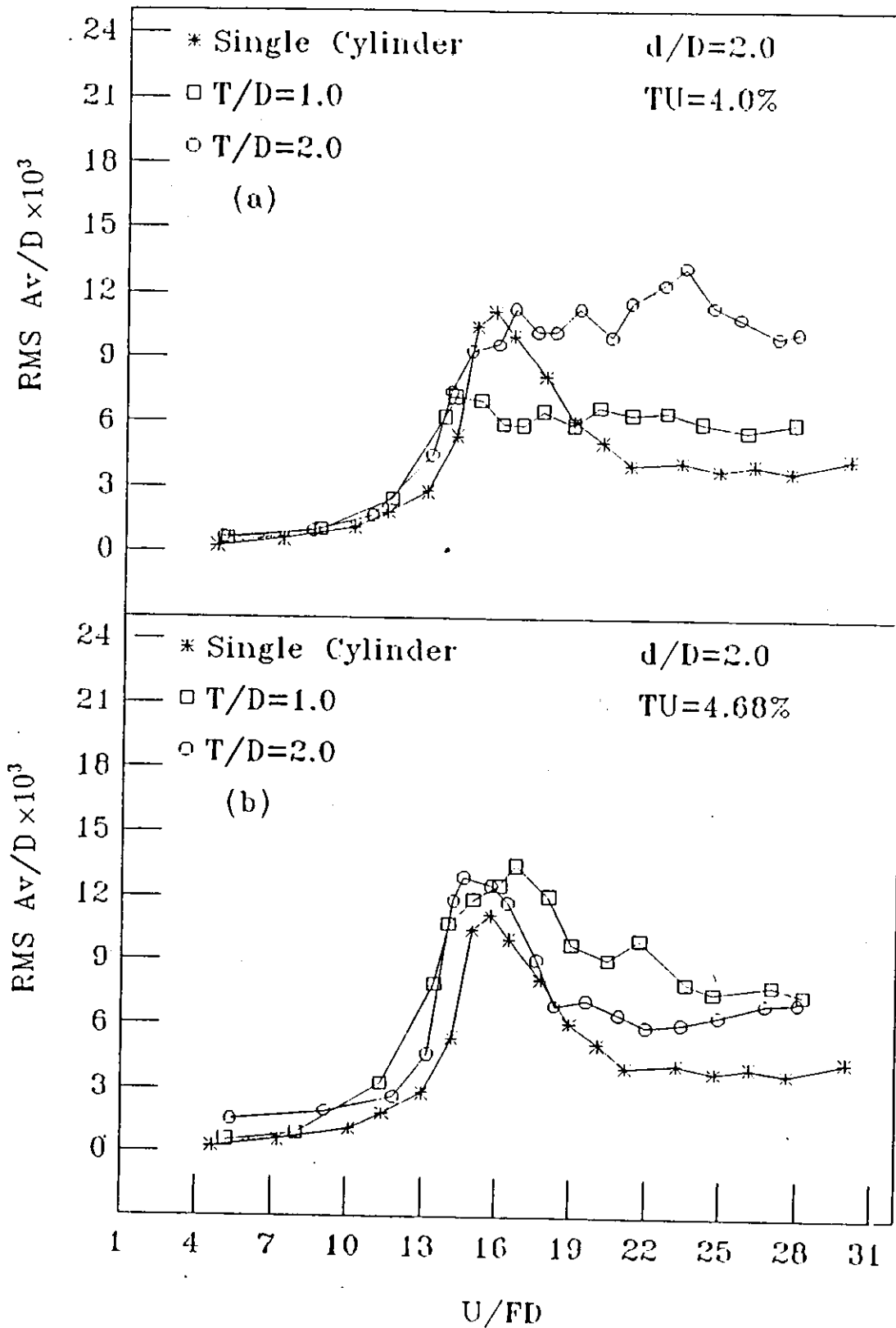
Fig(4-35). Effect of turbulence intensity in the streamwise direction for side-by-side arrangement; $d/D = 1.0$, (a) $TU = 4.0\%$, (b) $TU = 4.68\%$.



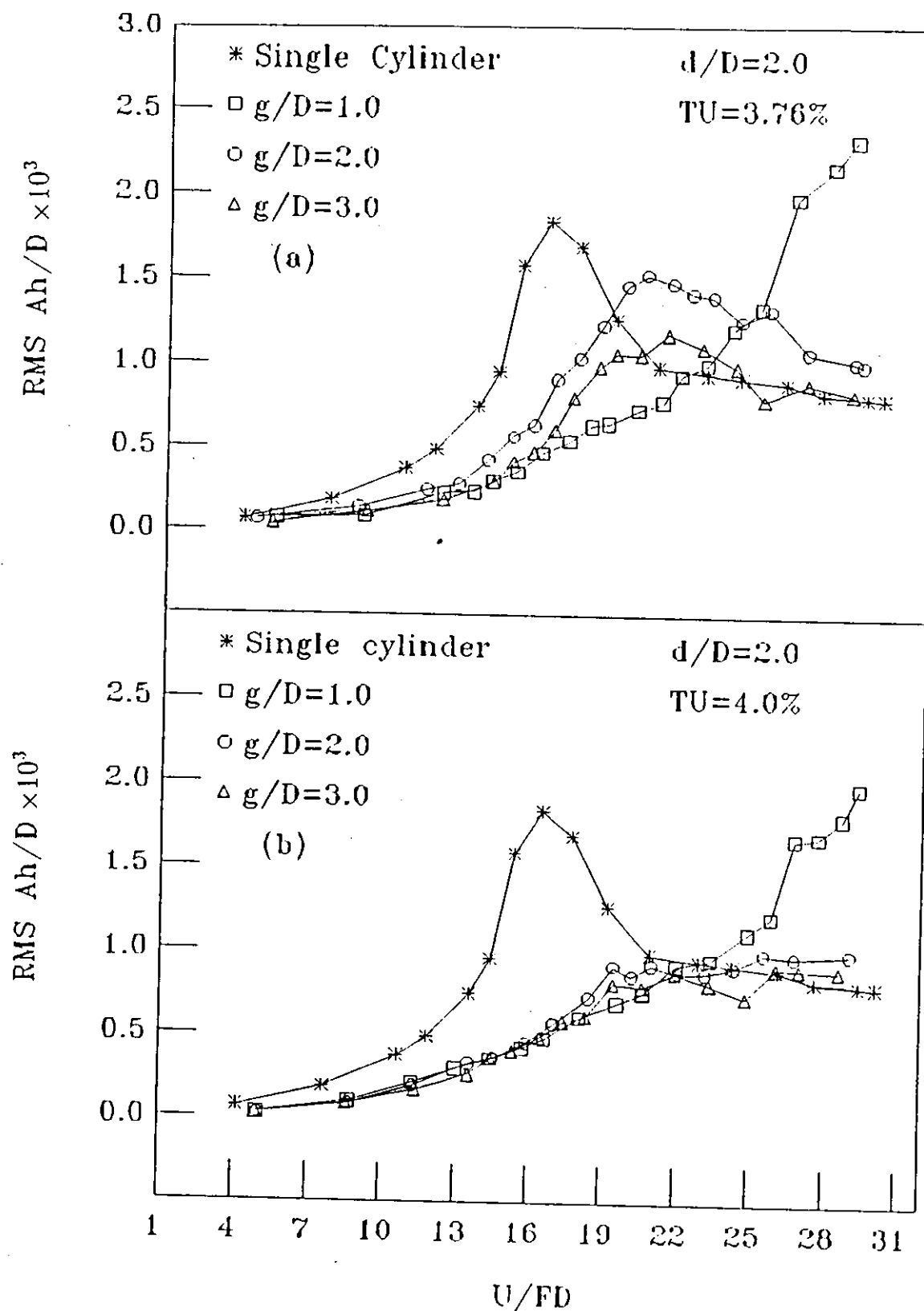
Fig(4-36). Effect of turbulence intensity in the transverse direction for tandem arrangement; $d/D = 2.0$, (a) $TU = 3.76\%$, (b) $TU = 4.0\%$.



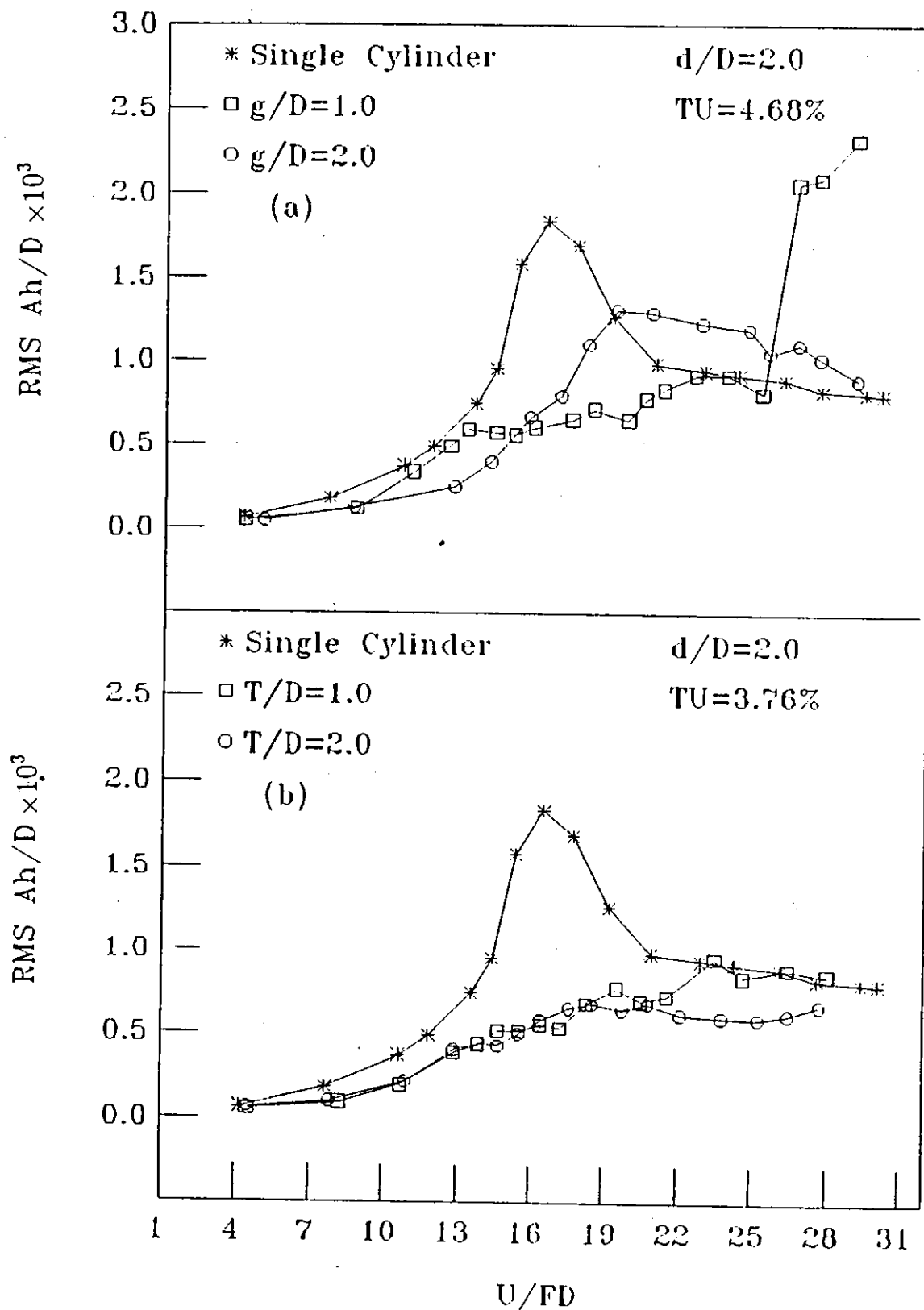
Fig(4.37). Effect of turbulence intensity in the transverse direction; $d/D = 2.0$, (a) tandem arrangement $TU = 4.68\%$, (b) side-by-side arrangement $TU = 3.76\%$.



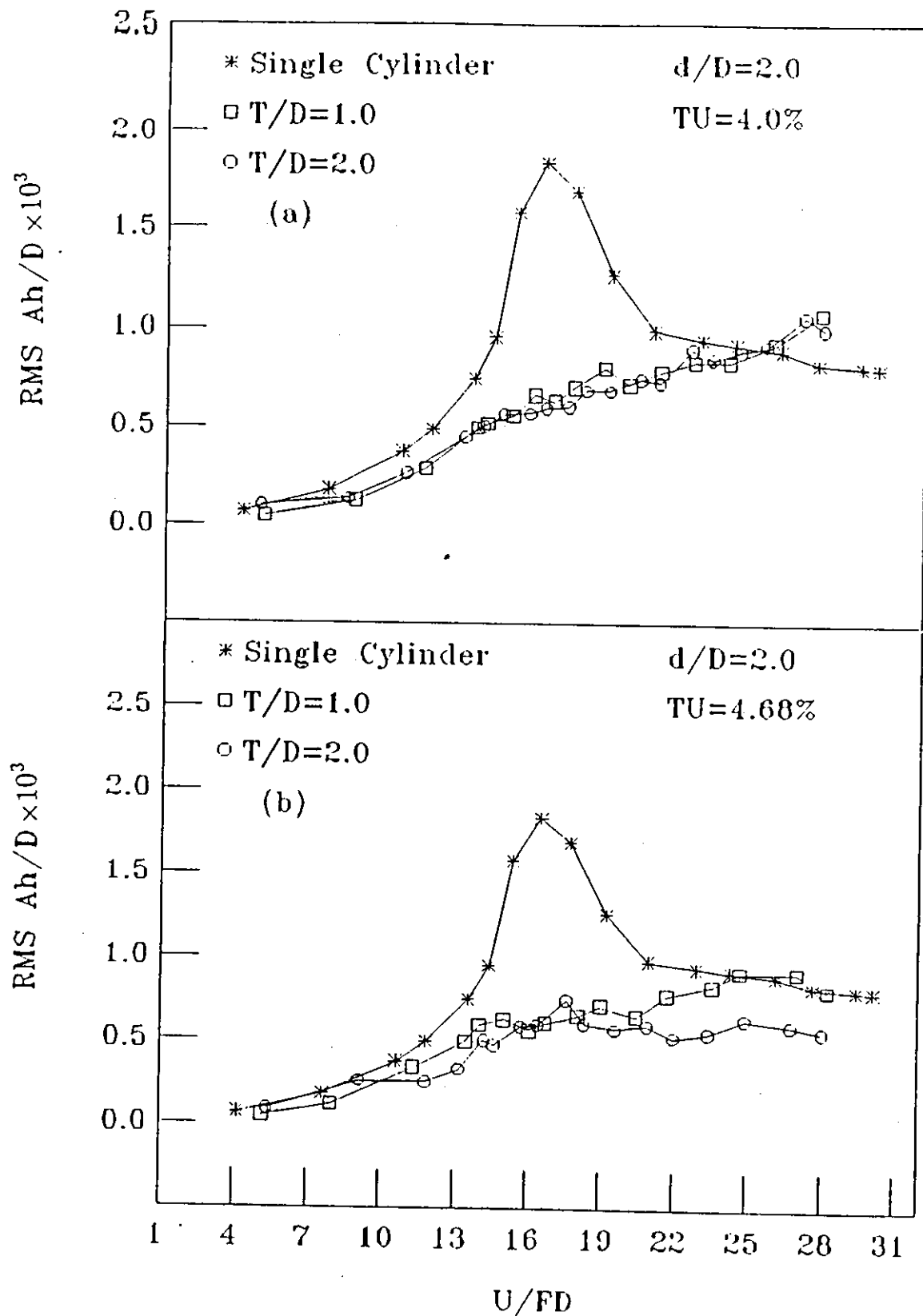
Fig(4-38). Effect of turbulence intensity in the transverse direction for side-by-side arrangement; $d/D = 2.0$, (a) $TU = 4.0\%$, (b) $TU = 4.68\%$.



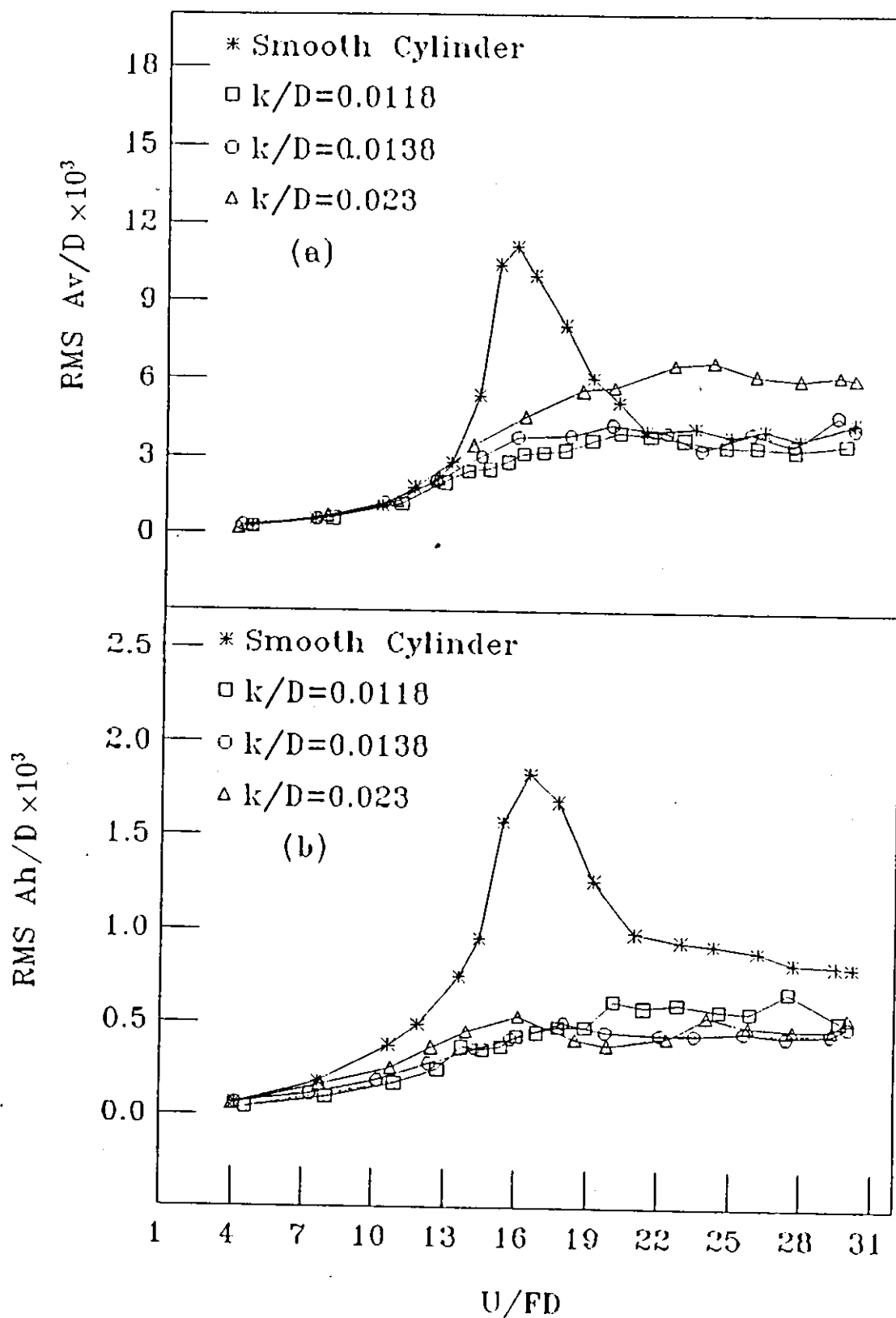
Fig(4-39). Effect of turbulence intensity in the streamwise direction for tandem arrangement; $d/D = 2.0$, (a) $TU = 3.76\%$, (b) $TU = 4.0\%$.



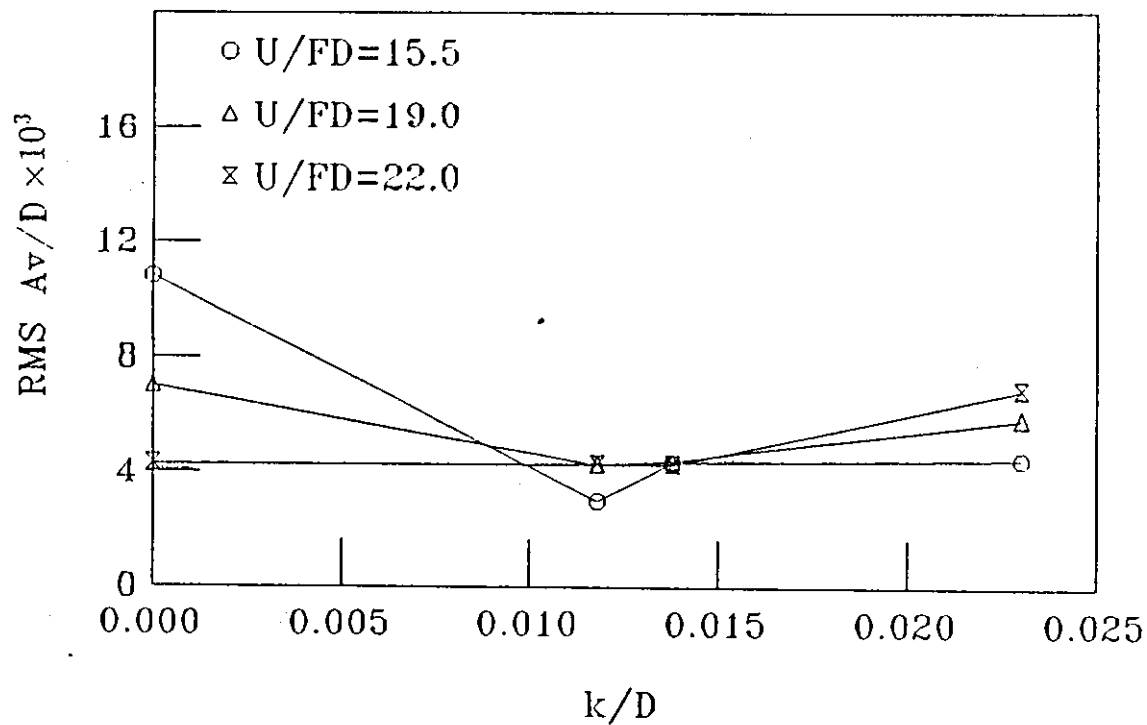
Fig(4-40). Effect of turbulence intensity in the streamwise direction; $d/D = 2.0$, (a) tandem arrangement $TU = 4.68\%$, (b) side-by-side arrangement $TU = 3.76\%$.



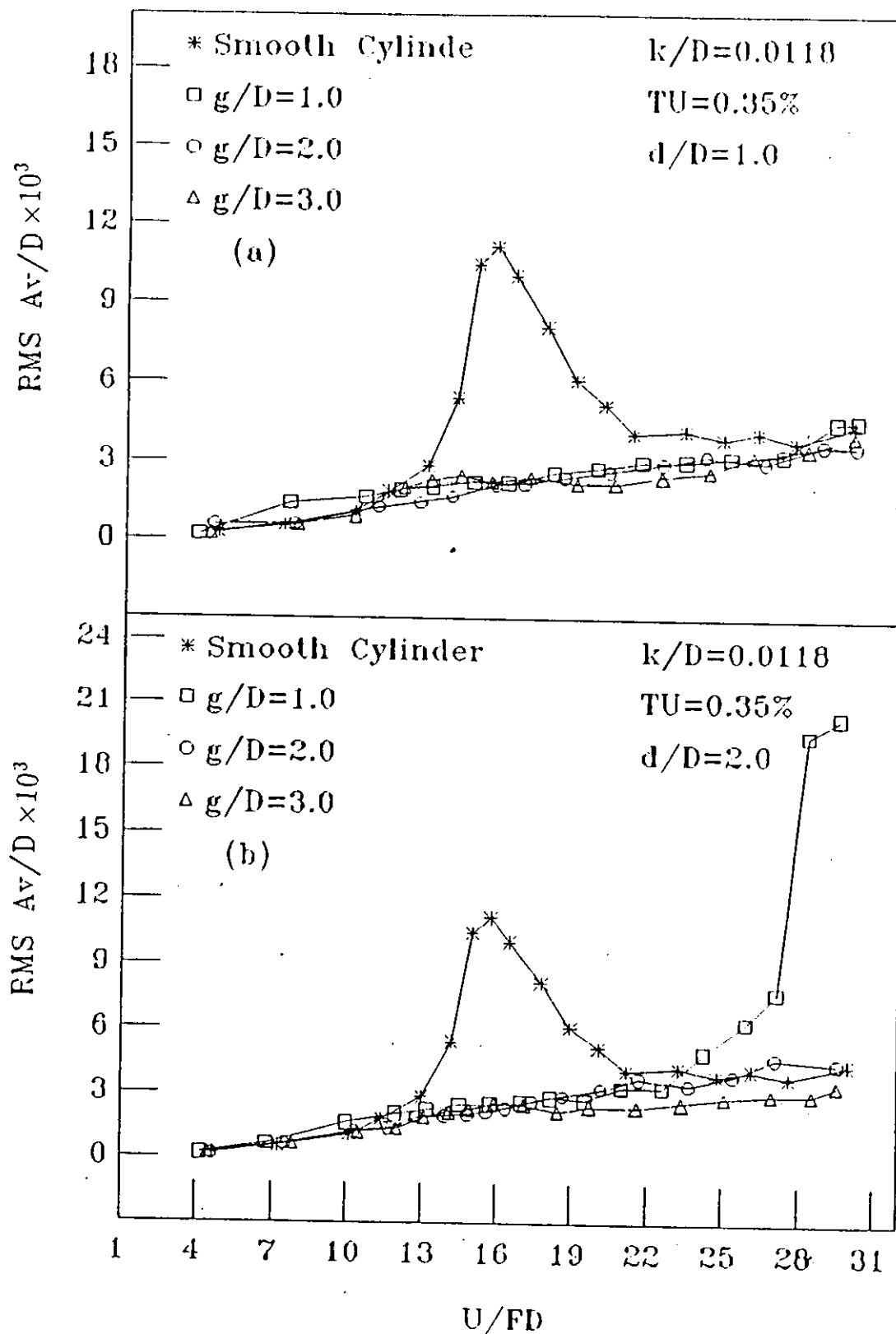
Fig(4-41). Effect of turbulence intensity in the streamwise direction for side-by-side arrangement; $d/D = 2.0$, (a) $TU = 4.0\%$, (b) $TU = 4.68\%$.



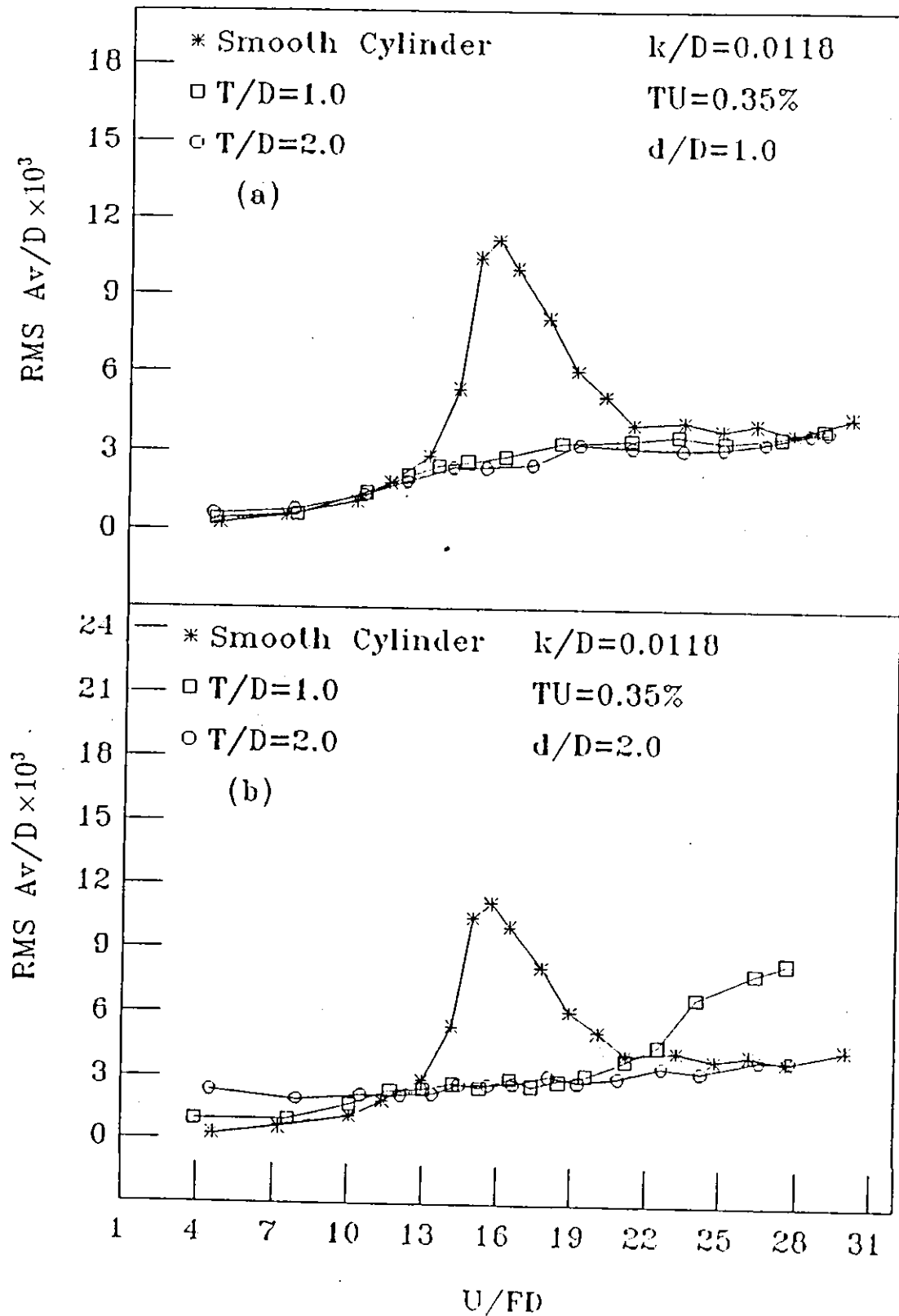
Fig(4-42). Effect of surface roughness on the flow-induced vibration of single cylinder; (a) transverse direction, (b) streamwise direction



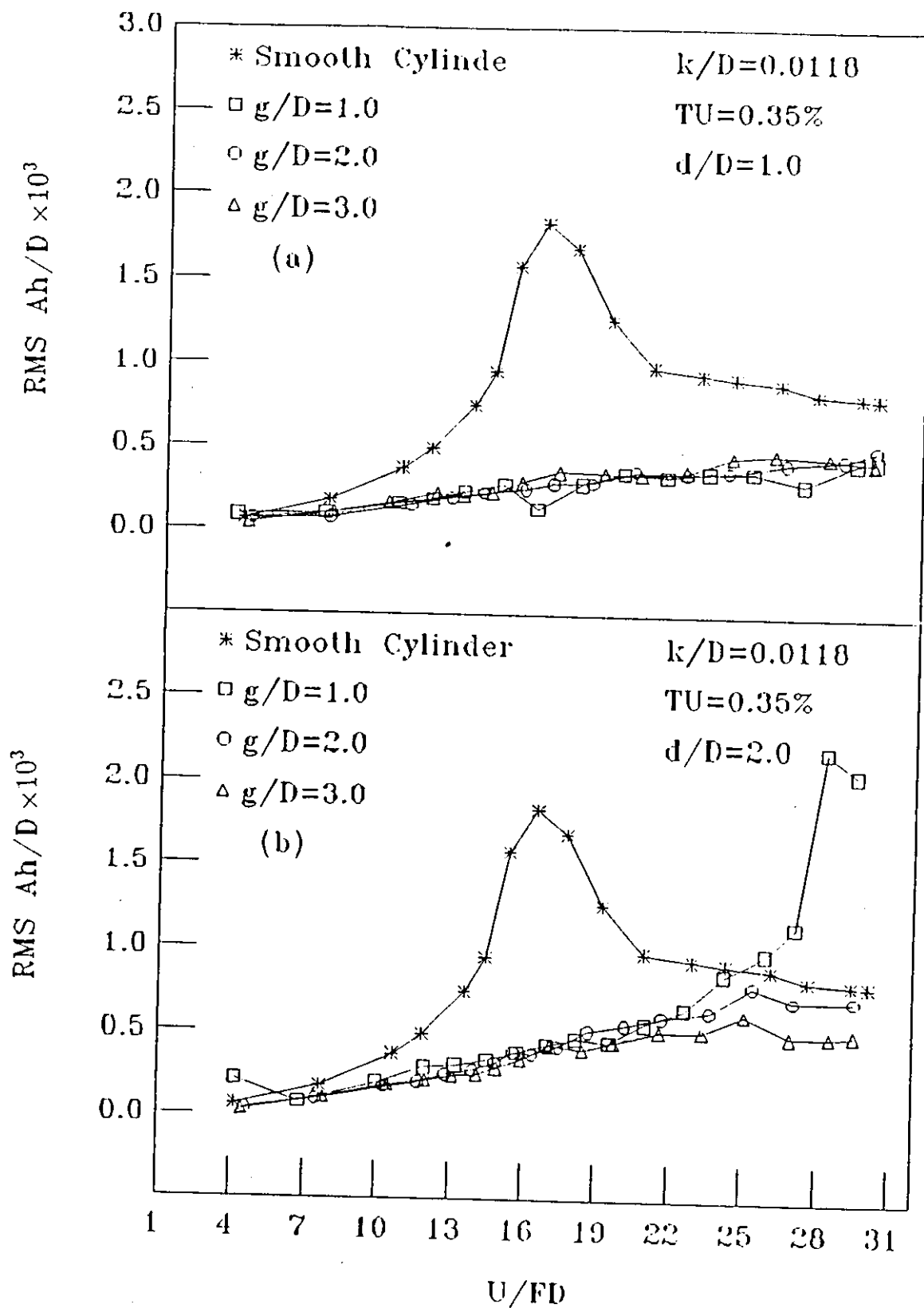
Fig(4-43). RMS vibration amplitude with roughness height (k/D) in the transverse direction.



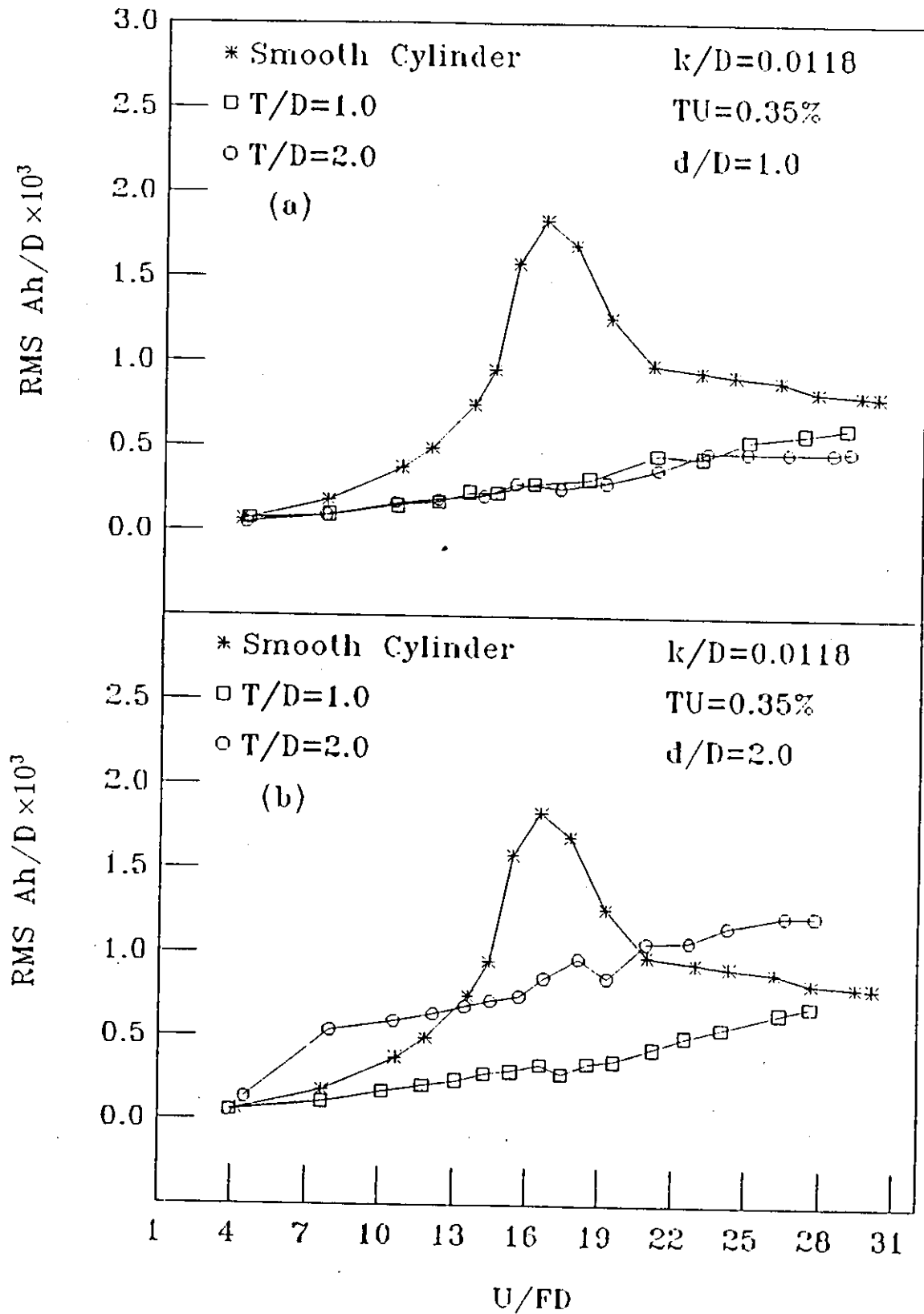
Fig(4-44). Effect of surface roughness in the transverse direction for tandem arrangement (a) $d/D = 1.0$, (b) $d/D = 2.0$.



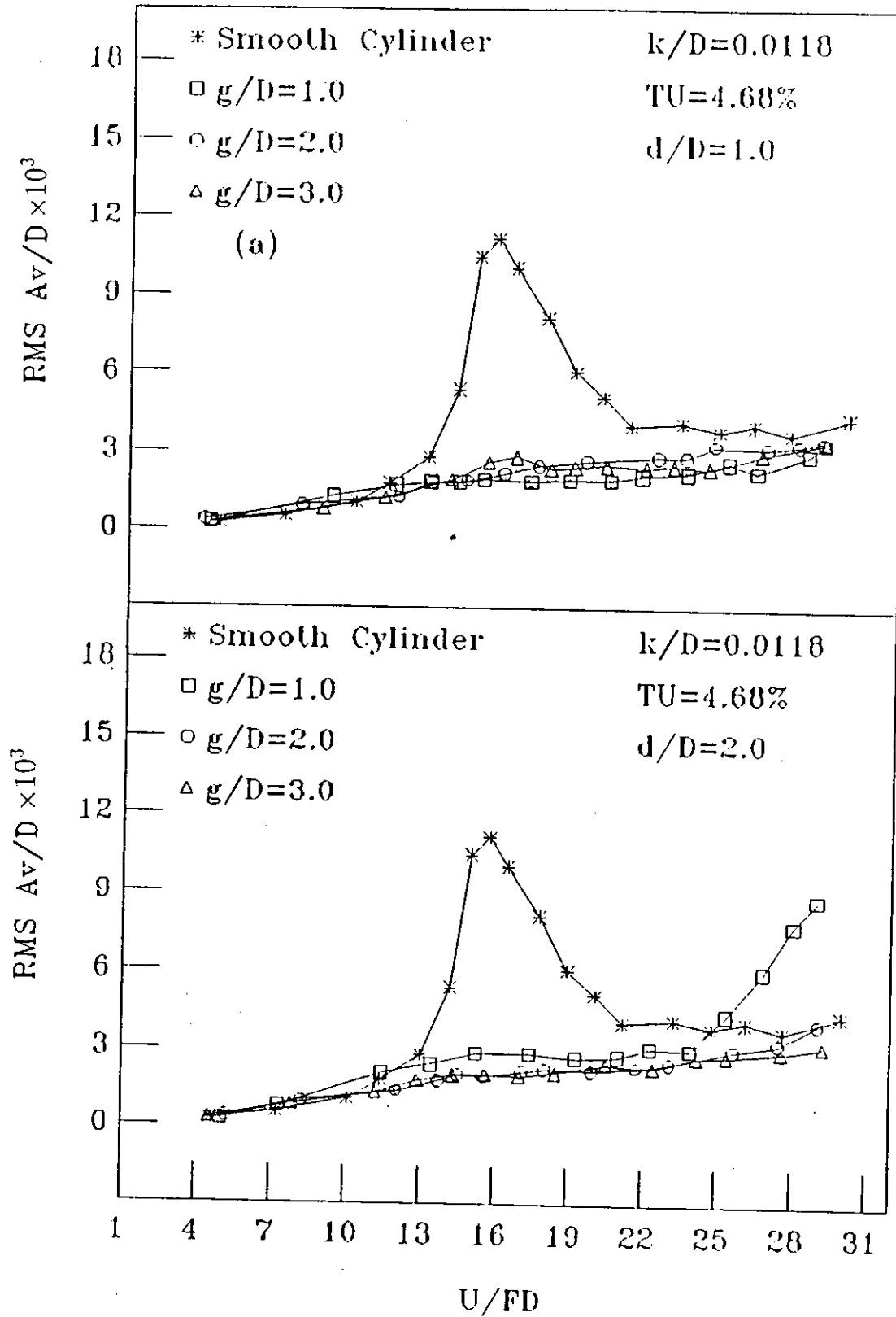
Fig(4-45). Effect of surface roughness in the transverse direction for side-by-side arrangement, (a) $d/D = 1.0$, (b) $d/D = 2.0$.



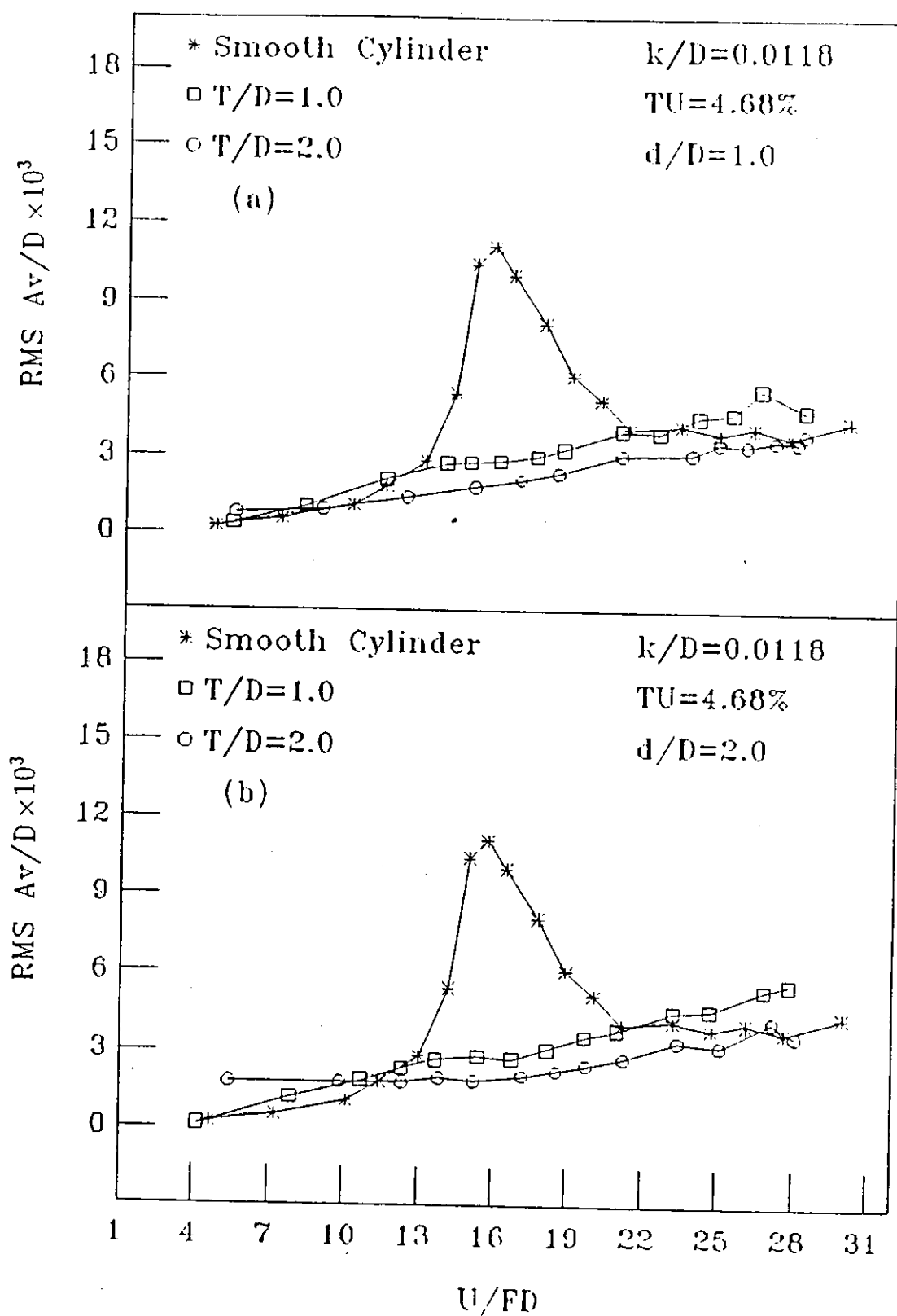
Fig(4-46). Effect of surface roughness in the streamwise direction for tandem arrangement, (a) $d/D = 1.0$, (b) $d/D = 2.0$.



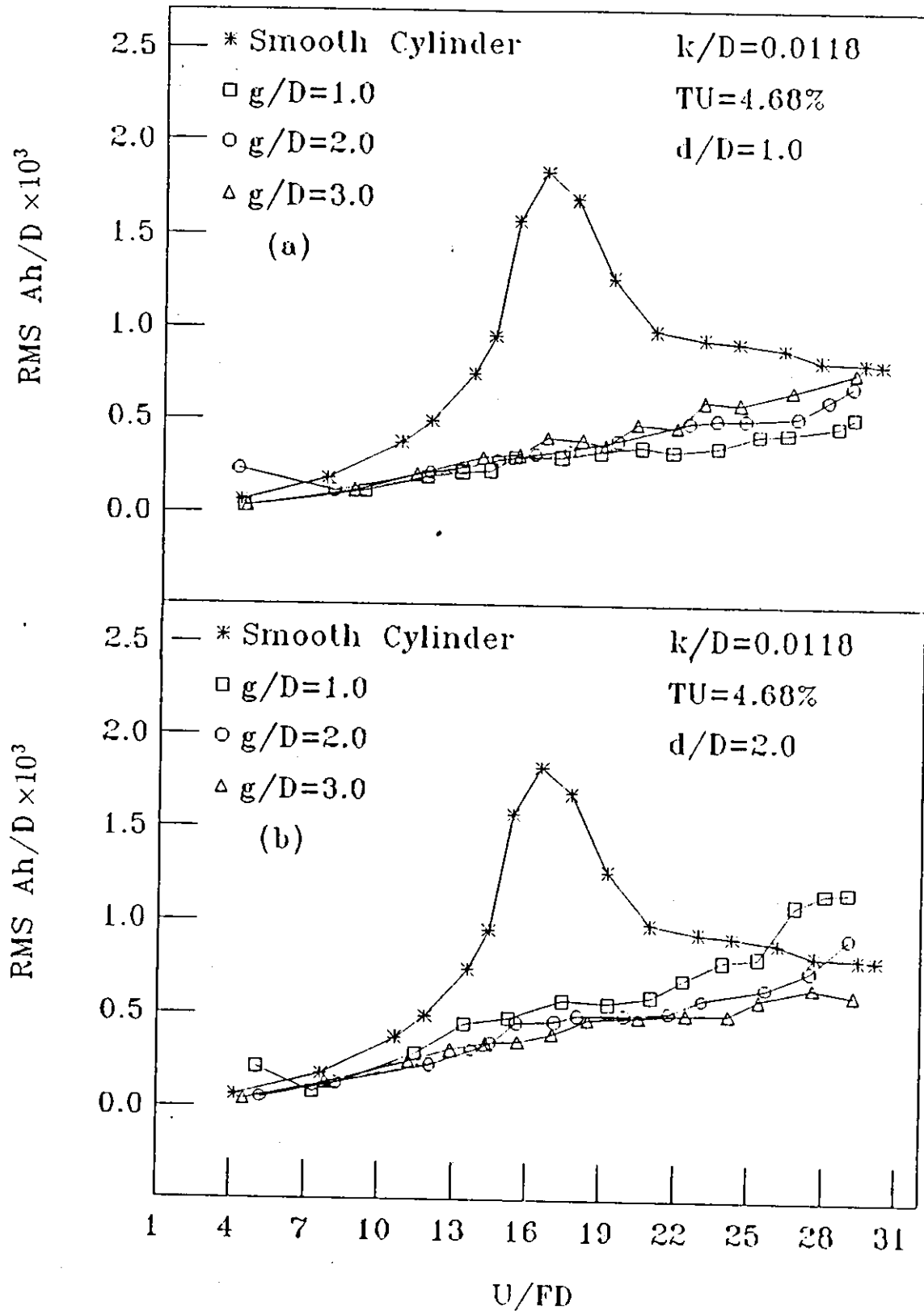
Fig(4-47). Effect of surface roughness in the streamwise direction for side-by-side arrangement, (a) $d/D = 1.0$, (b) $d/D = 2.0$.



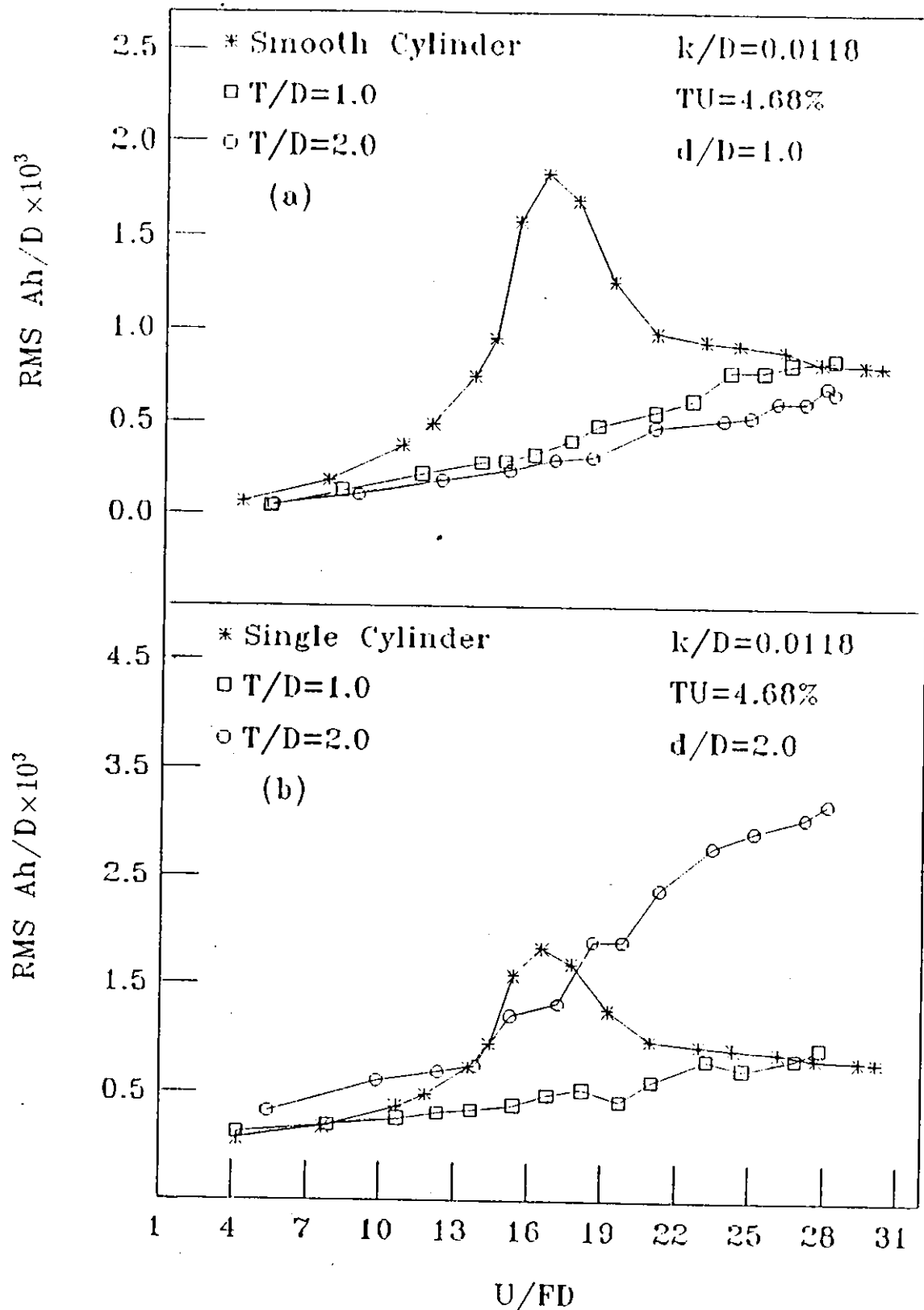
Fig(4-48). Effect of surface roughness and turbulence intensity in the transverse direction for tandem arrangement, (a) $d/D = 1.0$, (b) $d/D = 2.0$.



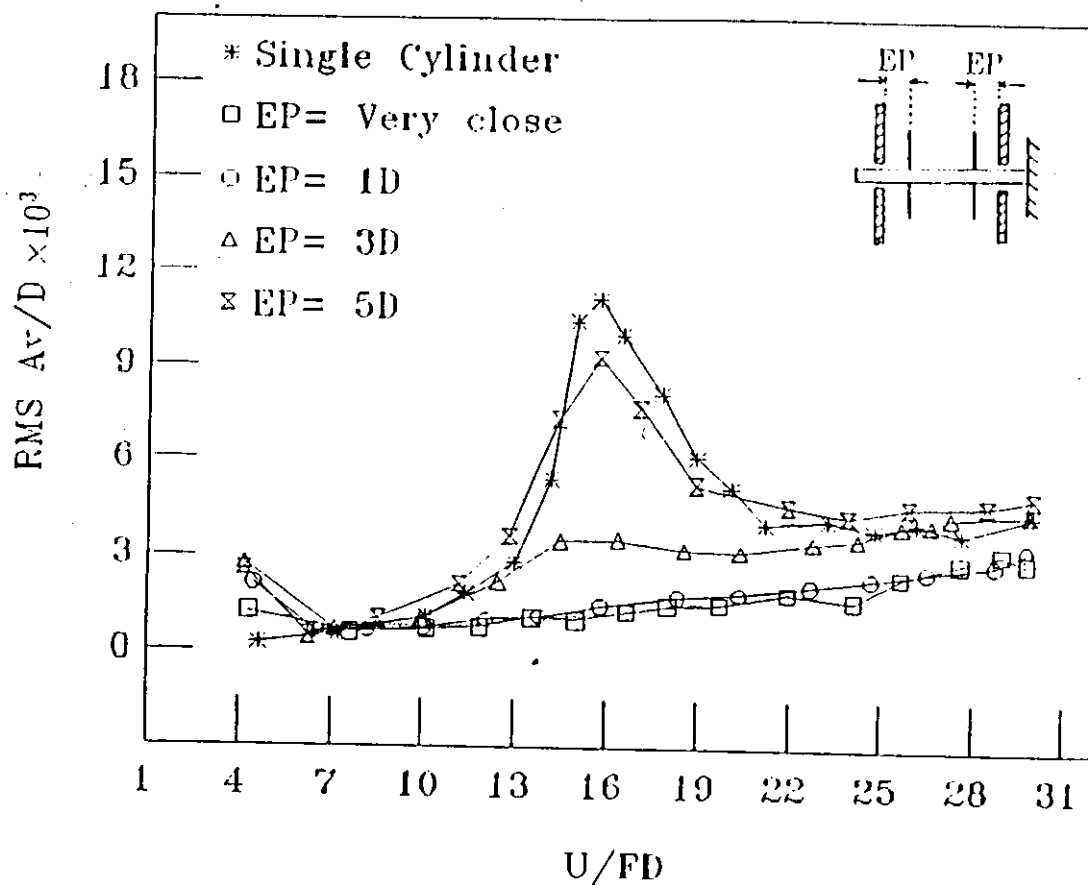
Fig(4-49). Effect of surface roughness and turbulence intensity in the transverse direction for side-by-side arrangement, (a) $d/D = 1.0$, (b) $d/D = 2.0$.



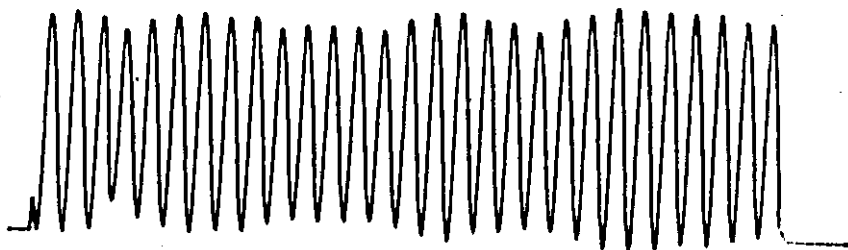
Fig(4-50). Effect of surface roughness and turbulence intensity in the streamwise direction for tandem arrangement, (a) $d/D = 1.0$, (b) $d/D = 2.0$.



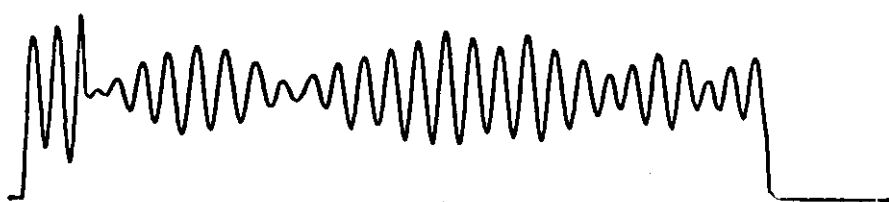
Fig(4-51). Effect of surface roughness and turbulence intensity in the streamwise direction for side-by-side arrangement, (a) $d/D = 1.0$, (b) $d/D = 2.0$.



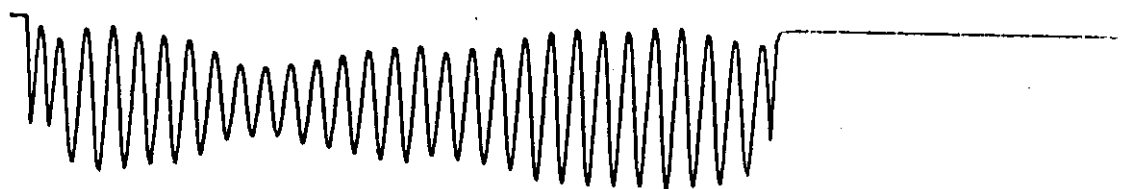
Fig(4-52). Effect of end plates on the flow-induced vibration of single cylinder.



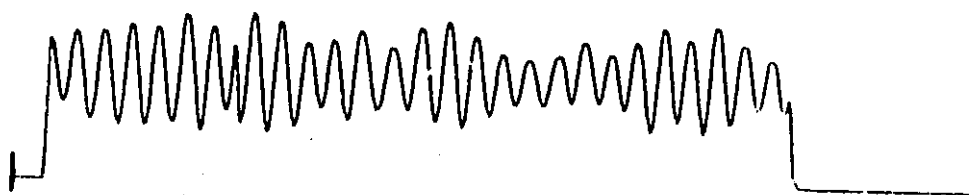
Fig(4-53). Signal wave form of the vibrating cylinder; $TU = 4.4\%$ and $U/FD = 15.55$



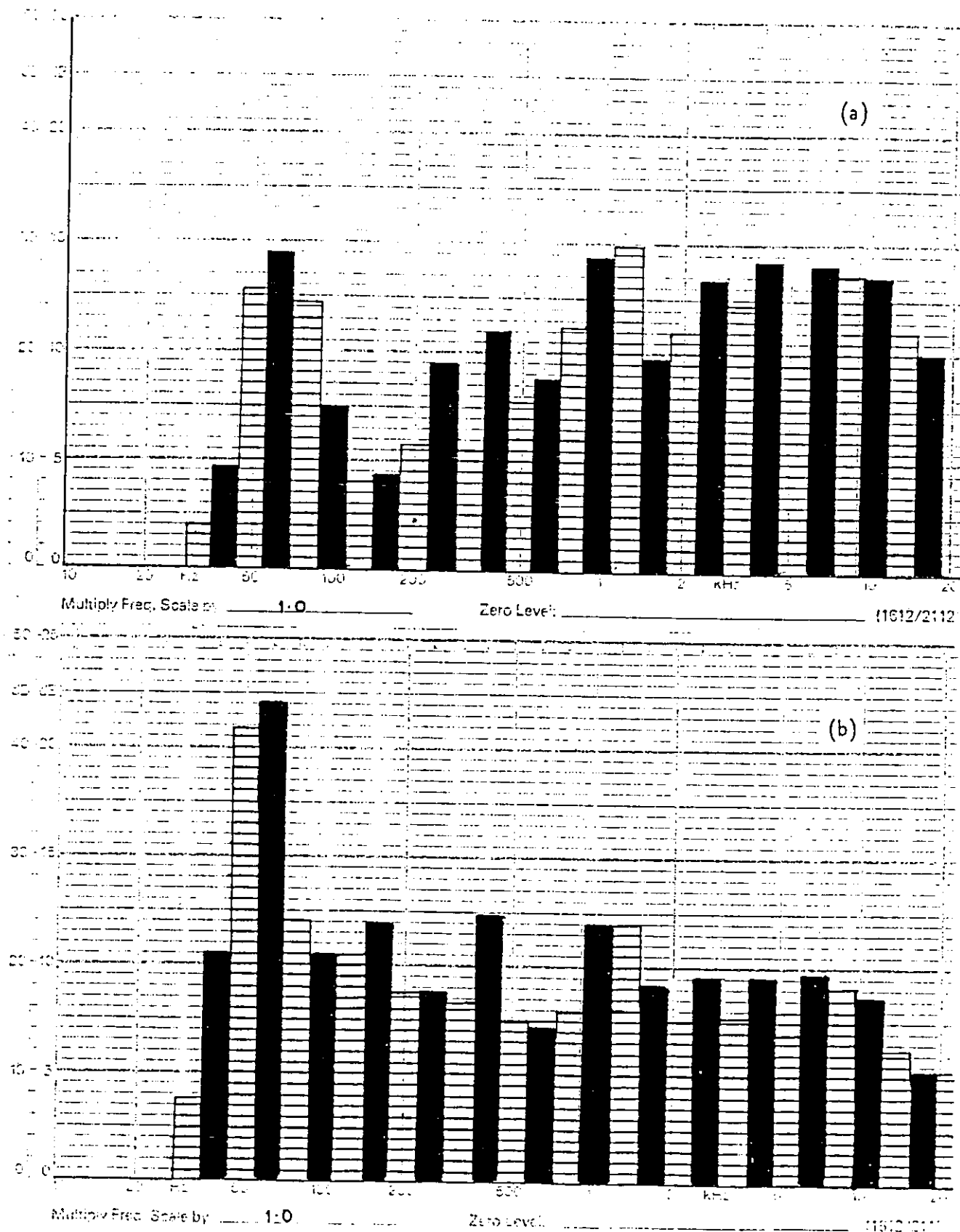
Fig(4-54). Signal wave form for side-by-side arrangement; $d/D = 2.0$, $T/D = 1.0$, $TU = 3.76\%$, and $U/FD = 13.14$



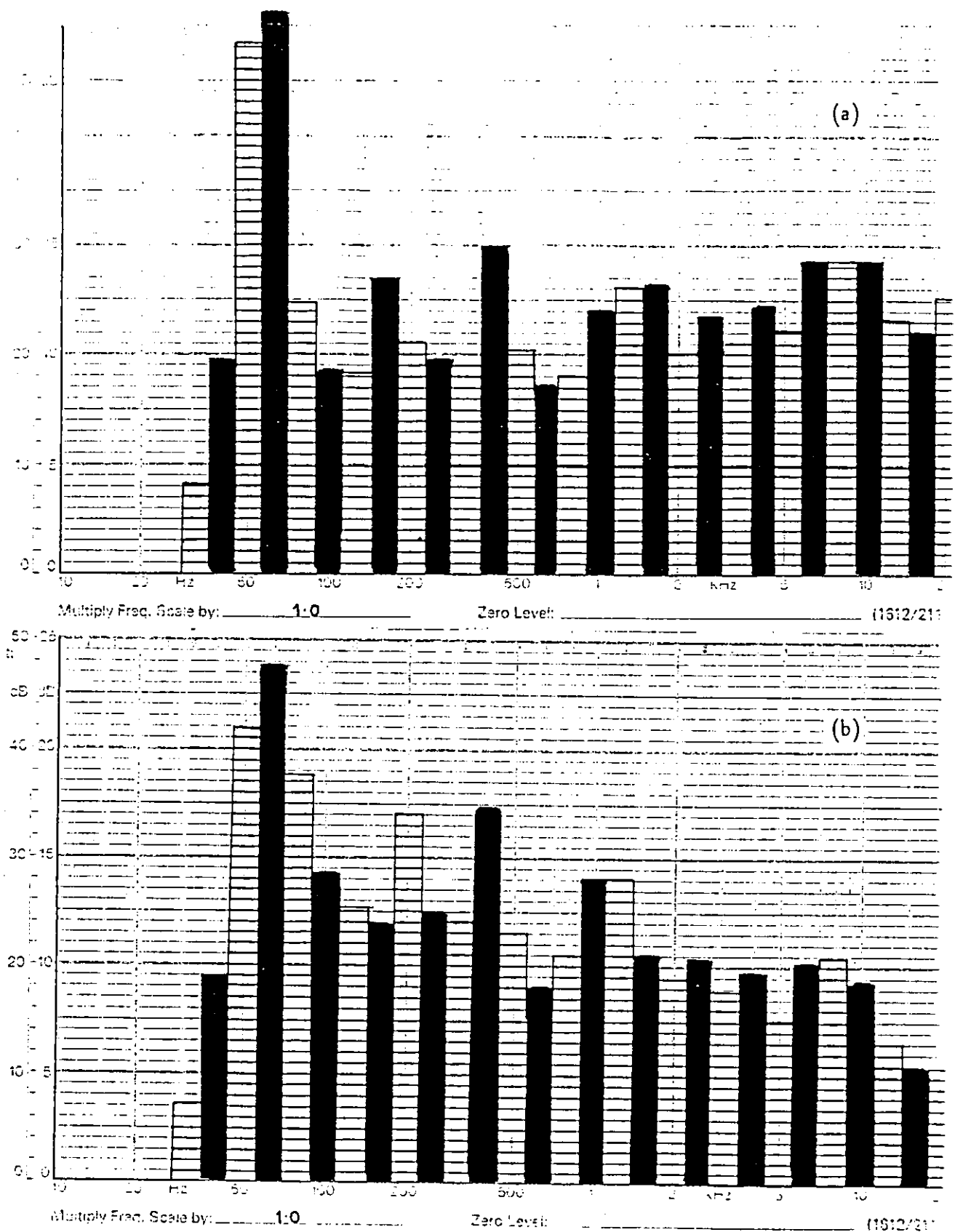
Fig(4-55). Signal wave form of the vibrating cylinder; $TU = 0.35\%$, $U/FD = 15.72$



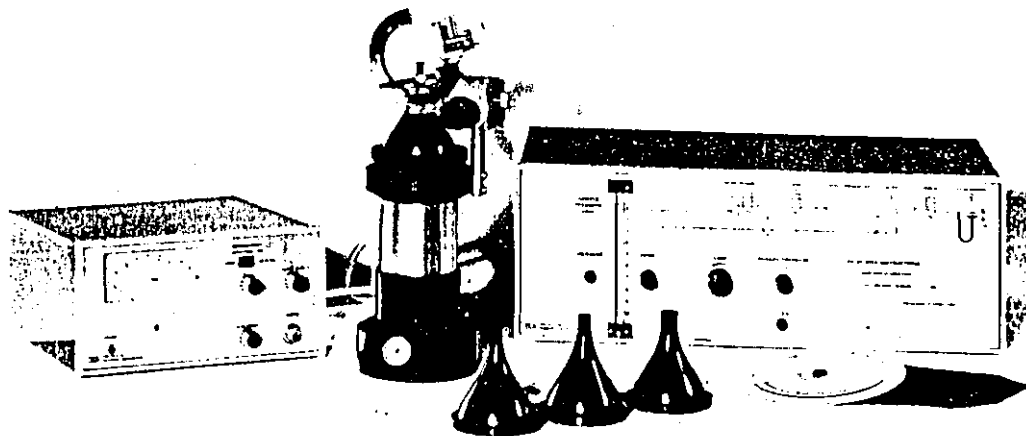
Fig(4-56). Signal wave form for tandem arrangement; $d/D = 2.0$, $g/D = 2.0$, $k/D = 0.0118$, $TU = 0.35\%$, $U/FD = 25.45$



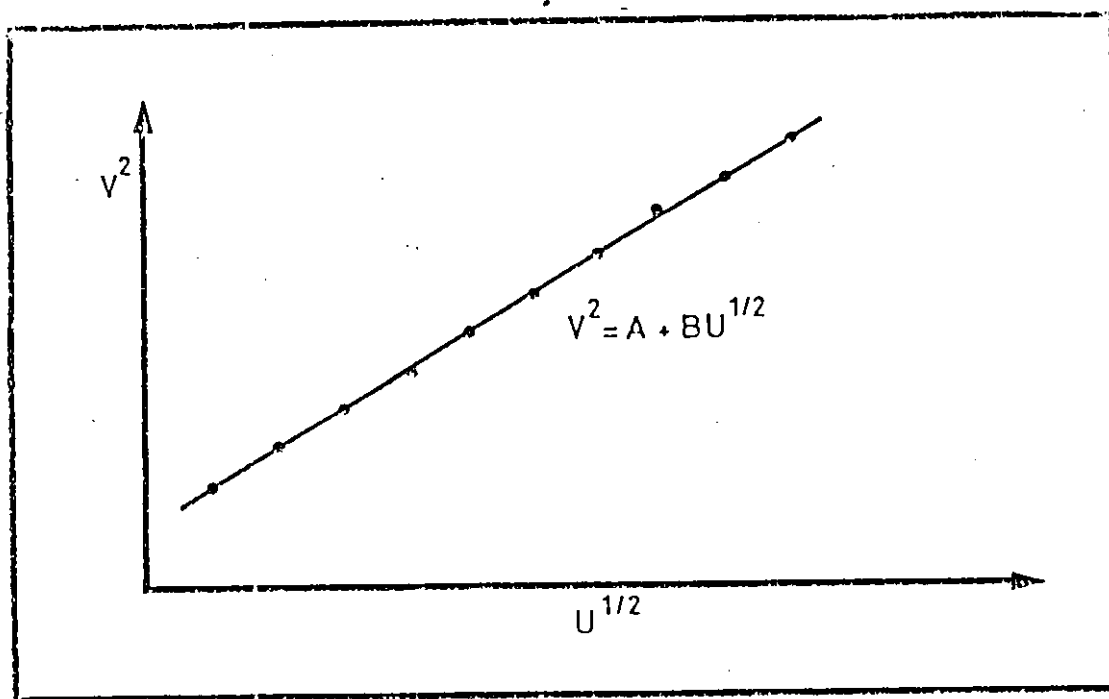
Fig(4-57). Frequency spectrum of the vibrating cylinder signal; (a) $U/FD = 7.65$,
 (b) $U/FD = 14.4$.



Fig(4-58). Frequency spectrum of the vibrating cylinder signal; (a) $U/FD = 15.38$,
 (b) $U/FD = 19.23$.



Fig(A-1). Calibration equipments.



Fig(A-2). Typical calibration curve

392970

ملخص الرسالة باللغة العربية

تتمثل أهمية هذه الدراسة في المساعدة على تصميم المنشآت الهندسية بحيث لا تتعرض لإنهيارات نتيجة الاهتزازات الذاتية المحثوثة الناتجة عن سريان الموائع فوق هذه المنشآت، وبالتالي يمكن الحصول على تصاميم ذات اعتمادية كبيرة وتكلفة اقل .

الدراسة الحالية هي دراسة مخبرية لمعرفة تأثير التداخل وشدة اضطراب الجريان وخشونة السطح على الاهتزازات الذاتية الناتجة عن سريان الهواء فوق سطح اسطوانة دائرية مربوطة بشكل كابولي . وقد تبين ان الإستجابة الديناميكية للإسطوانة تتمثل بقيمة واحدة عند سرعة مختزله حوالي (15.5) ، كما ان منطقة السيطرة تبدأ عند سرعة مختزله حوالي 13 وتنتهي عند 21 .

تم اختبار تأثير التداخل في ثلاثة ترتيبات مع الإسطوانة . في الترتيب الأول وضع الجسم المتداخل خلف الإسطوانة مع اتجاه الهواء، أما في الترتيب الثاني فتم وضع الجسم المتداخل فوق الإسطوانة والثالث كان بمزج الترتيبين الأول والثاني . ولجميع هذه الترتيبات فقد تم اختبار بعض المسافات بين الجسم والإسطوانة بالإضافة الى استعمال أكثر من جسم باقطار تتناسب مع الإسطوانة . وبعد إجراء التجارب تبين ان تأثير التداخل يكون أوضح في حالة الترتيب الأول أكثر منه في باقي الترتيبات حيث ظهر ازدياد ملحوظ في قيمة متسعذبذبة الاهتزاز خاصة عندما تكون المسافة قليلة وقطر الجسم المتداخل كبير . وقد أصبح متسعذبذبة الاهتزاز غير ملحوظ عند مسافات بعيدة ، أي ان الإستجابة الديناميكية للنظام أصبحت تشبه تلك في حالة اسطوانة فردية .

أثبتت النتائج المخبرية ان تأثير شدة الاضطراب يعتمد على مدى شدة الاضطراب وسرعة الهواء وابعاد المسافات والاقطار للجسام المتداخلة . أما تأثير خشونة السطح فقد تمثل في تخفيض متسعذبذبة الاهتزاز الى قيمة قليلة مقارنة مع تلك للسطح الناعم .

في المرحلة النهائية للتجارب تم دراسة تأثير أكثر من عامل مع بعض ، وقد بيّنت النتائج انه في حالة زيادة خشونة السطح فإن متسعذبذبة الاهتزاز يبقى قليلاً حتى مع وجود جسم متداخل قريب من الإسطوانة وله قطر كبير .